The Future of Carbonaceous Aerosol Measurement in the IMPROVE Monitoring Program

Bret Schichtel[1], William Malm[2], Melinda Beaver[3], Scott Copeland[2], Jenny Hand[2], Anthony Prenni[1], Joann Rice[3], John Vimont[1]

[1] National Park Service
[2] Colorado State University
[3] Environmental Protection Agency

Abstract

Carbonaceous aerosols are a signification fraction of fine particulate matter, often accounting for more than 50% of the mass in urban and rural environments. In the Interagency Monitoring of Protected Visual Environments (IMPROVE) program, thermal optical reflectance (TOR) is used to determine the total carbon (TC) concentration, separated into organic carbon (OC) and light absorbing carbon (LAC) fractions. TOR is an operationally defined analysis that cannot be referenced to traceable standards that reflect ambient compositions, so it is challenging to prevent potential instrument drift over long periods. The OC-LAC split can depend on the aerosol composition, which has spatial and long-term trends. These issues can introduce patterns and trends in the data records, complicating assessments of the spatial and temporal patterns of carbonaceous aerosols. In addition, TOR analysis is relatively expensive, and recent decreases in ambient concentrations are challenging the TOR detection limits, particularly for LAC. Due to these issues, two alternative carbonaceous measurements are being explored to supplement or replace TOR analysis in the IMPROVE network. The first is the use of Fourier transform infrared spectroscopy (FTIR), where FTIR spectra are calibrated against a subset of the measured TOR OC and LAC data. The second is a system using TC derived from a thermal method and filter absorption (fabs) measured using a hybrid integrating plate and sphere (HIPS) system. Estimates of LAC are then derived from the fabs data, and OC is estimated from the difference between TC and LAC. These methods have different benefits and drawbacks. FTIR is cost effective, but being calibrated to TOR, has the same inherent problems as an operationally defined method. TC and fabs measurements are also cost effective and known to produce stable long-term trends. However, fabs is subject to filter loading artifacts and relating TC and fabs to TOR OC and LAC is challenging. These three carbonaceous measurement methods are reviewed and contrasted with final recommendations for monitoring in the IMPROVE network.

Executive Summary

There are two national speciated particle-monitoring networks in the United States that are similar in design but serve different objectives. The Interagency Monitoring of Protected Visual Environments (IMPROVE) network, managed by a consortium of federal and state agencies, monitors primarily in rural areas and is used to track trends of haze in class I areas, consistent with the needs of the Regional Haze Rule (RHR). The Chemical Speciation Network (CSN), managed by state and local agencies, monitors primarily in urban and suburban settings and supports fine particulate matter less than 2.5 microns in diameter ($PM_{2.5}$) compliance monitoring for human health concerns. Together these networks provide an expansive characterization of PM in urban and rural settings, and the data are used for validating regional and global air quality

models; source apportionment modeling; radiative forcing assessments; and linking health effect endpoints to constituents in $PM_{2.5}$.

A defining characteristic of IMPROVE and the CSN is that they are long-term networks designed to track changes in fine mass and its composition over decades with IMPROVE initiating operations in 1988 and CSN in 2001. Both networks collect 24-h $PM_{2.5}$ samples that are analyzed for their elemental composition, ions, and carbon content. In addition, filter absorption (fabs), primarily due to carbon that absorbs light, is measured using a hybrid integrating plate and sphere (HIPS) system. With reductions in atmospheric sulfate and nitrate compounds, carbonaceous aerosols are now generally the largest or second-largest contributor to both rural and urban $PM_{2.5}$, accounting for on average ~60% in parts of the western United States and 25–40% in the East. The increasing relative importance of carbonaceous aerosols has made them a central focus of research activities to better understand their levels, trends, atmospheric processes, and origins. Critical to the success of using the IMPROVE and CSN carbonaceous data in these analyses is that changes in measured concentrations reflect real atmospheric changes and not changes in sampling or analysis protocols.

In IMPROVE and CSN, a thermal-optical reflectance (TOR) method is used to measure the total carbon (TC) content, which is divided into the operationally defined fractions of organic carbon (OC) and light absorbing carbon (LAC). LAC is simply defined as carbon that absorbs light, but it comes in a variety of forms. Elemental, graphitic, and refractory carbons, which are often referred to as black carbon (BC), primarily absorb incident light with little light scattering. As BC ages in the atmosphere, it can become internally mixed with other aerosol components that scatter light and enhance the absorption. Brown carbon (BrC), typically emitted from biomass burning, is OC that scatters and absorbs light, and as it ages it tends to become less absorbing. Consequently, LAC is composed of a complex mix of compounds with a range of absorbing and scattering properties. The TOR OC and LAC fractions are interpreted as pure scattering and pure absorbing, respectively, when in fact both scatter and absorb light to some degree.

TC is a well-defined atmospheric constituent. Thermal analyzers for TC can be calibrated, and it has been shown that TC concentrations are independent of the analysis methods. The ill-defined nature of the OC and LAC fractions, coupled with the difficulty in generating stable atmospherically relevant samples, hinders the development of reference standards that could be used to calibrate the TOR filter analysis for all ambient compositions. Consequently, the separation of TC into OC and LAC is dependent on the TOR operational protocols. Furthermore, the underlying assumptions of the TOR analysis are often not met, and the OC–LAC split can depend on the composition of the noncarbonaceous compounds in the $PM_{2.5}$ sample analyzed. Changes in the instruments or analysis protocols also can introduce discontinuities and drifts in the OC–LAC split, which are evident in the long-term IMPROVE record. When current sampling protocols are used, the low concentrations that increasingly occur at IMPROVE sites are near the TOR method's quantifiable limits. These issues complicate assessments of the carbonaceous aerosols' spatial and temporal patterns and their causes. LAC is the most sensitive to these issues since it is a smaller fraction of TC, typically 10–15% in the IMPROVE network. TOR is also a relatively resource-intensive analysis methodology. Due to these issues with TOR, alternative carbonaceous measurements are being explored to supplement or replace TOR measurements of OC and LAC in the IMPROVE program. Results are also informative for to the CSN program.

Alternative Carbonaceous Analysis Methods

Ideally, a long-term, routine carbonaceous aerosol-monitoring program should include the following:

- Ability to calibrate OC, LAC, and TC concentrations to ensure a consistent and accurate OC–LAC split
- Measurements that are not sensitive to analytic protocol or instrument type
- Ability to measure low concentrations found in remote environments as well as high concentrations found in urban centers and biomass burning plumes
- Cost-effective implementation
- Easy implementation in remote environments

In addition, any method must be suitable to meet the objectives of the monitoring programs. It is also important that measurements are relatable to with existing OC and LAC data measured using TOR analysis such that trends in these variables can be compared and tracked with past spatial and temporal trends.

The requirements for incorporation into routine monitoring programs limit the possible carbonaceous aerosol analysis methods, and only two alternatives have been explored. The first is the use of Fourier transform infrared spectroscopy (FTIR), where FTIR spectra are calibrated against a subset of the measured TOR OC–LAC data. The second is a system in which TC is measured using a thermal method and fabs is measured using HIPS. Estimates of LAC are then derived from the fabs data, and OC is estimated from the difference between TC and LAC. FTIR analysis has been employed in IMPROVE and CSN post-2015, though not as part of the routine measurements. HIPS analysis was first employed in IMPROVE in 1995 and CSN in 2018.

Table E1 summarizes and intercompares these two methods along with TOR and how they meet network requirements. As shown, unlike TOR, FTIR measurements are neither instrument nor protocol dependent. However, the estimation of OC and LAC from the FTIR spectra requires calibrating the system to TOR OC and LAC concentrations. Therefore, it suffers from the same issues as TOR OC and LAC, including not being fundamentally calibrated and ultimately dependent on the TOR operational protocols.

Table E1. Summary of requirements for three carbonaceous aerosol measurement methods for implementation into the IMPROVE long-term monitoring programs. Y and N are "yes" and "no", respectively, while H, M, L are "high", "medium", and "low", respectively.

	TOR[a]			FTIR[b]		TOA-HIPS[c]	
	TC	OC	LAC	OC	LAC	TC	(fabs)
Calibrated to standards	Y	N	N	N	N	Y	Y-N
Stable and reproducible measurements	Y	N	N	N	N	Y	Y
Instrument/method universality	N			Y		Y	Y
Measures at relevant low and high concentrations	Y	Y	N (biased)	Y	N (biased)	Y	N (unbiased)
High precision	Y	Y	N	Y	N	Y	Y
Cost	H			M		M	L
Implementable in remote settings	Y	Y	Y	Y	Y	Y	Y

Relatable to TOR	Y	Y	Y	Y	Y	Y	Y (today)
Organic aerosol compositional information	M			H		L	L

[a] thermal-optical reflectance
[b] Fourier transform infrared spectroscopy
[c] hybrid integrating plate and sphere

Measurement of TC can be calibrated to reference standards and is independent of instruments and protocols. The HIPS fabs measurement has been shown to be instrument independent, but it is not calibrated for loaded filters. HIPS is calibrated to blank filters and demonstrated to respond linearly at low filter loadings; however, at high filter loadings, HIPS is subject to artifacts and underestimates fabs. In IMPROVE, 6–12% of the filter samples in the last 12 years have sufficient loadings to result in an appreciable bias. Retrospective analyses of 15 years of IMPROVE samples have demonstrated that HIPS fabs measurements are stable and reproducible. The stability of HIPS and the low fraction of filters impacted by the artifact indicates that long-term trends in fabs should reflect changes in ambient absorption.

TOR TC and OC are quantifiable at low concentrations measured in the IMPROVE program. However, approximately 30% of IMPROVE LAC concentrations, and thus FTIR-derived LAC, are near or below the lower quantifiable limit (LQL) and have high uncertainty. These low values also appear to be significantly overestimated, which would bias aggregated LAC values. HIPS fabs has a similar fraction of values near and below the LQL as TOR LAC. However, due to the HIPS calibration procedures, these low values are not biased and generally have higher precision than TOR LAC.

All three carbon analysis methods have been successfully implemented into both rural and urban monitoring programs. Among the three methods, TOR is the most expensive analysis. FTIR is a relatively inexpensive analysis that is conducted on Teflon filters. Calibrating FTIR to OC and LAC concentrations requires the continued collection of $PM_{2.5}$ samples on quartz fiber filters for TOR analysis at about 20% of the monitoring sites as well as new monitoring sites. Therefore, using FTIR to derive OC and LAC is a moderately expensive analysis. The estimation of OC and LAC from TC and fabs would also be moderately expensive, since TC measurement using thermal methods requires the continued collection and analysis of samples on quartz fiber filters.

Although not a requirement for implementation into a speciated PM monitoring program, it is important that any changes to the carbonaceous measurements in IMPROVE are relatable to previous TOR OC and LAC to evaluate spatial and temporal patterns in the data across the change in filter analysis methods. The FTIR-derived OC and LAC have been shown to be generally within the uncertainty of the TOR and FTIR measurements and thus are comparable. This is not necessarily the case for the TC and fabs system, where the derived OC and LAC concentrations are dependent on the fabs to LAC relationship, which in turn depends on the optical properties of the carbonaceous aerosols. These optical properties can vary spatially and temporally, increasing the error in the estimated LAC. It has been shown that across the IMPROVE network from 2008 through 2018, fabs-estimated 24-h LAC concentrations were unbiased, but the error was more than twice the measurement uncertainty. In addition, trends in the IMPROVE LAC and fabs over the past 10 years are similar, but as the composition of ambient carbonaceous aerosols continues to change, the LAC and fabs trends could deviate.

A change in the measurement of carbonaceous aerosols in IMPROVE could bring other benefits. The fabs is an optical measure of $PM_{2.5}$ light absorption and is likely be more closely related to

ambient absorption than LAC. This is currently under investigation, and if accurate, then trends in fabs would be more closely aligned with trends in ambient absorption, which is important for RHR and climate science. The FTIR data contain additional information on the organic and inorganic composition of the carbonaceous aerosols that can be used to assess the organic mass to carbon ratios needed to reconstruct PM mass and light extinction, as well as information concerning the origins and history of the aerosols.

Recommendations

Based on this assessment, all three carbonaceous measurement methods have different benefits and drawbacks. They all can be easily implemented in IMPROVE and produce similar estimates of carbonaceous aerosol light extinction; thus all three methods are suitable for tracking trends in haze for the RHR, the primary objective of the IMPROVE monitoring program. A differentiating characteristic of the measurement methods is the ability to track long-term trends in the OC and LAC carbon aerosol fractions that are not influenced by changes in analytical procedures. This is ideally accomplished by fundamentally calibrating the system. In the measurement methods discussed, only TC fully meets this requirement and fabs meets it partially, though fabs has been shown to be stable and reproducible over decades.

The current approach of using TOR to measure TC, OC, and LAC and HIPS to measure fabs provides the most flexibility in that TC and fabs would be available for long-term trend analysis, but the TOR OC and LAC concentrations would continue to be measured, reported, and used in various analyses. However, cost constraints are driving changes to the IMPROVE program. Using TC and fabs to estimate OC and LAC and track trends in carbonaceous aerosols and haze would provide cost saving over TOR OC and LAC, produce the most stable and defensible long-term trends, and be suitable for use in the RHR analysis. Therefore, as a cost-saving measure, it is recommended that a TC-fabs system be used to measure carbonaceous aerosols in IMPROVE.

Introduction

The U.S. Environmental Protection Agency (EPA), the federal land management agencies (National Park Service, U.S. Fish and Wildlife Service, U.S. Forest Service, and Bureau of Land Management), and state and local air monitoring agencies are responsible for the operation of two extensive speciated particle monitoring networks that are similar in design but serve different objectives. The Interagency Monitoring of Protected Visual Environments (IMPROVE) monitoring network began in 1988 with ~20 sites, and today consists of about 160 sites primarily located in rural areas. The IMPROVE monitoring program is used chiefly to track long-term trends in visibility in class I areas, consistent with the needs of the Regional Haze Rule (RHR). Progress under the RHR is based on reconstructed aerosol mass and light extinction using particulate data measured in IMPROVE. Data collected in IMPROVE are also used to identify chemical species and emission sources responsible for existing man-made visibility impairment in federal class I areas; for identification of episodes of long-range transport; to serve as a regional backdrop for special studies; for regional modeling validation studies; and to support the development and implementation of particulate matter less than 2.5 microns in diameter ($PM_{2.5}$) National Ambient Air Quality Standards (NAAQS) by characterizing nonurban regional background aerosol levels (see Sections 169A and 169B of the Clean Air Act (42) U.S.C. §§ 7491, 7492 and implementation regulations at 40 CFR 51.308 and 51.309 containing legally binding requirements).

The Chemical Speciation Network (CSN) first began sampling in 2001 and consists of approximately 50 long-term-trend sites located primarily in urban and suburban settings, with about another 100 sites that are operated by state and local agencies. The purpose of the CSN program is to support $PM_{2.5}$ compliance monitoring for human health concerns. CSN objectives include tracking progress of emission control programs, aiding in the development of emission control strategies, and characterizing annual and seasonal spatial and temporal trends.

The data from both networks are also used for validating regional and global air quality models (Ridley et al., 2018); source apportionment modeling (Kim and Hopke, 2006; Schichtel et al., 2008, 2017; Chen et al., 2010; Ridley et al., 2018); radiative forcing assessments (Murphy et al., 2011; Bond et al., 2013); and linking health effect endpoints to constituents in particulate matter less than 2.5 microns in diameter ($PM_{2.5}$) (Cormier et al., 2006). A defining characteristic of IMPROVE and the CSN is that they are long-term networks designed to track changes in fine mass and its composition over decades. This allows for assessments of the responses of atmospheric concentrations to changes in emissions (Malm et al., 2004, 2017; Hand et al., 2013b) and climate (Ellis et al., 2013; Martin et al., 2015); epidemiological studies characterizing aerosol health effects (Hopke et al., 2006); as well as assessments of ecosystem responses to changing aerosol levels (Li et al., 2016).

The IMPROVE and CSN networks collect 24-h $PM_{2.5}$ samples that are analyzed for their elemental composition, ions, and carbon content. These data are used to estimate the major aerosol constituents, which include sulfates assumed to be in the form of fully neutralized ammonium sulfate, nitrates in the form of ammonium nitrate, soil mass estimated from assumed oxides of measured soil elements, sea salt, and carbonaceous aerosols. Carbonaceous aerosols are composed of thousands of compounds. In IMPROVE and the CSN, these compounds are grouped into two categories: a non-light-absorbing organic carbon (OC) and a light absorbing carbon (LAC) component. In the literature the carbon content of light-absorbing aerosols is often referred to as elemental carbon (EC), black carbon (BC), soot, and LAC (Bond and Bergstrom, 2006). Following the recommendations of Malm et al. (1994) and Bond and

Bergstrom (2006), LAC is used here to represent the broad set of carbon compounds that absorb light. In addition to OC and LAC, the absorption of the filter deposit, i.e., filter absorption (fabs), is measured in IMPROVE using a hybrid integrating plate and sphere (HIPS) method (White et al., 2016) since 1994 and in the CSN since 2019.

The goals and objectives of the IMPROVE and CSN monitoring programs are somewhat different. In the case of IMPROVE, the focus is on visibility, so a primary goal is to derive atmospheric extinction from measured aerosol species to track trends in haze for the RHR; atmospheric absorption (babs) from LAC is a component of extinction. In the CSN, the measurement of carbonaceous aerosols is more closely aligned with understanding its epidemiological effects. Currently, for tracking trends in haze for the RHR, the strategy is to measure LAC and derive babs from that measurement, while EC is of direct interest to the goals of the CSN. An alternative approach is the use of fabs, a measurement more directly related to atmospheric absorption, and relating fabs to LAC to meet the requirements of both monitoring programs.

Carbonaceous aerosols are generally the largest or second-largest contributor to both rural and urban $PM_{2.5}$, accounting for on average ~60% in parts of the western United States to 25–40% in the East (Hand et al., 2013a; Malm et al., 2017). Both OC and LAC have a number of adverse effects, but LAC has received more attention due to its potential adverse health effects (Grahame and Schlesinger, 2007; Janssen et al., 2011; Samoli et al., 2016) and climate effects (Ramanathan and Carmichael, 2008; Jacobson, 2010). LAC has also been used as a marker species for mobile sources (Schauer et al., 2003; Chiappini et al., 2014; Atkinson et al., 2016), though biomass burning is also a significant source (Schichtel et al., 2017). The relative importance of carbonaceous aerosols is expected to increase as emissions of particulate sulfate and nitrate precursors continue to decrease (Hand et al., 2020; Malm et al., 2020). However, OC and LAC concentrations have also decreased over the past two decades (Hand et al., 2013a, 2019; Chen et al., 2012), which may partly be due to decreased biogenic secondary organic aerosols resulting from decreased ambient sulfate concentrations, particularly in the eastern United States (Malm et al., 2017).

The increasing relative importance of carbonaceous aerosols has made them a central focus of research activities to better understand their levels, trends, atmospheric processes, and origins. Critical to the success of using the IMPROVE and CSN data in these analyses is that changes in measured concentrations reflect real atmospheric changes and not changes in sampling or analysis procedures. Many of the particulate measurements and analyses are subject to known and unknown artifacts and biases (Malm et al., 2011). In addition, it is a challenge to maintain consistent and equivalent measurements in the face of changing personnel, procedures, and manufacturers of consumable supplies, as well as changing and aging equipment. Known and unknown changes in the sampling artifacts and network operations can create discontinuities and biases in time series that can influence trends and complicate the use of the data (Kirchstetter et al., 2008; Hyslop and White, 2009; Murphy et al., 2011; Chen et al., 2012; Hyslop et al., 2012, 2015). The long timescales used for trends make consistent and verifiable calibration of the measurements to minimize such discontinuities a key focus in the monitoring programs (Bond and Bergstrom, 2006; Baumgardner et al., 2012; White et al., 2016; Hyslop et al., 2019).

Although the measurement of total carbon (TC) is relatively straightforward (Currie et al., 2002), separating TC into OC and LAC fractions is challenging (Currie et al., 2002; Baumgardner, et al., 2012). In IMPROVE and the CSN, TC is divided into OC and LAC using a thermal-optical reflectance (TOR) technique (Chow et al., 2007). As discussed in detail below, this division

depends on the operational protocols used in the measurement; different protocols can cause wide variability in the OC–LAC split (Chow et al., 1993, 2005, 2007; Watson et al., 1994, 2005; Yu et al., 2002; Cao et al., 2003). Changes in the analysis protocol can introduce systematic biases into the OC–LAC split that could potentially affect the long-term trends. In addition, the OC–LAC split may depend on the loading and composition of the carbonaceous aerosol deposits on the filters (Boparai et al., 2008; Conny et al., 2009). These issues are compounded by the complexity of carbonaceous aerosols and a lack of standards to calibrate the TOR instruments for both OC and LAC. In addition, the low concentrations that increasingly occur at IMPROVE sites are near the TOR method's quantifiable limits.

TOR is a relatively resource-intensive analysis methodology, and the potential varying biases in the OC–LAC split complicate its use for trend analysis and meeting the objectives of the IMPROVE and CSN programs. Due to these issues, alternative carbonaceous measurements are being explored to supplement or replace TOR analysis. Ideally, a long-term routine carbonaceous aerosol-monitoring program includes the following requirements:

- Ability to calibrate OC, LAC and TC concentrations to ensure a consistent and accurate OC–LAC split
- Measurements that are not sensitive to analytic protocol or instrument type
- Ability to measure low concentrations found in remote environments as well as high concentrations found in urban centers and biomass burning plumes
- Cost-effective implementation
- Easy implementation in remote environments

In addition to the above requirements, any method must be suitable to meet the objectives of the monitoring program. It is also important that measurements are relatable to existing OC and LAC data measured using TOR analysis such that trends in these variables can be compared and tracked with past spatial and temporal trends.

These requirements limit the possible measurement methods suitable for carbonaceous aerosol, and only two alternative approaches for measuring OC and LAC have been explored. The first is the use of Fourier transform infrared spectroscopy (FTIR), where FTIR spectra are calibrated against a subset of the measured TOR OC–LAC data (Russell, 2003; Ruthenburg et al., 2014). The second is a system using TC measured using a thermal method and fabs measured using HIPS. Estimates of LAC are then derived from the fabs data, and OC is estimated from the difference between TC and LAC. Both of these methods have benefits and drawbacks.

In this report, the current TOR method used in the IMPROVE and CSN programs is reviewed, and its benefits and limitations and issues are examined. The focus of the analysis and discussion is on the IMPROVE network. The two alternative carbonaceous measurement methodologies also are discussed and evaluated in the context of the above requirements. Finally, a recommendation for future carbonaceous measurements for IMPROVE is made.

Thermal-Optical Analysis of Filter Sample for Carbonaceous Aerosol

The most common analytic technique for estimating ambient carbon aerosol mass is the thermal evolution of carbon from particles that have been collected on quartz filters (Watson et al., 2005). There have been at least 15 thermal combustion methods identified (Cadle et al., 1980; Huntzicker et al., 1982; Novakov, 1982; Tanner, 1982; Mizohata and Ito, 1985; Cachier et al., 1989a,b; Fung, 1990; Chow et al., 1993, 2001; Rupprecht et al., 1995; NIOSH, 1999; Mader et al., 2001; Sharma et al., 2002; Yang and Yu, 2002). Although certain "standardized" thermal

evolution techniques have been adopted, there is not one common definition of what constitutes LAC or OC, and the sensitivity of the OC–LAC split to the operational protocols causes wide variability in the reported OC and LAC concentrations across the different thermal analysis techniques (Currie et al., 2002).

Early thermal methods involved heating the filter in an oxidizing environment. When heated, a fraction of organic aerosol can char or pyrolyze, essentially converting OC into LAC. This occurs most severely in nonoxidizing environments. To account for the pyrolyzed carbon, some methods combine thermal evolution of carbon while simultaneously monitoring the filter transmittance or reflectance. The optical data are then used to correct for the influence of charring during heating. These techniques are referred to as thermal-optical analysis (TOA). A wide variety of temperature programs have been used in TOA, often with differing results (Schmid et al., 2001; Watson et al., 2005). The combination of temperature program and optical analysis best suited to analyzing different types of samples is still a subject of debate and many papers have pointed out challenges in interpreting TOA results (Cadle et al., 1983; Chow et al., 2001; Conny et al., 2003; Subramanian et al., 2006).

IMPROVE TOR Protocol

The specific IMPROVE TOR protocol (Chow et al., 2007; DRI, 2012) is to heat the filter in a nonoxidizing environment of helium (He) up to 580 °C in four steps (Figure 1). During this heating under the He environment, a fraction of organic aerosols is charred and does not evolve from the filter. An oxidizing environment containing 2% O_2 is then introduced, resulting in both charred and native EC evolving, labeled as the EC1 peak in Figure 1. Note that in most of the thermal-optical literature, EC is used instead of LAC. In the following discussion, both terms are used interchangeably. Also shown in Figure 1, is the carbon that evolved at various temperatures under He, which is referred to as the OC1, OC2, OC3, and OC4 peaks. Carbon evolved at 740 °C and 850 °C in an oxidizing environment is referred to as EC2 and EC3, respectively.

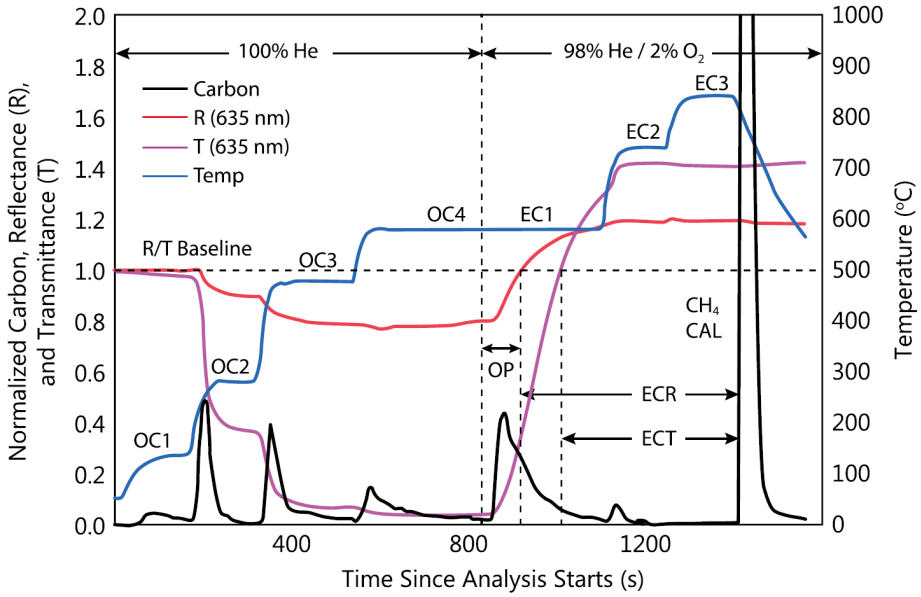

Figure 1. Typical thermogram showing the normalized evolved carbon signal, chamber temperature, laser reflectance (R) and transmittance (T) signals, and carbon concentration signals corresponding to OC1, OC2, OC3, OC4, EC1, EC2, and EC3. ECR and ECT refer to the

assigned elemental carbon concentrations corresponding to the R and T signals, respectively. OP is that portion of EC1 that is interpreted as pyrolyzed carbon (Chow et al., 2007).

To divide EC1 into native and charred LAC, filter reflectance (R) and transmittance (T) of the laser are continuously monitored as the sample is heated. During heating in the He environment, both R and T decrease as some of the organic mass is charred. In the oxidative environment, the R and T increase as EC is volatilized and eventually return to their initial or baseline value. Carbon that evolves before R or T returns to its baseline value is interpreted as OC, while the remaining carbon associated with the EC1 peak is assigned to the LAC fraction. Pyrolyzed OC (referred to as OP) is that portion of the EC1 peak that evolves before the reflectance or transmittance returns to its original value. Therefore, OC = OC1 + OC2 + OC3 + OC4 + OP and EC = ECR + EC2 + EC3. Dividing EC1 carbon into OP and EC is predicated on the assumptions that charred carbon volatilizes before native EC or that charred and native carbon have the same optical properties. Both assumptions are invalid in most cases (Yang and Yu, 2002; Subramanian et al., 2006; Boparai et al., 2008; Conny et al., 2009) resulting in under- and overestimates of OC and LAC.

Implementation in IMPROVE and CSN Monitoring Programs

Both IMPROVE and the CSN currently use the IMPROVE-A TOR protocol to measure OC and LAC concentrations (Chow et al., 2007). Prior to 2007, the CSN used the National Institute for Occupational Safety and Health (NIOSH) thermal-optical transmittance (TOT) method, and from 2007 to 2010 the CSN transitioned to the IMPROVE-A TOR protocol. The NIOSH protocol used a different temperature profile than IMPROVE-A and used transmittance to correct for pyrolyzed carbon during heating. These CSN LAC concentrations were on average lower than those measured in IMPROVE using the TOR protocol. Malm et al. (2011) present a method to reconcile the differences between the measurements.

TOA methods only yield a measurement of the carbon component of the organic aerosol. To estimate the organic mass, the OC must be multiplied by a scaling factor. Carbon aerosols are chemically complex, with OC to organic mass ratios (R_{oc}) that vary from values near 1 for aerosols containing mostly LAC to as high as 3.75 for oxalic acid. (El-Zanan et al., 2005; Nicolosi et al., 2018). The mass of organic aerosols (OMC, for organic mass by carbon) can be expressed as

$$OMC = \sum_i R_i OC_i \quad (1)$$

where OMC is the aggregate mass concentration of ambient OC aerosols, and R_i is the ratio of the mass of the i^{th} organic species to its carbon mass, OMC_i/OC_i. It is assumed that

$$\sum_i R_i OC_i \approx R_{oc} OC \quad (2)$$

where R_{oc} is the average OMC/OC ratio of an ambient organic aerosol and $OC = \sum_i OC_i$. In the IMPROVE program, the R_{oc} factor was initially assumed be a spatially and temporally constant value of 1.4 (Malm et al., 1994). Based on a literature review and statistical analyses of the IMPROVE data, the R_{oc} factor was revised to 1.8 (Malm and Hand, 2007). Recent work by Hand et al. (2019) and Malm et al. (2020) has shown that R_{oc} is seasonally and spatially variable and may have increased in recent years, and today an average R_{oc} of 1.8 to 2 is appropriate for rural areas in the United States.

Quartz filters absorb organic gases, resulting in a positive artifact (Chow et al., 2010). To account for this, backup quartz fiber filters were used at a small subset of sites that are also analyzed by TOR. The reported carbon concentrations are corrected for an approximate positive

artifact estimate from the monthly median OMC measured on the backup filters. Starting in 2015, field blanks were used in place of the backup filters (http://vista.cira.colostate.edu/improve/Data/QA_QC/Advisory/da0032/da0032_OC_artifact.pdf). This artifact correction is applied across the entire IMPROVE network. This assumes that the adsorbed gaseous material mass is equal throughout the continental United States. The method also assumes that the vapors are adsorbed uniformly throughout the sampled filters and field blanks (adsorption capacity is attained). Both these assumptions may not always be true. There is also a negative artifact of about 20% thought to be the loss of semivolatile organics during sampling due to the large pressure drop across the filter (Malm et al., 2011). The data are not corrected for this loss.

Advantages of Thermal-Optical Analyses

TOA methods have been implemented in national urban and remote monitoring programs. In addition, they provide estimates of TC, OC, and LAC. The TC has been shown to be operationally independent (Currie et al., 2002) and can be calibrated to various standards including sucrose, potassium hydrogen phthalate (KHP), and the National Institute of Standards (NIST) standard, reference material 8785, which was developed to calibrate TOA methods (Klouda et al., 2005; Baumgartner et al., 2012). This ability to calibrate TOA methods to TC standards should allow the tracking of TC long-term trends uninfluenced by analytical changes.

There is a long history of using TOAs on collected samples in the IMPROVE program since 1989 and in the EPA CSN program since 2001. It is also being used to characterize air quality in other countries with rapidly growing air quality problems (e.g., Venkataraman et al., 2002; Cao et al., 2003). The OC to LAC ratio has been used to infer changes in the carbonaceous aerosol composition, including contributions from secondary organic aerosol (e.g., Strader et al., 1999; Lim and Turpin, 2002; Polidori et al., 2006). Receptor- and inverse-modeling techniques have incorporated TOA results to infer sources of OC and LAC (e.g., Watson et al., 1994; Park et al., 2003; Hakami et al., 2005; Schichtel et al., 2017). In the United States, OC and LAC concentrations are being used to track decadal trends as their contributions to haze (Murphy et al., 2011; Chen et al., 2012; Hand et al., 2012, 2019, 2020). LAC is also highly correlated with filter-based absorption measurements (Kirchstetter et al., 2008; White et al., 2016) and associated with health effects (Grahame et al., 2007; Janssen et al., 2011; Samoli et al., 2016). Consequently, the existing short- and long-term carbonaceous data sets from TOAs have been critical for understanding the roles of organic aerosols and LAC in affecting visibility (Hand et al., 2020); radiative balance (Murphy et al., 2011); model development and evaluation (Heald et al., 2006); tracking changes in absorbing and organic carbon (Malm et al., 2017); and health (Janssen et al., 2011).

Limitations of Thermal-Optical Analyses

There are several important limitations in using TOA methods in monitoring networks such as IMPROVE and the CSN. These methods do not have accurate OC–LAC splits due to difficulty in calibration and violation of TOA assumptions. Consequently, the OC–LAC split is dependent on the TOA protocol as well as the composition of the PM on the filter. In addition, in the rural United States and many urban areas, the LAC concentrations are near or below the detection limits, leading to high uncertainties. Combined, these errors can potentially lead to changing biases in the data that can affect trends. The following sections include detailed discussions of these limitations.

Variable OC–LAC Splits

No Reference Standards to Calibrate TOA OC and LAC Concentrations

There is currently no methodology that unambiguously separates the TC into its OC and LAC components. The fundamental problem is that there is not an objective definition to distinguish between the two analytes (Baumgardner et al., 2012). Without such a definition, this distinction in the carbonaceous aerosols cannot be traced to fundamental principles, and there is no way to directly ensure no analytical drift in the OC–LAC split. Instead, the OC–LAC split is defined by the operational protocol, and steps are taken to ensure a consistent protocol. For example, the IMPROVE TOR system is calibrated for TC using sucrose standards; the temperature at the sample and the temperature heating protocols are calibrated; and the system is checked for oxygen leaks during the inert heating phase. These system checks help to minimize and prevent instrument drift, but they do not eliminate the potential for drift. Past efforts have been taken to develop specific definitions of LAC and OC and standards suitable for calibration of TOA instruments (Baumgardner et al., 2012). Though not successful to date, even if suitable standards are eventually developed, the analysis of ambient samples often violates the underlying assumptions of TOA methods, resulting in increased uncertainties and potentially biases and trends in the OC–LAC splits.

Violation of TOA Assumptions

The proper split of TC into OC and LAC using the IMPROVE TOR protocol and all other TOA analyses is dependent on the assumptions that 1) all nonabsorbing and nonpyrolyzed OC volatilizes prior to LAC; 2) all OP volatilizes prior to LAC, or OP and LAC have the same mass absorption efficiency (MAE); 3) the optical properties of LAC and other aerosols remain constant during heating; and 4) changes in laser reflectance or transmittance account for all changes in the sample absorption during heating.

In a series of lab experiments, it has been shown that there can be significant slip of non-pyrolyzed OC into the oxidative phase of the TOA, leading to overestimations of LAC (Subramanian et al., 2006). In one study it was found that a few percent of biogenic secondary organic aerosols analyzed by TOR was reported as LAC (Schauer et al., 2003). The amount of the OC slip was dependent on the temperature profile with low temperature protocols, e.g., IMPROVE TOR, having more slip. It was also dependent on the type of aerosol, which complicates any potential corrections for the OC slip. Alternatively, LAC can volatilize in the inert phase of the TOA, leading to LAC underestimations (Yu et al., 2002; Subramanian et al., 2006; Boparai et al., 2008). For example, it has been demonstrated that when various salts or metal oxides are present, there can be a catalytic degradation of the LAC during the inert heating stage when only OC is supposed to evolve (Novakov and Corrigan, 1995; Yu et al., 2002; Subramanian et al., 2006; Cavalli et al., 2010; Bladt et al., 2012; Nash et al., 2013).

The second assumption requires that all OP volatilizes prior to LAC or that OP and LAC have the same MAE. Neither of these assumptions hold. Laboratory experiments have shown that LAC and OP co-evolved when oxygen was added to the analyzers (Conny et al., 2003, 2009), and an implication of LAC volatilizing in the inert phase of TOA, as noted above, is that LAC can volatilize before OP. It has also been shown in laboratory-generated aerosols that the MAE of OP is typically significantly larger than for LAC, by a factor of 2 or more (Subramanian et al., 2006; Boparai et al., 2008). Chow et al. (2004) used a regression analysis on a subset of samples collected in 2002 and 2003 from the IMPROVE network to estimate the apparent effective OP and LAC MAEs and found that the OP MAE was more than a factor of 3 larger than for LAC at

70 m^2/g versus 20 m^2/g. Hand (personal communication, 2020) extended this analysis to all IMPROVE samples measured in 2016 and 2017 and found similar results, with OP MAE ~ 70 m^2/g and LAC MAE ~ 15 m^2/g. The implications from these results are that LAC volatilizes from the filters prior to all of the OP volatilizing, and due to the lower MAE of LAC, the optical corrections in TOAs will overcorrect for the OP artifact, resulting in underestimated LAC.

The third assumption for a valid TOA OC–LAC split is that the optical properties of the aerosols do not change during heating. It is known that some iron (Fe) oxides can become more absorbing when heated. This is explored in Figure 2, where the TOR LAC divided by the TOA black carbon (BC) is plotted against the Fe concentrations for all IMPROVE samples for the years 2007–2016. TOA BC is derived from the attenuation of the laser transmittance through the sample on the filter and is defined as

$$BC = ln\left(\frac{LTfinal}{LTintial}\right)/MAE \quad (3)$$

where LTinitial and LTfinal are the initial (before heating) and final (at the end of heating) laser transmittance values, respectively, and MAE is the effective MAE of BC deposited on a quartz filter. Equation 3 is analogous to how an aethalometer operates. The MAE used in equation 3 was assumed to be 23 m^2/g, which is a similar MAE to what is used in an aethalometer (Ram and Sarin, 2009) and is greater than ambient BC MAE due to filter measurement artifacts. Orange dots in Figure 2 signify filter punches that are red in appearance, an indication of Fe oxides. Because Fe does not evolve over the temperature range used during the TOR analysis, the BC is not expected to depend on the absorption by Fe oxides.

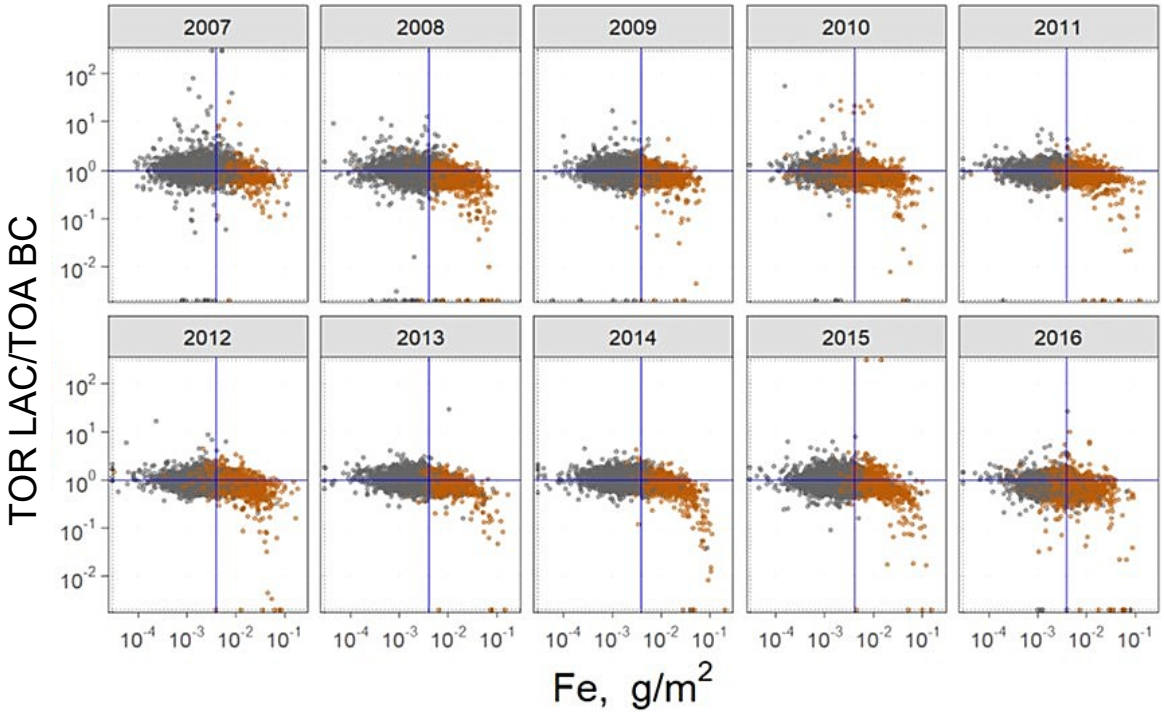

Figure 2 (Adapted from White, 2017). TOR LAC/TOA BC ratio scattered against the Fe filter density for IMPROVE samples from 2007 to 2016. Orange data points signify filter punches with a reddish hue after the TOR analysis.

As shown in Figure 2, at the higher Fe concentrations the TOR LAC/TOA BC ratio is depressed, suggesting that TOR LAC is dependent on the level of Fe on the filter. It is well established that minerals such as Fe have a catalytic effect on soot oxidation (e.g., Nash et al., 2013) causing the

premature volatilization of LAC in the inert environment. The optical correction should compensate for this loss, but if not, the Fe catalytic effect would cause an underestimation in the TOR LAC concentrations and overestimation in the OC concentrations.

An alternative explanation for the potentially low LAC concentrations at high Fe loadings is that the Fe oxides become more absorbing during heating. This is explored in Figure 3 where the change in the filter reflectance per unit change in temperature (ΔRefl/ΔTemp) for all CSN samples analyzed by TOR in 2019 is plotted against the sample Fe concentration (Zhang and White, 2020). The ΔRefl/ΔTemp was calculated from data collected during the cool-down period in the TOR analysis. Consequently, all carbonaceous aerosols were volatilized from the filter, and any changes in optical properties of the sample are due to changes in the inorganic aerosol. The strong relationship with Fe concentrations suggests that the Fe-containing particles become less absorbing as the temperature cools. The dependence of the filter reflectance on temperature can explain at least a part of the change in TOR LAC/TOR BC with Fe concentrations in Figure 2.

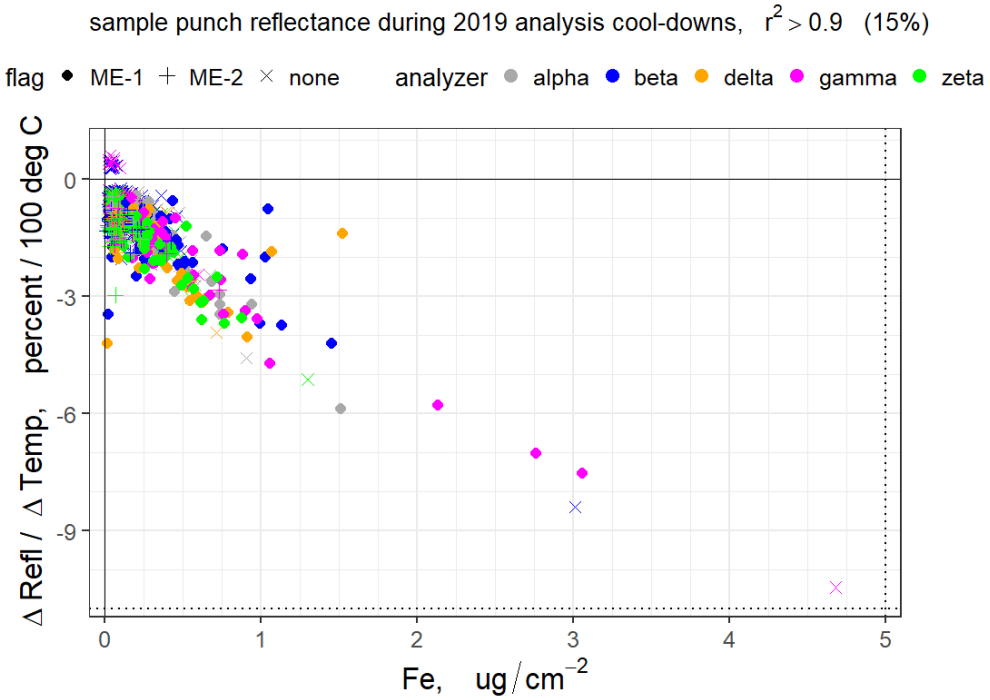

Figure 3. Temperature sensitivity of the reflectance of noncarbonaceous $PM_{2.5}$ as measured by the ratio of the percent change in the sample reflectance per 100 ºC in the post-TOR analysis cool-down phase. Ratios, or slopes, were calculated using ordinary least squares regression on the reflectance vs. temperature data, and only data with $r^2 > 0.9$ are shown. CSN 2019 samples were analyzed using multiple Sunset OCEC instruments. Color of the symbols identifies the specific analyzer used (e.g., alpha, beta, delta, gamma, and zeta). Samples flagged as ME-1 and ME-2 have red/orange- and gray/black-colored punches after analysis, respectively (Zhang and White, 2020, personal communication).

Operationally Defined OC–LAC Split

The primary differences between TOA methods are in the temperature profiles used during heating and the optical detection technique (transmission versus reflectance) used to correct for pyrolyzed OC. A wide variety of temperature programs have been used in TOAs, often with differing results (Schauer et al., 2003; Watson et al., 2005; Subramanian et al., 2006; Piazzalunga

et al., 2011). In general, higher maximum temperatures in the inert heating phase result in lower LAC. In one study (Subramanian et al., 2006) 43 ambient samples were analyzed using TOT with two different temperature protocols. The maximum temperature during the inert heating phase was 700 ºC (He4-700) in one protocol and in the second it was 800 ºC (He4-870). Samples were collected using various sampling durations and with and without volatile organic compound denuders. As shown in Figure 4, the He4-700 protocol resulted in 25 ± 13% higher LAC than the He4-800 protocol. The consistency in these results across the samples has not been found by others. In the TOT intercomparison by Schauer et al. (2003), the fractions of LAC measured in wood smoke were found to be sensitive to the temperature profiles used in the analysis, while samples of coal fly ash had moderate sensitivity to temperature profiles, and samples of BC and secondary organic aerosol were found to have the same OC–LAC split in all temperature programs used.

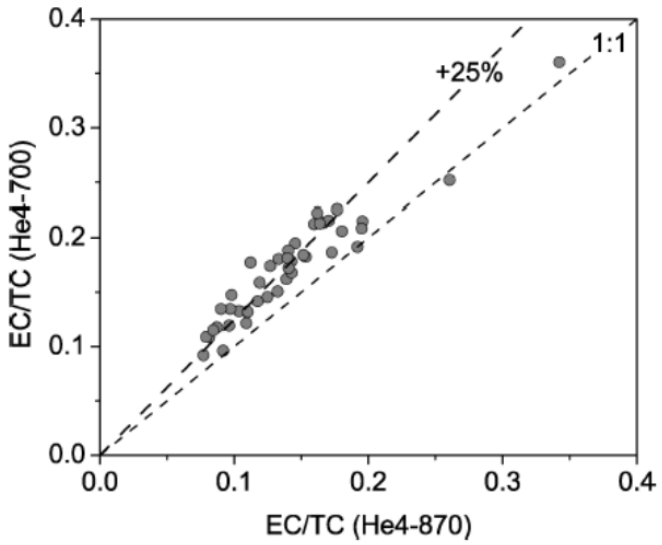

Figure 4. Scatter plot of EC (LAC) as a fraction of TC measured using two TOT temperature protocols for parallel punches taken from 43 different ambient samples, including 24-h denuded and undenuded samples with sampling durations of 8, 24, 48, 96 hours. Figure is from Subramanian et al. (2006).

These studies used transmittance (i.e., TOT) to correct for pyrolysis. Chow et al. (2004) used samples collected from a number of rural and urban IMPROVE sites to test the sensitivity of the OC–LAC split to different temperature profiles in TOR. Consistent with other studies, they found that higher maximum temperatures used in the inert phase resulted in lower LAC concentrations when transmittance was used to correct for charred carbon but that reflectance (TOR) corrections yielded equivalent OC–LAC splits for widely divergent temperature protocols (Figure 5). They attributed the difference in the LAC response between TOT and TOR to substantial charring that took place within the filters, possibly due to adsorbed organic gases or diffusion of vaporized particles. Filter transmittance is more influenced by the within-filter char, whereas filter reflectance is dominated by charring of the near-surface deposit that appears to evolve first when oxygen is added.

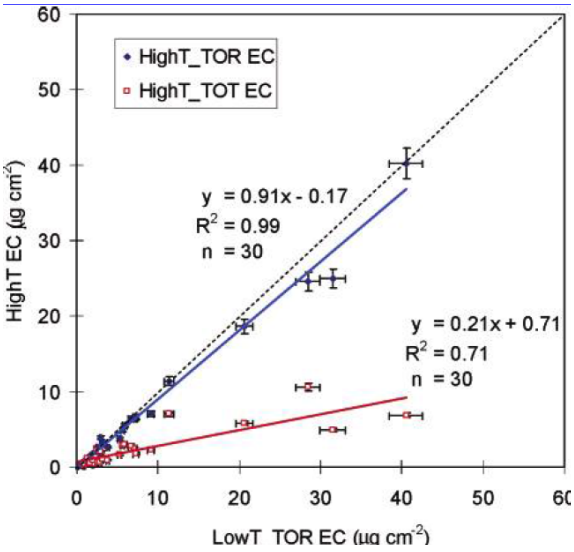

Figure 5. TOR-corrected LAC from a low-temperature protocol and both TOR- and TOT-corrected LAC from a high-temperature protocol. Thirty samples from 16 IMPROVE sites were used in the analysis. Figure is from Chow et al. (2004); TOA EC is referred to as LAC in this document.

As evidenced in Figure 5, the optical correction method for charred carbon can affect the OC–LAC split in TOA analyses. Chow et al. (2004) made simultaneous TOT and TOR measurements from the samples and found that LAC determined by TOT was 30% lower than LAC by TOR for the same temperature protocol. Subramanian et al. (2006) found similar results in their study. Karanasiou et al. (2015) pointed out that the differences between reflectance and transmittance corrections tend to be larger than the differences between different thermal protocols. However, both transmittance corrections and higher maximum temperatures in the inert heating phase result in lower LAC. Combined high-temperature TOT resulted in LAC concentrations that were 70–80% lower than the low-temperature TOR protocol used in the IMPROVE program (Figure 5).

LAC Signal to Noise Ratio

The IMPROVE LAC concentrations have relatively large errors of 22% compared to 17% for OC and 4% for sulfate as estimated from collocated data (Hyslop and White, 2008). Contributing to this uncertainty is the fact that LAC concentrations in rural areas are low and near or below the lower quantifiable limits (LQLs), defined as three times the minimum detection limit (3 × MDL) (US EPA, 2000). In IMPROVE the MDL is derived from the LAC measured on field blanks. In 2017–2019 the LAC MDL ranged between 0.008 and 0.48 µg/m^3 with an average of 0.02 µg/m^3. The uncertainty is estimated as $\sqrt{0.6 * MDL^2 + precision^2}$ where the LAC precision is 14%.

Figure 6 presents the cumulative frequency of the ratio of the LAC to MDL concentrations for IMPROVE data measured at rural sites from 2017 to 2019. As shown, about 30% of all LAC concentrations were below the LQL. The fraction of LAC below the LQL varies widely, from 0% at near-urban sites to over 90% at sites in Hawaii and Alaska where LAC concentrations are very low (Figure 7). As shown in Figure 7, there is a general decrease in the fraction of LAC below 3 × MDL from the western to the eastern United States, which is expected based on the typical LAC concentrations (Hand et al., 2013a). In total, 32 out of the 150 nonurban sites used in the analysis, or 21%, have 50% or more of the LAC below the LQL. These large fractions of

unquantifiable LAC concentrations hinder tracking of LAC trends and using the data and source marker species at these sites.

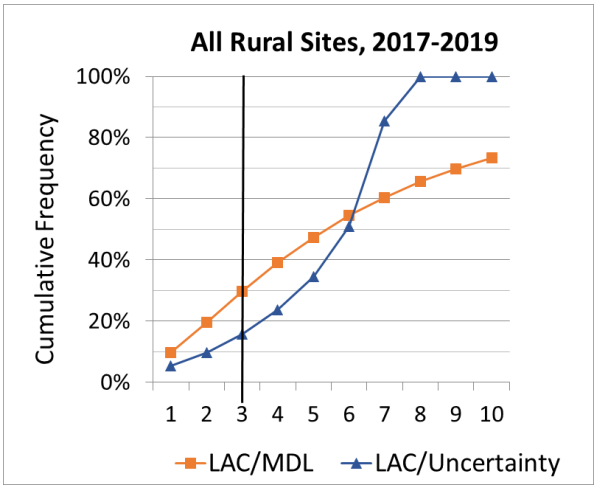

Figure 6. Cumulative frequency distribution of the ratios of LAC/MDL and LAC/measurement uncertainty for data from all IMPROVE rural sites measured in 2017–2019.

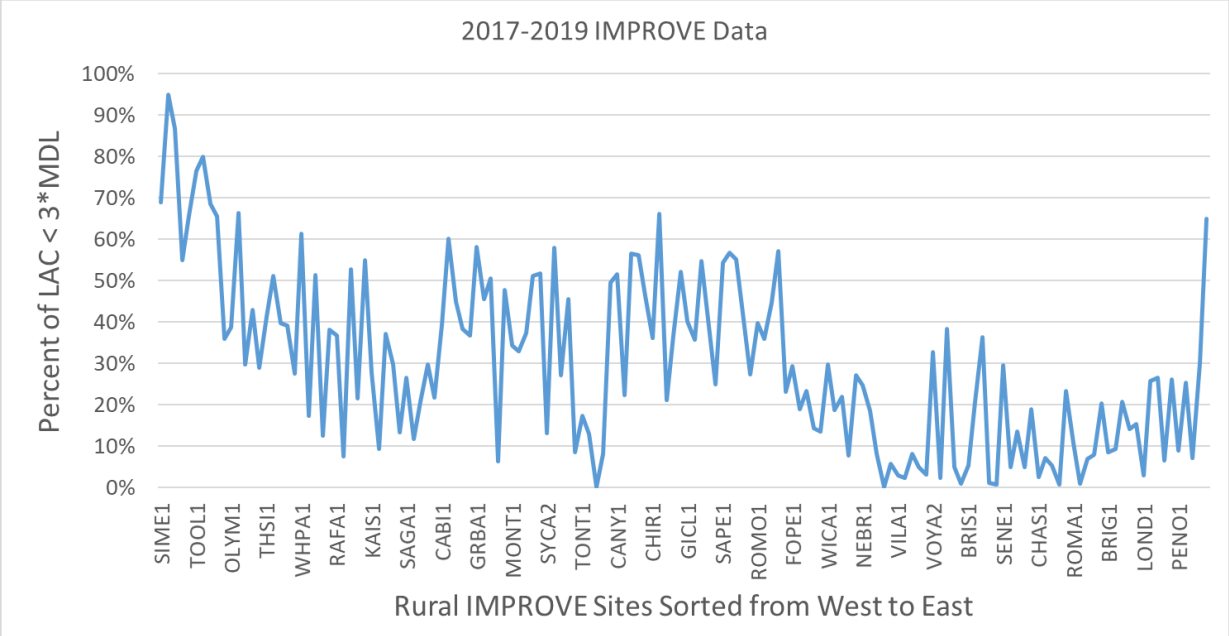

Figure 7. Fraction of LAC concentrations less than 3 × MDL, i.e., the LQL, measured at 150 rural IMPROVE sites from 2017 to 2019. Sites are sorted by longitude from west to east. X-axis is the IMPROVE site code for every 4th site.

Potential Discontinuities and Biases in Long-term Trends

The issues with TOA methods and the lack of a fundamental calibration for the system for ambient aerosols can potentially result in discontinuities and biases in long-term trends. This is illustrated in the timeline of network-wide, median, deseasonalized daily LAC/TC ratios in Figure 8. All valid measured data from 1990 through 2017 were included. Daily LAC/TC data were deseasonalized by multiplying each value by the ratio of the annual median to the monthly median LAC/TC ratios calculated using all data. Due to the changing number of sites during the period of operation, trends in the ratio do not necessarily represent changes in the composition of the carbonaceous aerosols. However, by using all valid data, the measurement uncertainty in the

aggregated data is small, allowing the identification of shifts or discontinuities in the data record. Changes in analytical procedures that cause a change in the OC–LAC split would cause a discontinuity in the data record. A sudden change in the composition of the aerosol could also cause a discontinuity in the data record, but this change would have to simultaneously occur across the United States, which is unlikely.

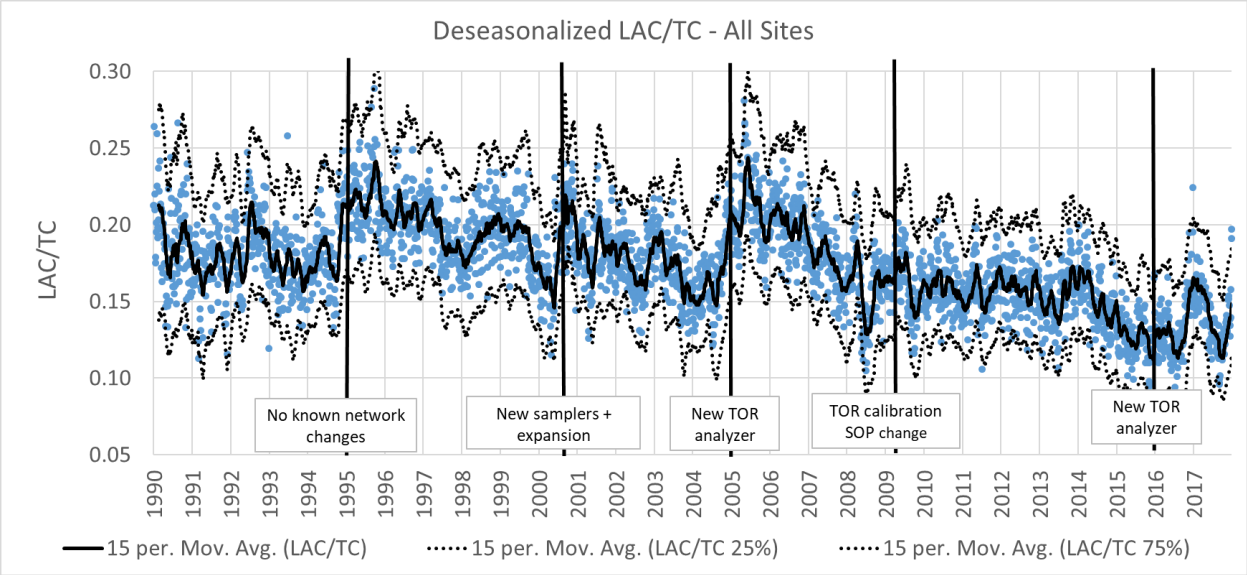

Figure 8. Deseasonalized daily network median LAC/TC ratios from the IMPROVE monitoring network from 1990 through 2018. Each circle is the median of all 24-h LAC/TC ratios measured in the IMPROVE program on the given sample day. Solid line is a 15-point moving average of these daily data. Dotted lines are 15-point moving averages of the 25th and 75th percentiles of the LAC/TC ratios on a given sample day. Daily LAC/TC data were deseasonalized by multiplying each value by the ratio of the annual median to the monthly median LAC/TC ratios calculated using all data.

As shown in Figure 8, since the early 1990s there are at least three discontinuities in the temporal data record, two abrupt ones in 1994 and 2000 and a third in 2005 that appears to have occurred over several months at the end of 2004. There are no known changes to the IMPROVE monitoring program that occurred at the end of 1994 that could explain that discontinuity. The discontinuity in 2000 is associated with the large expansion in the IMPROVE monitoring program to support the RHR, and in 2005 a new TOR analyzer was introduced. Tests revealed that oxygen leaks had occurred in the old analyzers during the inert heating phase, which could cause a loss of LAC in the inert phase and an underestimation in the LAC concentrations (Chow et al., 2007). The optical correction should compensate for this loss of LAC, but the increase in LAC/TC ratio in 2005 suggests that it did not fully compensate for the loss. Marked on the figure are two periods when changes did occur in the TOR analysis with no evident discontinuities. One was a minor change to the calibration procedure in 2009, and the second was the introduction of a new model of TOR analyzer in 2016. Consequently, not all changes to the TOR analysis result in discontinuities in the time series.

Potential Biases in LAC Trends due to Misapportionment of Charred Carbon to OC

The pyrolyzed carbon (OP) from the TOR analysis is assumed to be equivalent to the fraction of OC pyrolyzed during heating. However, due to the violation of the TOR assumptions the OP fraction may overestimate the OP and be a mix of OC and LAC resulting in an underestimation in LAC. Through a series of regression analyses on the IMPROVE data, Malm et al. (2020)

investigated the potential for a systematic underestimation of LAC due to an overestimation of OP in the IMPROVE TOR data. Results from this analysis are shown in Figure 9 where the average fraction of OP that is LAC and its uncertainty are plotted for eight regions of the United States averaged over 2006–2017. Error bars reflect the standard error of the analysis. On average, within the uncertainty of estimated values, the fraction of LAC in OP across the United States is 25–40%. The estimated fraction for the eastern United States is highest at 42% and has the least uncertainty at about ±0.01. Generally, the fraction of LAC in OP has decreased over the 2006–2017 timeframe by about 25% except in the central United States, Northwest, and Southwest regions where it has remained constant. The average fraction of OP that is LAC over the entire continental United States (CONUS) was estimated to be 34%±0.05 (Malm et al., 2020).

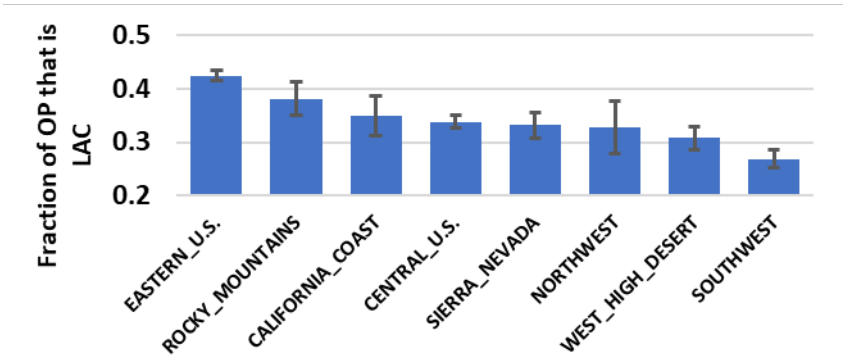

Figure 9. Regional annual average fraction of OP that is LAC for 2006–2017. Error bars are the standard errors of the analysis.

Chow et al. (2004) put forth an alternative method for estimating LAC and OP from the optical transmittance measurements (LAC_o and OP_o, respectively) that is independent of the TOR-derived LAC and OP. Specifically, they assumed that

$$[Carbon\ after\ O_2] = [LAC] + [OP] = \frac{\tau_{a,LACo}}{MAE_{LAC_o}} + \frac{\tau_{a,OPo}}{MAE_{OP_o}} \qquad (4)$$

where [LAC] and [OP] are the mass concentrations of light absorbing and charred carbon, respectively, as determined by TOR; LAC_o and OP_o refer to optically derived LAC and OP; MAE_{LAC_o} and MAE_{OP_o} are the MAEs of LAC_o and OP_o, respectively; and $\tau_{a,LACo}$ and $\tau_{a,OPo}$ are the attenuation of light or optical depth due to [LAC_o] and [OP_o], respectively.

[LAC] and [OP] are measured in the thermal analysis, and $\tau_{a,LACo}$ and $\tau_{a,OPo}$ are estimated from the measured initial (T_i), final (T_f), and minimum (T_m) transmittance values using

$$\tau_{a,LACo} = -ln\left(\frac{T_i}{T_f}\right);\ \tau_{a,OPo} = -ln\left(\frac{T_m}{T_i}\right). \qquad (5)$$

The MAEs are unknown. However, under the assumption that the MAEs are reasonably constant, Chow et al. (2004) used linear regression to estimate the MAEs and thus the [LAC_o] and [OP_o] concentrations. In this work, a similar regression analysis was conducted using IMPROVE data for each year from 2006 to 2017 and each region defined in Figure 9 to estimate the regional annual average LAC_o. In Figure 10, these average optically derived LAC_o concentrations are compared to the corresponding corrected LAC (CLAC) values, which were calculated by adding the fraction of OP that is LAC to the reported LAC concentrations. As shown, the agreement between the two variables is surprisingly good, with an ordinary least

squares (OLS) slope of 1.01±0.04 and an $R^2 = 0.83$, further suggesting that reported LAC concentrations obtained using TOR are an underestimate of true concentrations by about 60%.

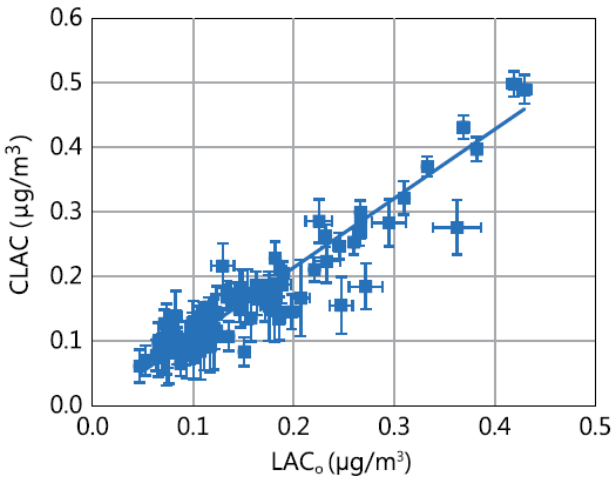

Figure 10. Regional annual average LAC derived from the optical thickness plotted against the corrected LAC (CLAC) derived from the corrected OP. Each data point is an annual average for all sites in one of the eight regions.

Suitability of TOR for Long-term Monitoring Networks.

The long history of measurement of OC and LAC by TOR in the IMPROVE, CSN, and other networks is evidence of the ability of TOR to be implemented in rural and urban monitoring programs. The TOR OC and LAC data have proven to be good surrogates for organic mass and LAC used to understand the composition of $PM_{2.5}$ and its trends. In addition, they can be related to light scattering and absorption, thus meeting the needs and goals of the IMPROVE program and its support of the RHR. TOR TC can also be calibrated, is operationally independent, has reasonable precision, and is thus suitable for tracking long-term trends.

The TOR approach has several drawbacks for use in long-term monitoring programs. First, TOR OC and LAC are not fundamentally calibrated, and the split of TC into OC and LAC is dependent on the instrument protocol. The underlying assumptions in the OC–LAC split are often not met, and the split can depend on the composition of the particulate sample. The sensitivity of the TOR OC–LAC split to instrument protocols and aerosol composition introduces the possibility of discontinuities in the time series as instruments and analytical protocols change. Drifts in the OC–LAC split can also occur due to changes in aerosol composition and unknown drifts in the instruments, e.g., as the instrument ages. This complicates the assessment of spatial and temporal patterns and trends and their causes. These potential issues mostly affect the LAC fraction, since in the IMPROVE network, LAC is generally a small fraction of TC, typically 10–15%; thus it is more sensitive to small changes in the TOR OC–LAC split than the OC fraction. LAC also has a significant fraction of concentrations below the LQL, with as much as 90% of the data below the LQL at some IMPROVE sites. Finally, using TOR to measure OC and LAC is a relatively expensive measurement when compared to some other options.

Fourier Transform Infrared Spectroscopy (FTIR) to Estimate OC and LAC

FTIR has been investigated as an alternative for quantification of TOR OC and LAC concentrations (Ruthenburg et al., 2014; Dillner and Takahama, 2015a,b; Debus et al., 2019; Takahama et al., 2019). FTIR measures the absorbance of inorganic and organic aerosols

collected on filters in the mid-infrared (IR) range, 2500–25,000 nm or 4000–400 cm^{-1}. The frequency-dependent absorption in the mid-IR range induces changes in the dipole moment of molecular bonds of functional groups such as aliphatic and aromatic CH, carbonyl (CDO), alcohol OH (C-OH), carboxylic acid OH (C-OH), and others (Blando et al., 2001; Maria et al., 2003; Coury and Dillner, 2008). The amount of light absorbed in specific regions of the spectrum is proportional to the quantity of the functional group, and it has been found that even in complex mixtures, organic functional groups can be quantified (Reff et al., 2007; Coury and Dillner, 2008; Russell et al., 2011; Takahama et al., 2013; Ruthenburg et al., 2014).

There are two methods for calibrating the FTIR spectra to estimate the concentrations of particulate compounds (Figure 11) (Dillner and Takahama, 2015a; Takahama et al., 2019). The traditional approach is to develop laboratory standards to build semiempirical calibration models for individual functional groups present in a mixture. The observed absorption is then related to the reference measurements. This has been used to measure nitrate and sulfate salts (Pollard et al., 1990) and organic functional groups (e.g., Coury and Dillner, 2008; Russell et al., 2011) from filter deposits. The primary issue with this approach is that OC and OMC are often underestimated with typical recoveries from 70% to 100% (Takahama et al., 2019). This bias results from a number of issues. One is that the carbonaceous aerosol can contain nonfunctionalized carbon, which is not measured by FTIR. Also, a functional group is composed of multiple compounds with different numbers of carbon atoms, and it is challenging to scale the results from the simple compounds used in the calibration to the complex atmospheric compounds (Takahama et al., 2019). The benefits of this method are the information on the composition of the aerosol as well as an estimation of organic mass as opposed to only OC.

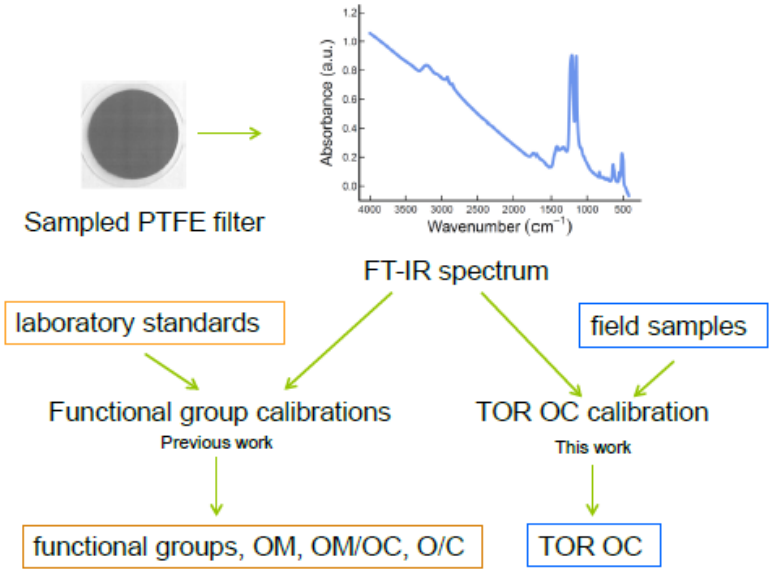

Figure 11. FTIR absorbance spectra from PM collected on Teflon (PTFE) filters can be used for measuring OM, OM/OC, organic functional groups, and TOR OC.

An alternative approach to the lab-generated references is to use collocated field samples to calibrate the FTIR spectra to complex mixtures of carbonaceous aerosol with known OC and LAC concentrations (Figure 11). The benefits of this data-driven calibration model are that it

does not rely on expensive or difficult to obtain standards, it can encompass the complex composition of carbonaceous aerosols, and it should not suffer from systematic biases.

Significant effort has been expended in developing data-driven calibration models and procedures for estimating TOR equivalent OC and LAC in the IMROVE and CSN networks using FTIR analysis of the Teflon filter deposits (Ruthenburg et al., 2014; Dillner and Takahama, 2015a,b; Debus et al., 2019; Takahama et al., 2019). The concept was to develop calibration models from TOR data measured at a small subset of sites in the monitoring program with errors on the order of those measured by TOR. The method is based on the linear equation

$$m_{c,i} = \sum_j b_j A_{i,j} + e_i \quad (6)$$

where $m_{c,i}$ is the concentration of OC or LAC for sample i, $A_{i,j}$ is the FTIR-measured absorbance for sample i at wavelength j, b_j is the calibration coefficient for wavelength j, and e_i is the error for sample i.

Given a series of samples analyzed by TOR and FTIR, equation 6 is inverted to estimate the calibration coefficients *b* for OC and LAC. Equation 6 is an ill-posed inverse problem, and solutions using standard linear regression methods can result in highly unstable coefficients with large positive and negative values. To avoid this, partial least squares (PLS) regression was used (Dillner and Takahama, 2015a). In PLS, the matrix of spectra is decomposed into a product of orthogonal factors (loadings) and their respective contributions (scores); observed variations in the OC mass are reconstructed through a combination of these factors and a set of weights simultaneously developed to relate features in the dependent and independent variables. Candidate models for calibration are generated by varying the number of factors used to represent the matrix of spectra.

The calibration coefficients *b* resulting from the inversion of equation 6 are then used on FTIR spectra from other filters to estimate the OC and LAC concentrations. The errors in the resulting OC and LAC concentrations are dependent on the distribution of carbonaceous aerosol compounds in the dataset used in the calibration (Debus et al., 2019; Takahama et al., 2019). It was found that if data with consistently low or high concentrations were used in the calibration, then the estimated OC and LAC data were biased. In addition, ammonium interferes with the IR absorption of some organic functional groups and the calibration dataset needed to contain the distribution of the ammonium to carbon ratios in the data to be derived (Dillner and Takahama, 2015a). Also, some carbonaceous aerosol compositions are unique and not well reproducible using general calibration models. For example, it was found that samples heavily influenced by biomass burning smoke and fresh mobile sources needed specific calibration models to estimate OC and LAC with acceptable uncertainty (Weakley et al., 2018).

To identify a suitable subset of sites with the appropriate distribution of concentrations and compositions, a Gaussian mixture model was used to cluster the sites (Debus et al., 2019). The application of the method to IMPROVE data resulted in 21 clusters from which data from individual sites were selected. Three urban sites broke into separate clusters. Due to the unique nature of the biomass burning smoke influence on filters, these filters were removed from the calibration dataset and used in a separate biomass burning calibration. This process resulted in two sets of calibration coefficients, one for smoke-impacted filters and another for non-smoke-impacted (global) filters. A method was developed to identify smoke-impacted filters, and the appropriate calibration was applied to a given FTIR spectrum to estimate the OC and LAC concentrations.

Figure 12 compares predicted FTIR OC to measured TOR OC for all 2015 data, and performance statistics are in Table 1. This includes the data used in the initial calibration (~13%) and all other data (~87%). Smoke-impacted samples are excluded from the comparison. As shown, the comparison is very good with errors of 12.5% and 27.1% for OC and LAC, respectively, which are similar to TOR OC and LAC errors found in collocated data (Hyslop and White, 2008). Similar results were found for the combined global and smoke-impacted filters for 2015–2018.

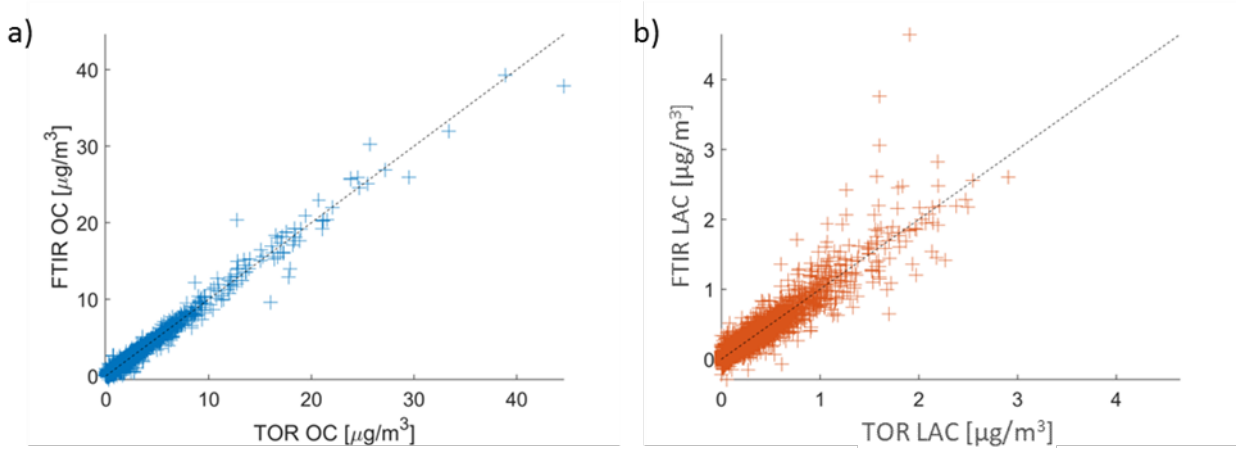

Figure 12. a) FTIR OC and b) FTIR LAC predicted concentrations achieved by the global model regressed against the corresponding TOR values. Predicted concentrations from both calibration and test samples from 2015 (n = 19,609) are shown (Debus et al., 2020).

Table 1. FTIR OC and LAC prediction performance for the global model, i.e., non-smoke-impacted samples in 2015. Reported metrics include both calibration and test samples (Debus et al., 2020).

	R^2	Bias [μg/m^3]	Bias [%]	Error [μg/m^3]	Error [%]	MDL [μg/m^3]	< MDL [%]	Precision [μg/m^3]
OC	0.979	0.01	1.7	0.08	12.5	0.06	0.4	0.08[a]
LAC	0.882	0.003	3.8	0.02	27.1	0.03	12.9	0.02[a]

[a] Precision was computed from the 538 parallel PTFE filters sampled at Mesa Verde National Park (CO), Phoenix (AZ), Proctor Maple Research Center (VT), Saint Marks (FL), and Yosemite National Park (CA) sites equipped with a collocated sampler.

The use of FTIR spectra calibrated to a subset of TOR OC and LAC data to estimate OC and LAC across the IMPROVE and CSN programs has several important advantages. First, provided a suitable calibration dataset is available, the method can generally reproduce TOR OC and LAC within the errors of the TOR data, and this method would maintain the current TOR data record. FTIR is a nondestructive analysis on the Teflon filter and is not directly dependent on carbon artifact corrections. However, it is indirectly dependent on the artifact correction in the TOR data. The FTIR spectra provide valuable information on the composition, origin, and history of the carbonaceous aerosols and could be used to estimate the organic mass and oxygen to carbon ratios. Last, it is a more cost-effective methodology than TOR analysis alone, in part because it can use Teflon filters.

There are also important disadvantages. First, the method is not fundamentally calibrated, and by calibrating to TOR OC and LAC, this method has all of the disadvantages of TOR as previously discussed. In addition, there is not a single universal set of calibration coefficients but at least two sets that are needed for smoke- and non-smoke-impacted filters typically

collected in the IMPROVE network. Samples heavily influenced by mobile sources are also unique, and FTIR-derived OC and LAC have large errors in those circumstances. This creates potential complications as new sites, such as international sites, are established that are impacted by unique sets of sources. Last, the method is dependent on a linear regression and will suffer from biases inherent in regression models. For example, it has been shown that FTIR estimates of LAC concentrations below the LQL are significantly overestimated. This exacerbates the apparent overestimation of these low concentrations by the TOR system (see discussion associated with Figure 16).

Suitability of FTIR-derived OC and LAC for Long-term Monitoring Networks.

OC and LAC concentrations derived by calibrating FTIR data to TOR data have been shown to be near equivalent to TOR OC and LAC. Therefore, FTIR has the same advantages as TOR in that it meets the objectives of the IMPROVE monitoring program. The method also has the same drawback as TOR in that a large fraction of LAC concentrations are below the LQL and low concentrations are likely biased high. The calibration of the FTIR spectra to TOR OC and LAC concentrations is also dependent on the composition of the carbonaceous aerosols, and a single calibration model cannot be used for all samples. Instead, multiple calibration models are needed to account for aged aerosols typically measured in the IMPROVE program, samples heavily impacted by smoke, and samples impacted by mobile sources.

The FTIR method for deriving OC and LAC has two important advantages compared to TOR. First, it should be a more cost-effective option for measuring OC and LAC concentrations. Second, FTIR provides additional information on the composition of the carbonaceous aerosols. This information has been used to assess contributions of biomass burning to carbonaceous aerosols and to estimate the organic mass concentration. This is important information for understanding the contributions of organics to fine particulate carbon and its radiative properties. On the other hand, FTIR has large errors for PM10 samples and cannot be used to assess carbonaceous aerosols in the coarse PM fraction since PM10 samples are not routinely analyzed by TOR.

TC and fabs to Estimate OC and LAC

Alternative OC and LAC concentration estimates can be derived from a measure of TC and an estimate of ambient absorption. Just as LAC is used in the RHR and other analyses to estimate light absorption, light absorption can be used to estimate LAC. Given TC and LAC, OC can be derived by the difference of the two. Most any TOA analysis can be used to estimate TC, and in IMPROVE and the CSN the absorption of the particle deposit on an exposed filter, i.e., fabs, is measured using a HIPS method. The following sections discuss the practicality and issues in using TC and fabs to estimate OC and LAC.

Total Carbon Measured using Thermal Approaches

TC can be measured by thermal approaches as either a product of thermal-optical methods that measure OC and LAC, e.g., IMPROVE TOR, or as an independent thermal measurement that does not bifurcate the carbon into different fractions (Rigler et al., 2020). The latter approach does not necessarily require an inert environment heating phase, calibrated temperature ramps, or optical corrections. However, it is a destructive analysis method using quartz fiber filters that require positive artifact corrections. These corrections increase the quantifiable limits and errors of the TC concentrations.

Carbonate compounds, e.g. calcium carbonate, can volatilize when heated contributing to the measured TC by thermal approaches and biasing the TC concentrations. In TOR carbonate carbon may be measured as either OC or EC depending on the carbonate compound and its thermal decomposition temperatures. Acid pretreatment of filter samples can eliminate the carbonate interference (Novakov, 1982) and carbonate carbon can be determined by measuring the CO_2 evolved upon acidification. Carbonate carbon has been found at only a few IMPROVE monitoring sites, and the levels at these sites do not appreciably the TC concentrations (Chow et al., 2001; Chow and Watson, 2002).

TC instruments can be calibrated to standards including atmospherically relevant standards such as NIST reference material 8785 (Klouda et al., 2005). This helps to make the measurements independent of operational protocols and reproducible across different methods and protocols (Schmid et al., 2001; Chow et al., 2004; Baumgardner et al., 2012). TC data have similar to better precision than TOR OC with higher fractions above the quantifiable limits than TOA-derived LAC and OC. For example, using the 2017–2019 IMPROVE data, 20% of the TC concentrations were less than the LQL compared to 23% and 30% for OC and LAC, respectively. Also, the median relative error was 11% compared to 12% and 16% for OC and LAC, respectively. These qualities of the TC measurement make it suitable for implementation into monitoring programs such as IMPROVE and the CSN.

Filter Absorption Measurements as a Surrogate for LAC

Filter absorption has been measured from the $PM_{2.5}$ Teflon filter in the IMPROVE program using the HIPS method since 1994 (Figure 13). In HIPS both the transmittance (t) and reflectance (r) of a 633nm laser light illuminating the backside of the filter are measured. White et al. (2016) developed a calibration method based on fundamental principles where the HIPS t and r are calibrated such that their sum for clean filters equals 1. Unexposed field and lab blanks are used for the clean filters (Figure 13). Filter absorption is calculated as

$$fabs = \frac{f}{V} * \tau_{abs} = \frac{f}{V} \ln\left(\frac{1-r}{t}\right) \quad (7)$$

where f is the area of the sample deposit, V is the volume of air sampled, and τ_{abs} is the absorption optical depth. The fabs measurements are not equivalent to ambient absorption (babs). This is partly due to potential changes in the aerosols' absorbing properties after they are deposited on a filter. Also, the illumination of the aerosol in the atmosphere is columnar, while the HIPS calibration model approximated the illumination as diffuse, which would yield twice the effective path length and resulting optical depth. Actual sample illumination is anisotropic and $1 \leq fabs/babs \leq 2$.

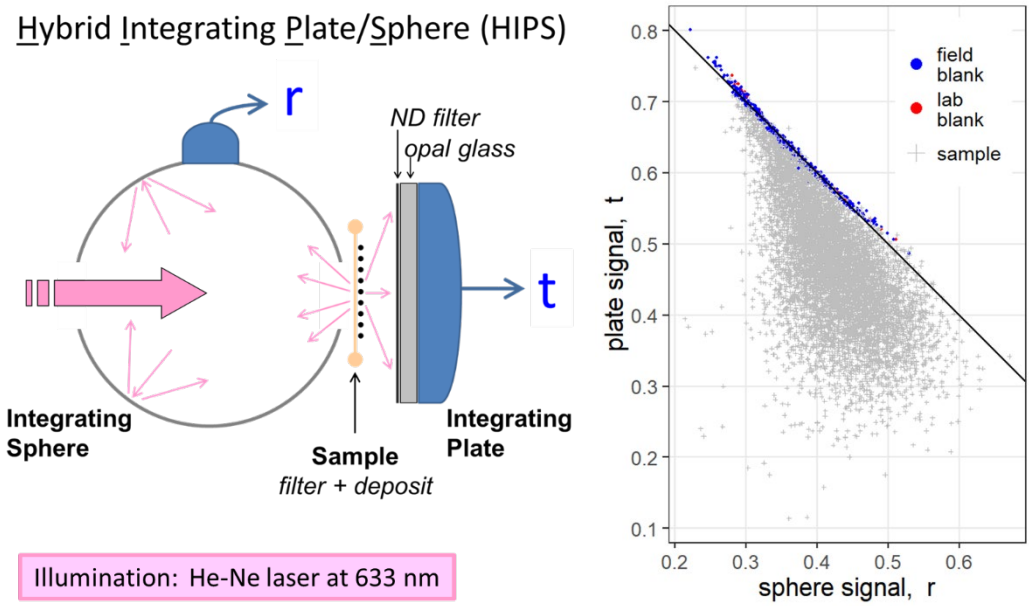

Figure 13. (Left) Schematic configuration of the HIPS system. Filters are oriented with sample deposit toward the plate. Output signals r and t are directly proportional to the illumination power reaching each detector. (Right) HIPS r and t signals for clean filters, i.e., field and lab blanks and sampled filters (White et al., 2016, 2019).

Calibrating the system to blank filters has the advantage that the system is demonstrably well calibrated at zero absorption and should not suffer from biases at low values. The measurement of both r and t accounts for changes in filter scattering properties. However, it was found that filters with significantly different light scattering properties require a separate calibration (White, personal communication, 2021). Consequently, filter acceptance testing is important to ensure the calibration is applicable to a given filter batch. HIPS is not a fully calibrated system since reference standards with known absorbing properties are not used in the calibration. However, there has been adequate theoretical and empirical evidence for the linearity of the response of HIPS to absorbing PM in lightly loaded samples (White et al., 2016). As discussed below, fabs is underestimated in heavily loaded filters.

In 2018 a new HIPS system was developed and incorporated into the IMPROVE monitoring program. The new HIPS instrument was used to reanalyze filters from four IMPROVE sites from 2003 through 2017 (White et al., 2019). The multiyear reanalysis fabs data are compared to the original fabs values in Figure 14. As shown in the scatter plots, there is very good correspondence between the two measurements, indicating that the fabs measurement is not instrument dependent; there was no instrument drift; and the filter absorption characteristics of the collected aerosols have remained stable over the 15-year period. The stability of the measurement is further illustrated by the fact that there is no long-term trend in the difference between the original and reanalyzed data (Figure 14). Data prior to 2003 were not included in the analysis because field blanks for these data were not available, and so these data could not be properly calibrated. Though not evident in Figure 14, the fabs data from the new HIPS system were on average 5% higher than the original system. The cause of this difference is not known, but this difference can be corrected for when combining data across the different instruments and it is recommended to increase the fabs prior to 2018 by 5%.

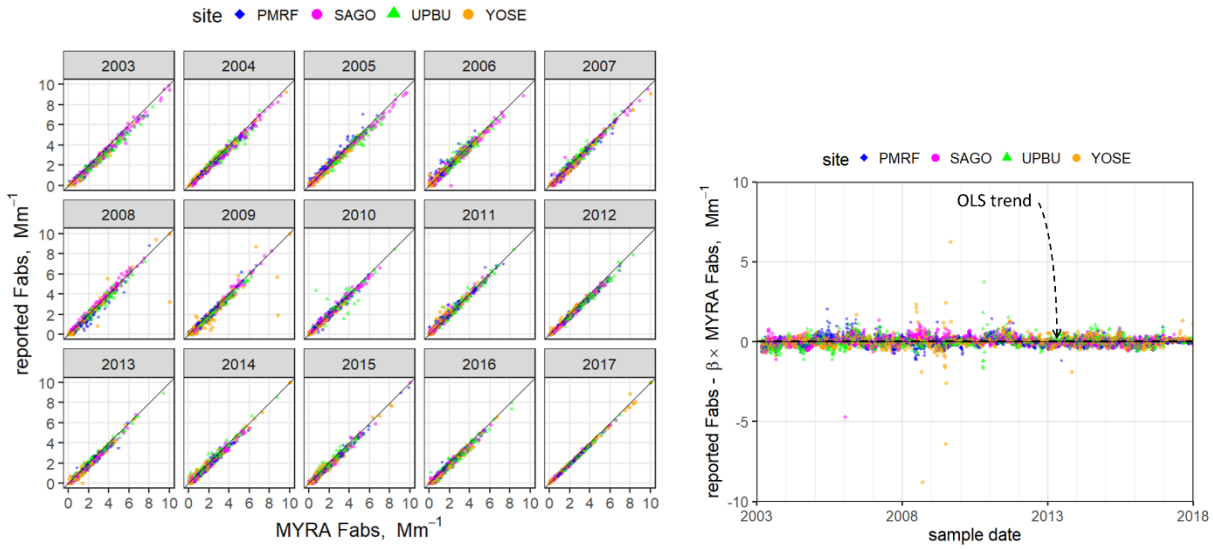

Figure 14 (White et al., 2019). (Left) Comparison of fabs measured using HIPS on filter samples from four IMPROVE sites from 2003 to 2017 to the reanalysis of the same filter samples by a new HIPS system in 2018. Straight line is the one-to-one line. (Right) Differences between originally reported fabs and the reanalysis. Dashed line corresponds to the OLS trend line. Sites include Procter Maple R.F., VT (PMRF); San Gorgonio, CA (SAGO); Upper Buffalo, AR (UPBU); and Yosemite, CA (YOSE).

As shown in Figure 15, about a third of the fabs values measured in 2017–2019 are below the LQL of 3 × MDL. This is a large fraction and somewhat larger than found for LAC in Figure 6. However, as shown in Figures 6 and 15, the uncertainty of the fabs data is smaller than for the LAC data even at values below the quantifiable limit, and 15% of the fabs and LAC data have values less than the uncertainty. The uncertainties for both fabs and LAC are calculated as $\sqrt{0.6 * MDL^2 + precision^2}$ where the precision is derived from collocated data and the MDL from field blanks (Hyslop and White, 2008). LAC and fabs have similar MDLs, but the fabs precision is smaller at 6% compared to 14% for LAC. This results in 50% of the fabs values being more than 9 times larger than the uncertainty (Figure 15), whereas 50% of the LAC values are 6 times larger than the uncertainty (Figure 6).

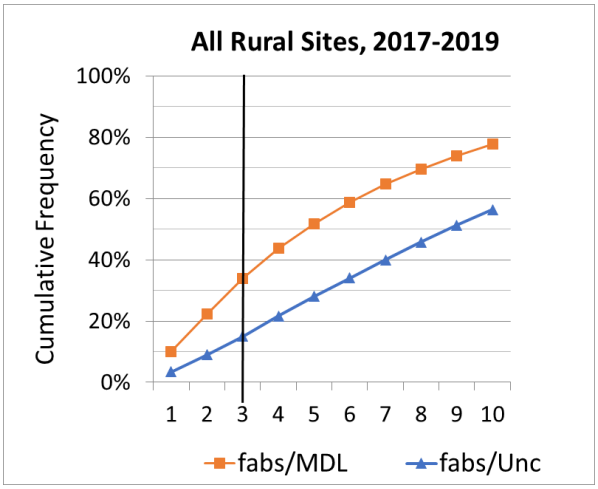

Figure 15. Cumulative frequency distribution of the ratio of fabs/MDL and fabs/uncertainty for data from all IMPROVE rural sites measured in 2017–2019. Vertical line denotes the LQL.

The HIPS instrument is essentially calibrated to zero absorption. Therefore, the variability in the filter blanks will create large errors in the fabs values below the quantifiable limit, but they should not be biased. As previously discussed, low-temperature TOAs such as IMPROVE TOR can result in OC slip, i.e., misapportioned OC into the LAC fraction. This misapportionment would be most apparent at low LAC concentrations where the optical correction could not counter the misapportionment. Figure 16 plots the ratio of the TOR LAC to fabs values for three time periods against the filter absorption optical depth τ_{abs} (equation 3). As shown, the ratio is relatively constant across the range of τ_{abs}, but below τ_{abs} = 0.1, the ratio increases by a factor of 2. At low τ_{abs}, the LAC concentrations will also be low. It is unlikely that such a change is due to atmospheric changes in the aerosol absorption properties and is indicative of low LAC concentrations being biased high. Also evident in Figure 16 is an increase in the LAC/fabs ratio at high τ_{abs}. This is thought to be at least partly due to the fabs being biased low due to a filter loading effect, which is discussed below.

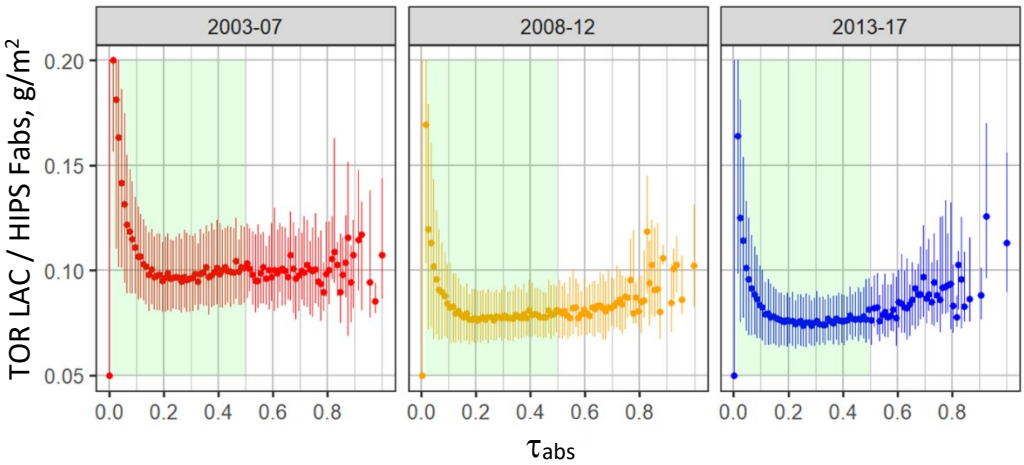

Figure 16. Ratio of TOR LAC to HIPS fabs vs. the absorption optical depth, τ_{abs}, for three time periods, 2003–2007, 2008–2012, and 2013–2017. Data from all IMPROVE sites with at least 50 samples were used. τ_{abs} values less than 0.5 are shaded in green. (White 2020, personal communication)

HIPS Issues

Filter Loading Artifact

Filter absorption measurements made using transmission-based instruments can suffer from filter loading artifacts. Absorbing particles on filters with heavy deposits can "shadow" other absorbing particles, while scattering particles can increase the reflectance of incident light. Both effects would cause an underestimation in the fabs measurement. On the other hand, increased light scattering by particles could increase the absorption by LAC. These are well-known artifacts (e.g., Bond et al., 1999) and various methods are used to reduce them. The measurement of both reflectance and transmittance by HIPS does reduce, but not eliminate, these effects (Bond et al., 1999).

White et al. (2020) assessed the potential loading artifacts on the HIPS measurement. In one assessment they compared fabs measured on collocated IMPROVE and CSN samplers. CSN samplers use a larger filter and lower flow rate than IMPROVE, and the resulting filter deposits are more than a factor of 10 lower in mass. The ratio of the CSN to IMPROVE fabs data as a function of IMPROVE τ_{abs} is presented in Figure 17. As shown, at τ_{abs} below 0.5, the ratios are mostly scattered around the one-to-one line, indicating no bias in either measurement.

However, at τ_{abs} above 0.5 there is a decreasing trend in the ratio. This trend indicates that the more heavily loaded IMPROVE filters have a negative loading artifact, and fabs data at $\tau_{abs} \sim 1$ are underestimated by more than 30%. These results are counter to tests with absorbing gels layers (White et al., 2016) and uniformly deposited layers of soot on Teflon filters, both of which showed no evidence of filter loading artifacts. This discrepancy is under investigation.

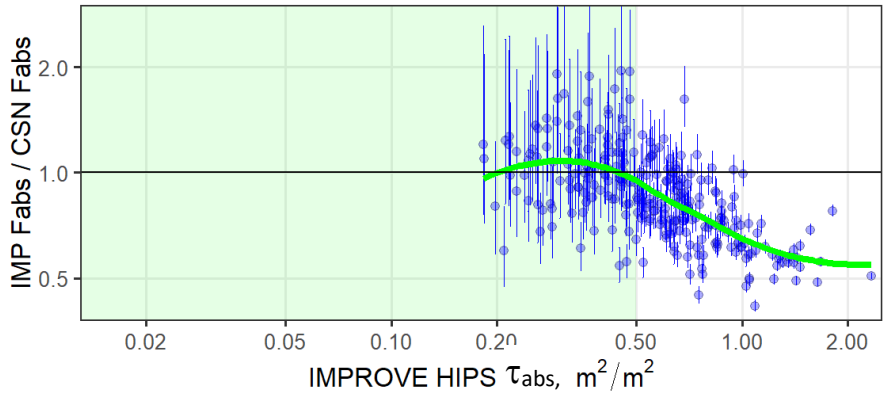

Figure 17. Ratio of fabs measured from collocated IMPROVE and CSN samplers as a function of the absorption optical depth (τ_{abs}) measured on the IMPROVE filters. The trend in the data is visualized by the green smooth curve, which is an unweighted fit by the LOESS function from the R STATS package. τ_{abs} less than 0.5 is shaded in green. (White 2020, personal communication)

Contributions of Fine Dust to Filter Absorption

Fine mineral dust containing Fe oxides is known to absorb in the visible spectrum, with "blue" light being absorbed preferentially over "red" light, hence the red color of Fe oxides (Alfaro et al., 2004; Moosmuller et al. 2012). Therefore, it is expected that fabs, a measure of absorption by all aerosols collected on a Teflon filter, will have contributions from Fe oxides in addition to LAC. Figure 18 is a scatter plot of fabs/BC (BC is defined in equation 3) versus density of Fe measured by x-ray fluorescence of filter substrates expressed as g/m^2 for 2007–2016. The orange-filled circles represent those filters that are visually identified as being red after the TOR analysis, presumably because of a higher content of Fe oxide. Because Fe does not evolve over the temperature range used during the TOR analysis, the BC is not expected to depend on the absorption by Fe oxides. Therefore, ratios of fabs/TOA_BC > 1 reflect enhanced fabs absorption due to soil particles. As shown, for each year from 2007 through 2016, the fabs/BC ratios increased for those filters that were identified as red and had elevated Fe concentrations, a clear indication of absorption by fine soil.

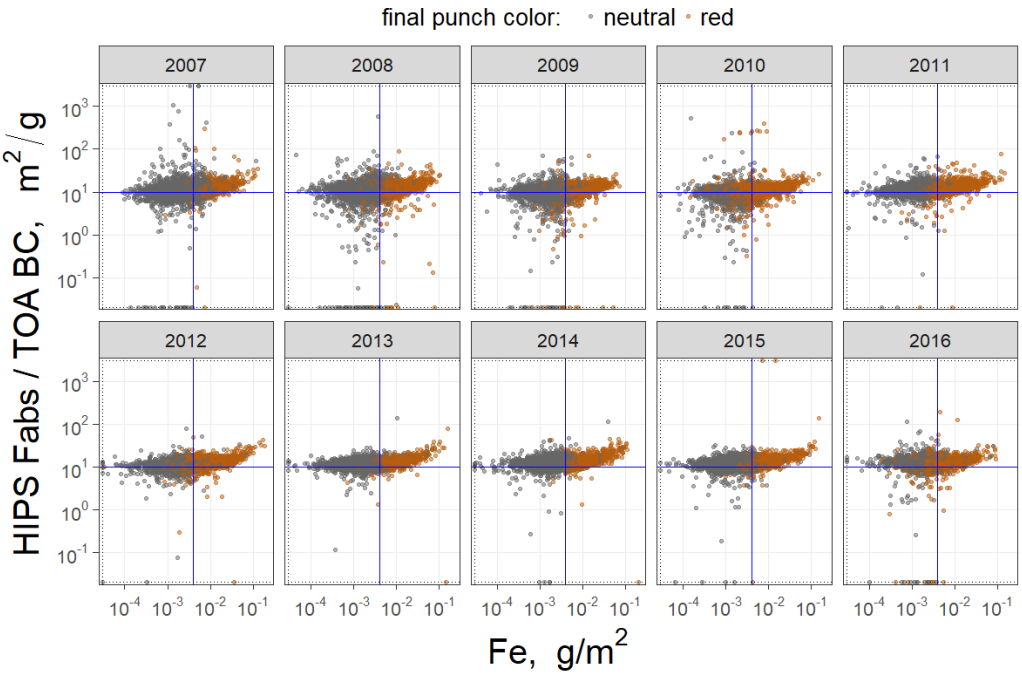

Figure 18 (White, 2017). Ratio of fabs to TOA BC, defined in equation 3, scattered against the Fe filter density for IMPROVE samples for each year from 2007 to 2016. Rust-colored data points signify filter punches with a reddish hue after the TOA analysis. Horizontal blue line is at 10, and vertical line is at 0.005 g/m^2 Fe, the approximate density when filters appeared red. Samples with TC < 1 µg/m^3 were excluded from the analysis.

Comparison of HIPS fabs to TOR LAC Concentrations

The ability of the HIPS fabs data to reproduce the spatial and temporal trends in TOR LAC data is explored in Figure 19, which shows the deseasonalized, long-term daily network median of LAC/TC, fabs/14/TC, and fabs/LAC ratios across the IMPROVE monitoring network. The LAC/TC ratios are the same as those in Figure 8. In Figure 19a fabs was divided by 14 to scale it to LAC. As shown, after 2008 the network-wide trends in fabs/14/TC ratios are similar to LAC/TC ratios, resulting in relatively flat fabs/LAC ratios from 2008 to 2017. Prior to 2008, the two time series differ. There are no trends in fabs/TC data from 2003 to 2008, but the LAC/TC ratios show an initial increase followed by a 25% decrease from 2005 to 2008, which is also reflected in the fabs/LAC ratios. The data in Figure 19 are across the entire IMPROVE monitoring network, and the set of sites with valid data can vary by the sample day and year. However, as shown in Figure 20a, similar differences are evident in the annual average LAC and fabs/12 data in eight regions across the United States where the same set of sites were used in each region across all years.

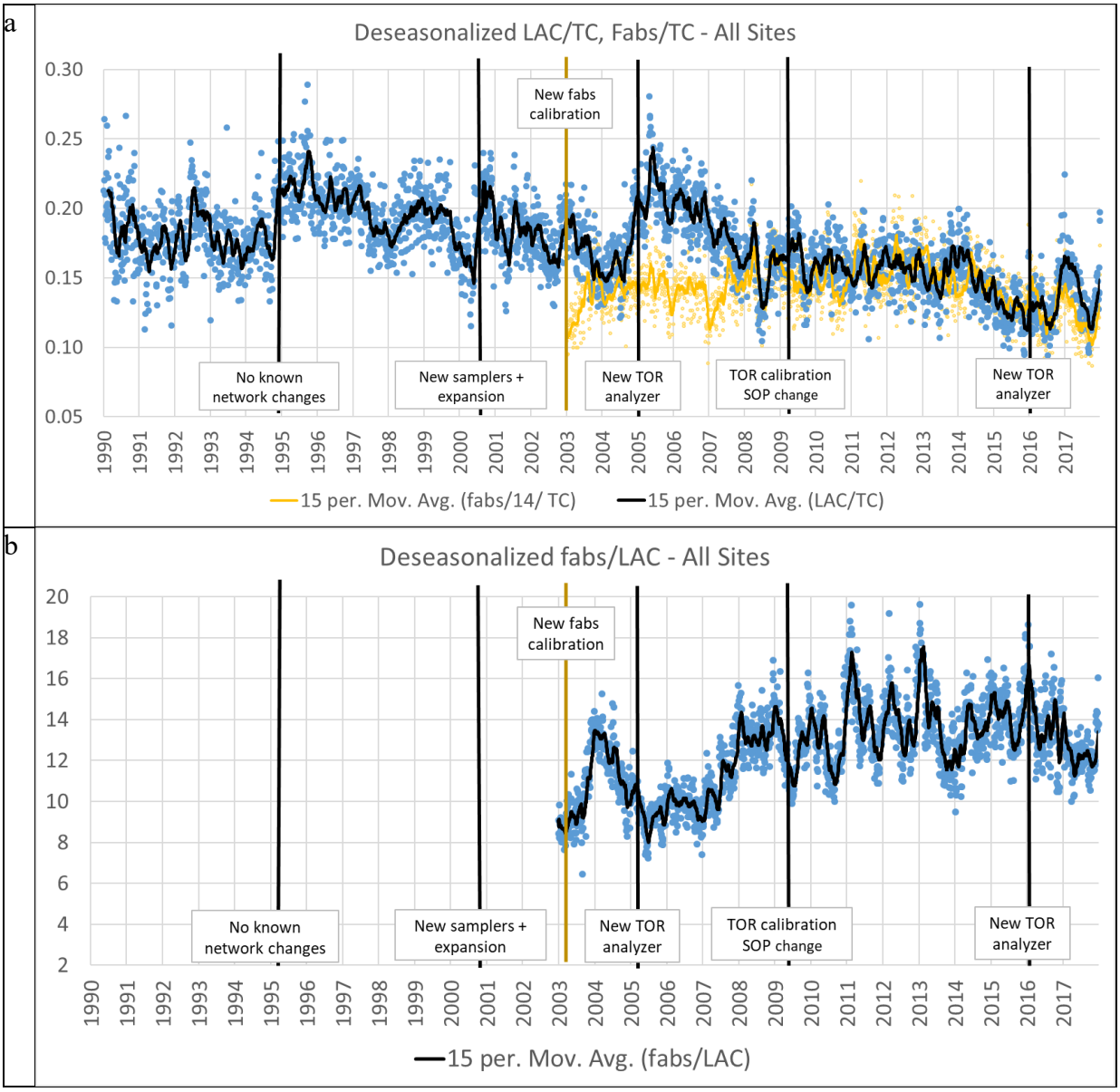

Figure 19. (a) Deseasonalized daily network medians of LAC/TC (black) and (fabs/14)/TC (yellow) and (b) fabs/LAC from the IMPROVE monitoring network from 1990 to 2018. Each circle is the median of all 24-h LAC/TC or (fabs/14)/TC ratios measured in the IMPROVE program on the given sample day. Solid line is a 15-point moving average of these daily data. Data were deseasonalized using the same method as in Figure 8.

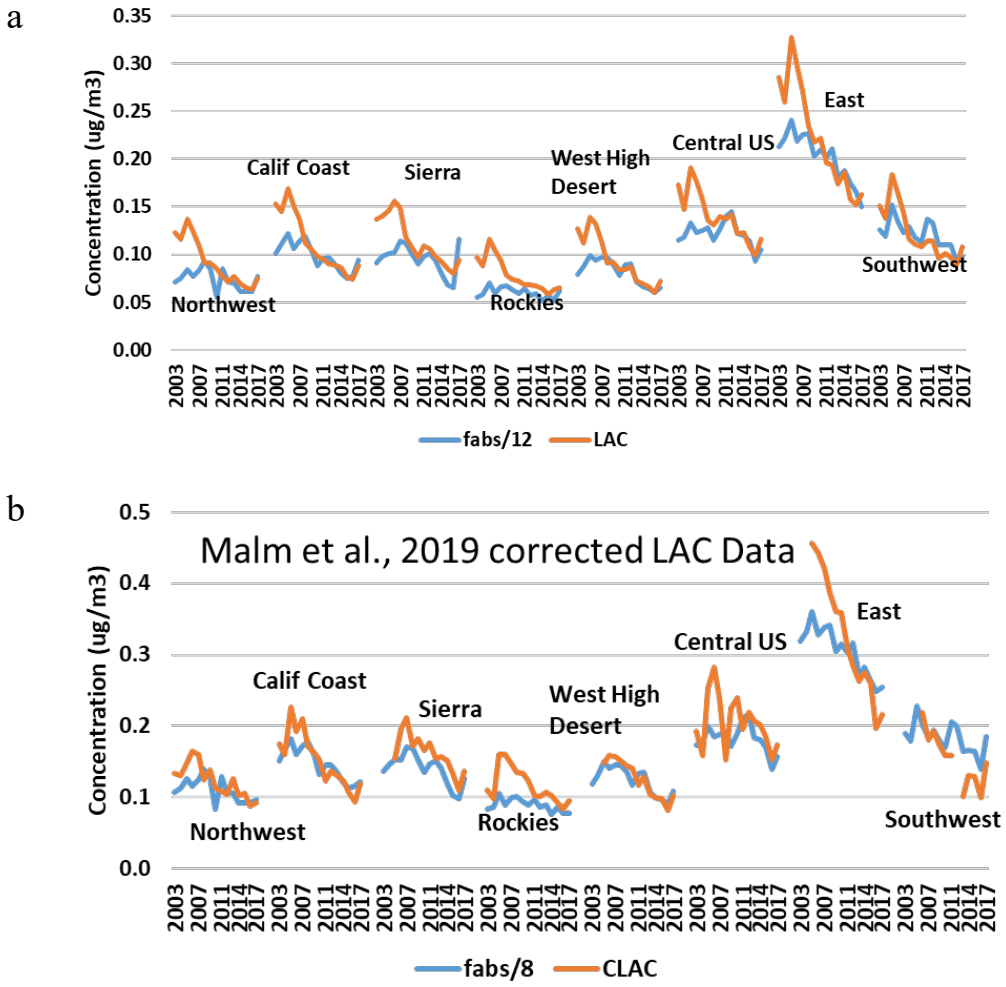

Figure 20. Timelines of IMPROVE regional and annual average (a) TOR LAC and fabs/12 data from 2003 to 2017 and (b) CLAC, i.e., LAC concentrations corrected for a bias in the bifurcation of the IMPROVE OC, and LAC concentrations using the method in Malm et al. (2020) and fabs/12.

The cause of the changes in the LAC/TC and fabs/LAC relationships around 2008 is not known. The ratio of fabs to LAC is an effective MAE and is dependent on the optical properties of the aerosols. There is a broad range of MAEs in the atmosphere, dependent on aerosol composition and atmospheric processing (Bond and Bergstrom, 2006), and MAEs will vary in space and time. However, it is unlikely that a change in the aerosol optical properties would occur across the entire IMPROVE network, as would be needed to explain the different trends in LAC/TC pre- and post-2008 in Figures 19 and 20a. The retrospective analyses of the IMPROVE Teflon filters by HIPS noted above demonstrate the reproducibility and precision of the fabs data, so a drift in the HIPS measurement would not explain the deviation. Such a retrospective analysis has not been done for TOR. It is also not currently possible to calibrate for the OC–LAC split in TOA methods, so instrument drift in the TOR analysis could be a cause for the change in the trends.

As explored by Malm et al. (2020) and discussed and demonstrated in Figures 9 and 10, it appears that TOR LAC is underestimated on average, and this underestimation varied in space and time with a long-term decreasing trend. Malm et al. (2020) developed an annual correction for the bias over different regions in the United States. Figure 20b compares the annual

corrected LAC (CLAC) to fabs/8. As shown, the difference in the concentrations from 2003 to 2008 in CLAC and fabs/8 was reduced in most regions compared to that in Figure 20a while maintaining the very good correspondence from 2008 to 2017. This is further evidence that the difference between the 2003–2008 LAC and fabs/12 values in Figure 20a is due to the TOR analysis and not due to changes in ambient aerosol absorption properties or HIPS measurements. The CLAC data derived by Malm et al. (2020) are coarse corrections to the TOR LAC data, meant to illustrate potential biases in the TOR LAC data record, and are not used in any further analyses.

Reproduction of TOR LAC from fabs Data

If filter absorption and TC measurements are used in lieu of the current TOR OC–LAC system, then it is necessary to be able to estimate LAC concentrations from fabs. Ambient LAC is a complex mixture of carbonaceous aerosols from near-elemental graphitic carbon to organic brown carbon, with MAEs dependent on the composition and morphology of the aerosols and the MAEs varying by more than a factor of 2. TOR LAC is an operationally defined PM constituent that is related to ambient LAC but dependent on the TOR method as well as the composition of the PM sample being analyzed. This relationship is complicated by the fact that TOR analysis of filter samples often violates some of the underlying assumptions for a valid OC–LAC split and the inability to calibrate the TOR analysis for OC and LAC. Based on statistical analyses of the IMPROVE data, it appears that on average the LAC is underestimated, and this bias varies in space and has a potential trend in time (Figure 20) (Malm et al., 2020). Consequently, the relationship of TOR-defined LAC and ambient LAC may also vary in space and time.

To maintain the long history of TOR OC and LAC data, it would be desirable to reproduce the TOR LAC using fabs data, which ideally would account for spatially and temporally variable MAEs as well as potential biases between ambient and TOR-derived concentrations. It may be possible to account for effects of constituents such as Fe oxides on TOR LAC and fabs but not potential instrument drift and effects of changing ambient concentrations and composition of PM. Consequently, relationships between fabs and LAC were sought that reproduced the IMPROVE LAC concentrations post-2008 when there was good correspondence between fabs and LAC (Figures 19 and 20). It is not possible to account for the TOR analytical issue or all of the spatial and temporal variability in the aerosol absorbing properties due to changing LAC compositions and atmospheric processing. Therefore, the developed relationships between fabs and LAC will not reproduce some of the historical trends and may not reproduce future TOR LAC trends. A detailed analysis of the relationship between fabs and TOR LAC is presented in Appendix A. In the next section is a summary of key findings.

Effect of Iron Oxides on TOR LAC and HIPS fabs

As shown in Figures 2 and 18, Fe in the filter samples has the apparent effect of increasing fabs measured by HIPS and decreasing derived LAC concentrations in TOR. Both increase the fabs/LAC ratio, and the effects of Fe need to be accounted for when estimating TOR LAC from an fabs measurement.

fabs can be related to LAC and Fe by

$$fabs_i = a_1 LAC_i + a_2 Fe_i \quad (8)$$

where i refers to the i^{th} sample, and a_1 and a_2 are the MAE efficiencies of LAC and Fe, respectively. The coefficients a_1 and a_2 can be found through linear regression models. LAC

concentrations on the average are more than an order of magnitude greater than Fe concentrations. To equalize their influence on the regression, equation 8 can be rearranged to

$$\frac{fabs_i}{LAC_i} = a_1 + a_2 \frac{Fe_i}{LAC_i} \quad (9)$$

Figure 21 presents the scatter plot of Fe/LAC against fabs/LAC using data from all IMPROVE sites in the mid-southeastern United States. As Fe/LAC increases, fabs/LAC also increases with an OLS regression line slope of 4.7 ± 0.05 and an intercept of 12.2 ± 0.08. Based on equation 9, this implies that the Fe MAE is 4.7 m^2/g and LAC MAE is 12.2 m^2/g at a wavelength of 633 nm. The Fe MAE is greater than those found in laboratory experiments on dust samples from the Gobi Desert, northern Sahara, and in the Sahel, which were ~0.56 m^2/g for Fe oxides or ~0.8 m^2/g for Fe (Alfaro et al., 2004). This supports the notion that the presence of Fe oxides in a filter sample analyzed by TOR reduced the measured LAC.

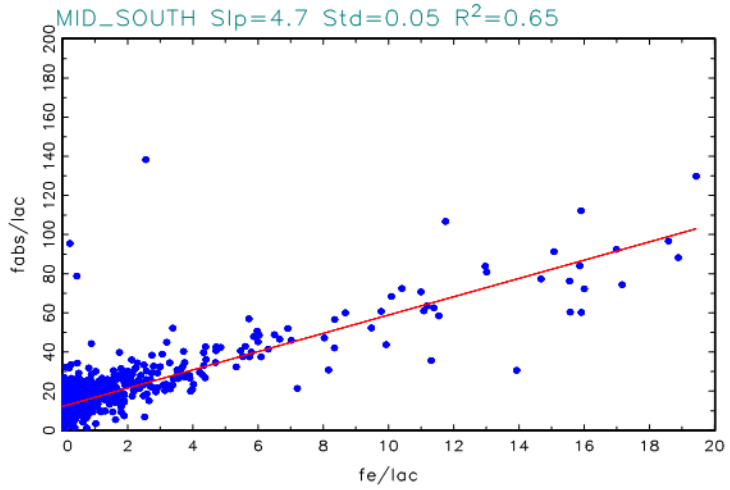

Figure 21. Scatter plot of the ratios of Fe/LAC against fabs/LAC for all IMPROVE sites in a region of the southeastern United States for 2008–2015.

A similar regression analysis was conducted for 23 regions across CONUS (Appendix A). The average Fe MAE was 4.8 ± 0.9 m^2/g. Based on these results, a corrected fabs (cfabs) is used in the following analysis and is defined as

$$cfabs = fabs - 5 \times Fe = LAC\_MAE \times LAC. \quad (10)$$

This corrected fabs accounts for both the contribution of Fe oxides to light absorption and the associated underestimation of LAC in TOR LAC for Fe oxides. The ratio of cfabs/LAC is then an estimate of the apparent filter LAC MAE.

Equation 10 implies a linear relationship between cfabs and LAC. As shown in Figure 22, there is a nonlinear relationship between the cfabs and LAC where cfabs decreases as a function of LAC. The data in Figure 22 are for all IMPROVE data measured at sites in the Ohio River valley region from 2008 through 2015. Similar relationships occurred in 23 regions throughout the United States, and it was found that on average cfabs in all regions could be explained well by the exponential function

$$cfabs = 13 \times (1 - e^{-LAC}) \quad (11)$$

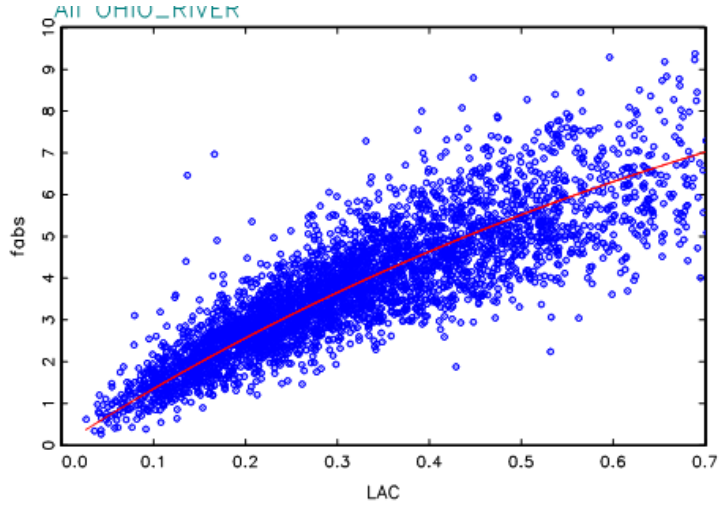

Figure 22. Scatter plot of the 24-h LAC concentrations and cfabs for all IMPROVE sites in the Ohio River valley region for 2008–2015. Red line is cfabs = 13.1 × (1 - e^{-LAC}) resulting from the exponential regression.

The overarching goal is to use measurements of fabs to derive an estimate of LAC concentrations measured using IMPROVE TOR analysis. LAC can be derived from fabs measurements by inverting equations 10 and 11 such that

$$LAC = cfabs/LAC\_MAE \quad (12)$$

$$LAC = -\ln(1 - cfabs/13). \quad (13)$$

Figure 23 plots the measured LAC against the cfabs for all IMPROVE sites using data from 2008 through 2018. To highlight the average pattern, these data were first rank ordered by the measured LAC, and every 50 data points were averaged together, resulting in about 3700 average values. Also plotted on Figure 23 are the predicted LAC from equations 12 and 13. In equation 12, LAC_MAE = 12 m^2/gm was used. As shown in Figure 23, the linear model reproduced the average LAC concentrations well for cfabs less than 5 Mm^{-1} but underestimates the LAC at higher cfabs due to the nonlinear relationship. The exponential model better reproduces the LAC at cfabs above 5 Mm^{-1} but then overestimates the LAC at cfabs above 8 Mm^{-1} where the relationship between LAC and cfabs becomes more linear again. Both the linear and exponential models reproduce the majority of the data since ~97% of the cfabs are below 8 Mm^{-1}. However, it is desirable to be able to reproduce the highest LAC concentrations.

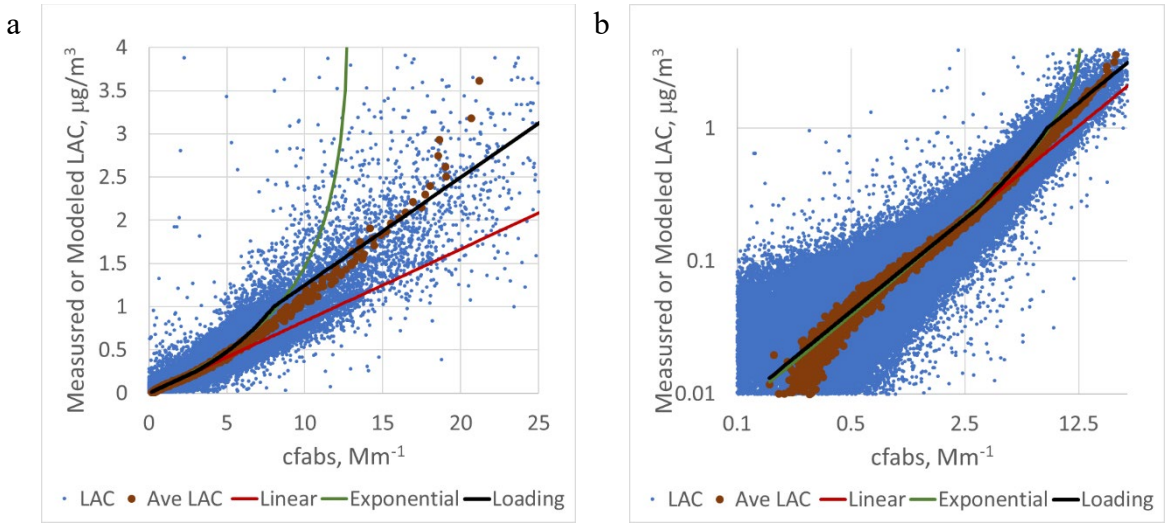

Figure 23. Scatter plot of measured or modeled LAC concentrations against the cfabs values on linear (a) and logarithmic (b) scales. Blue dots are the measured 24-hr values, and the brown circles are averaged values of 50 data points sorted by LAC. Red, green, and black lines are the modeled LAC concentrations using the linear, exponential, and loading models, respectively. Data from all IMPROVE sites from 2008 to 2018 were used.

The nonlinearity between cfabs and LAC at higher cfabs and LAC values is consistent with the fabs filter loading artifact shown in Figure 17 where fabs is progressively biased lower with increasing fabs above 4–5 Mm^{-1} until about 12 Mm^{-1} where an approximately 40% constant bias occurs. This nonlinear relationship can be accounted for by making the LAC MAE in equation 12 a function of fabs, with LAC MAE constant for lightly loaded filters, i.e., fabs < 3 Mm^{-1}, then with a linear decrease for more heavily loaded filters, i.e., 3 Mm^{-1} < cfabs < 8 Mm^{-1}, and finally with LAC MAE constant for heavily loaded filters, i.e., cfabs > 8 Mm^{-1}. LAC MAE = 12 m^2/g and 8 m^2/g for lightly and heavily loaded filters, respectively. These relationships can be represented by the equations

$$LAC\_MAE = fl \times light\_MAE + fh \times heavy\_MAE \quad (14)$$

$$fl = 1 - (cfabs - 3)/12 \quad (15)$$

$$fh = 1 - fl \quad (16)$$

where light_MAE = 12 m^2/g, heavy_MAE = 8 m^2/g and fl and fh refer to the fraction of filter aerosol material that corresponds to light_MAE and heavy_MAE, respectively. When cfabs is less than one, fl is set equal to one, and when equation 15 becomes negative, fl is set to zero.

Equations 14–16 are referred to as the loading model, and as shown in Figure 23, this model reproduces the average LAC concentration throughout the range of cfabs values, though it does overestimate the LAC for cfabs between 7 and 15 Mm^{-1}.

Figure 23 is the average performance of the LAC models across the IMPROVE network. The regional performance of these national models is explored in Figures 24 and 25, which plot the average bias and normalized root mean square errors (NRMSE), respectively, for the IMPROVE sites grouped into the 23 regions. As shown in Figure 24, biases range from ±25% depending on the region and model. The loading model has the lowest average bias of -0.025±0.1 compared to 0.066±0.1 and -0.058±0.1 for the exponential and linear models, respectively, with a range of +15% in southern California to -20% in Hells Canyon. The loading model also has the smallest

NRMSE at 0.79±0.68 compared to 0.82±0.73 and 1.19±0.62 for the linear and exponential models, respectively.

There is a clear spatial variation in the NRMSE with the northwestern and California coastal regions having the largest errors at over 2.0 (Figure 25). The smallest errors tend to occur in the eastern United States regions where the errors are less than 0.4. IMPROVE sites in the northwestern and northern California regions can have high LAC concentrations from intermittent impacts from biomass burning, and the models have the largest errors at these high concentrations (Figure 23). The eastern United States regions tend to have higher average LAC concentrations from anthropogenic combustion sources (Schichtel et al., 2017) but not the extremes from wildfire impacts. These LAC concentrations have the smallest measurement errors, and all of the models reproduce them well, suggesting a relatively constant LAC MAE across the East. There is no clear spatial variation in the average biases. For example, the California coast has among the highest NRMSE but lowest bias for the loading and linear models.

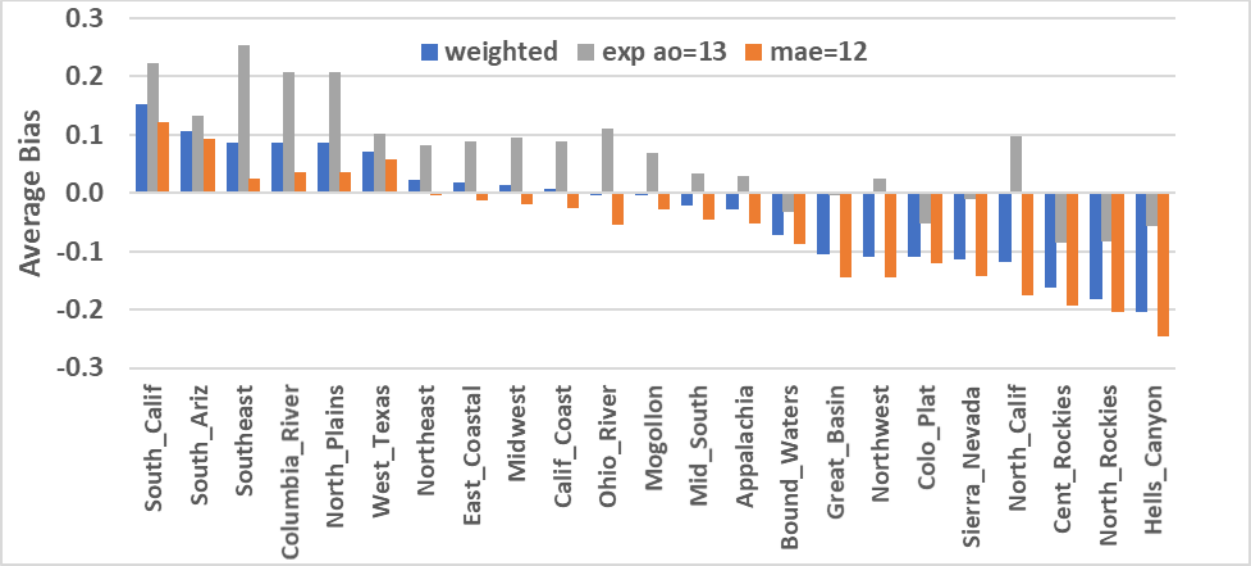

Figure 24. Average bias between measured LAC and LAC predicted using the weighted filter loading model (equation 14), the exponential model (equation 13), and linear model with LAC MAE = 12 for each of the 23 regions from 2008 through 2018.

The spatial variation in the errors and biases in the modeled LAC may reflect real differences in the LAC MAEs in the different regions. The model performance could be significantly improved by deriving a different model for each region. However, the causes of the model errors are not known, and they may represent measurement and other statistical errors. Without additional information, a single model applicable to all IMPROVE sites was sought, and overall, the loading model had the best regional and national performance.

The causes for the fabs loading artifacts are under investigation and correction is being developed. If successful, then the loading model would need to be revised, and a linear model may be more appropriate.

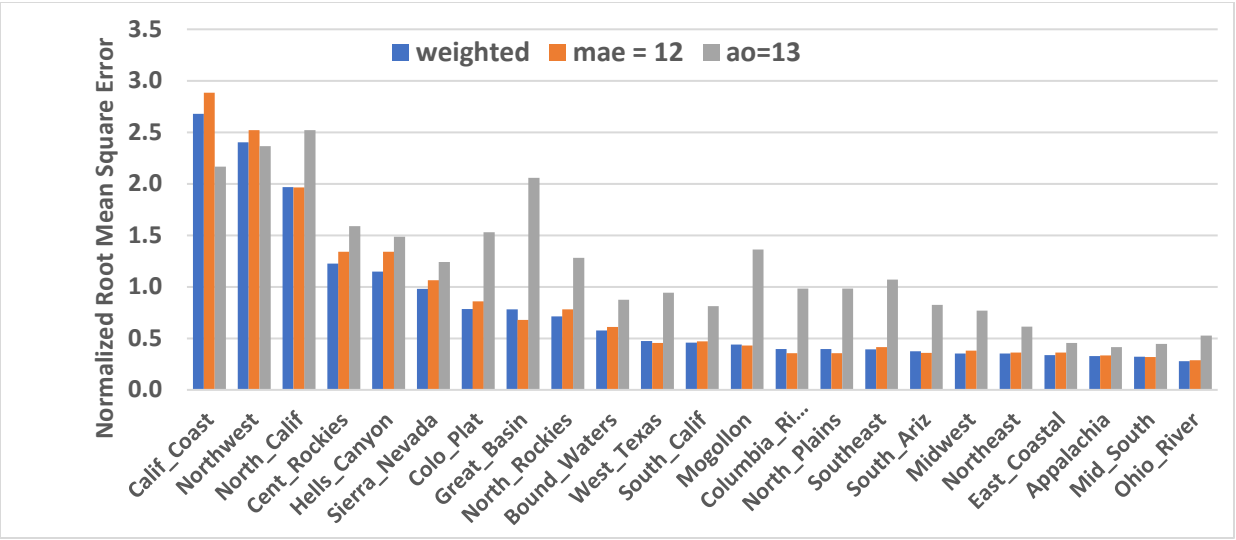

Figure 25. Normalized root mean square between measured LAC and LAC predicted using the weighted filter loading model (equation 14), the exponential model with (equation 13), and LAC = cfabs/12 for each of the 23 regions.

Suitability of TC and fabs-Derived OC and LAC for Long-term Monitoring Networks

TC is currently measured in the IMPROVE program and satisfies most requirements for use in a long-term monitoring program. Specifically, it is suitable for use in remote environments and is not biased at the low or high concentrations measured in the IMPROVE program. TC derived from thermal protocols can be calibrated, and the measured concentrations are not operationally defined and should produce stable and reproducible concentrations and trends. The primary issue with TC is that it is composed of OC and LAC, and by itself, it does not provide the information needed in IMPROVE to assess the contribution of carbonaceous aerosols to $PM_{2.5}$ and light extinction.

In order to meet the requirements of the IMPROVE program, an estimate of LAC is needed from which OC can be estimated by OC = TC - LAC. LAC can be derived from the HIPS fabs currently measured in IMPROVE. HIPS is an inexpensive fabs measurement with good precision. It is calibrated using clean filters with no absorbing aerosols, thus resulting in unbiased low concentrations. However, like TOR LAC, a large fraction of the fabs values is below the LQL. HIPS values have also been shown to be independent of the instrument and reproducible over a 15-year time span.

The HIPS fabs values have several important limitations. HIPS fabs has a loading artifact and underestimates high fabs values. This artifact is most apparent at fabs levels above 4–5 Mm^{-1} and affects 6–12% of recently measured IMPROVE data. HIPS fabs is not a direct measure of LAC but results from the absorption of light by LAC and soil deposited on the filter. To estimate LAC, the contribution of absorption from soil needs to be accounted for, though this is typically small. The relationship between absorption and species mass is defined by its MAE, which varies by more than a factor of two depending on the aerosol composition and morphology of the aerosols on the filter. It is not possible to account for the spatial and temporal variability in the MAEs, and average values are sought that can relate fabs to current TOR LAC concentrations. A semilinear relationship was developed that accounted for the HIPS loading artifact. It was found that it reproduced the measured LAC concentrations with little bias and errors of 52% for all concentrations and 42% for the lowest 95% of the values. Note that the combined fabs and TOR LAC measurement error was about 25% for the lowest 95% of the

values. As the composition of the atmosphere changes in time, these average MAEs may also change, and long-term trends in LAC derived from fabs could differ from those from TOR; however, the general patterns in the trends should be the same.

A primary use of LAC for the RHR is to estimate ambient absorption (babs). Procedures to estimate babs from fabs are under investigation. One procedure would be to use the derived LAC concentrations from the fabs data and assume a constant MAE of 10 m^2/g, which is what is currently used for the RHR rule. Alternatively, babs could be directly estimated from the fabs data. This is the desirable approach, but the loading artifact will also affect any estimates of ambient absorption, and the fabs to ambient absorption relationship will likely be nonlinear.

Impacts of Alternative Carbonaceous Aerosol Measurements for Tracking Trends for the RHR

In support of the RHR, light extinction is reconstructed from the IMPROVE aerosol concentrations. In the current RHR guidance documents, the organic mass scattering efficiency, used to convert organic concentrations to light scattering, varies between 2.8 and 6.1 m^2/g depending on the organic concentration (Prenni et al., 2021), but on average it is near 4 m^2/g. Therefore, using the OC data, scattering by organic mass can be approximated by

$$\text{OMbsp} \sim 1.8 \times 4 \times \text{OC} = 7.2 \times \text{OC} \quad (17)$$

where 1.8 is the organic mass to organic carbon ratio (R_{oc}), and 4 m^2/g is the approximate organic mass light scattering efficiency.

Light absorption is estimated from the LAC data assuming a MAE of 10 m^2/g:

$$\text{babs} = 10 \times \text{LAC} \quad (18)$$

The OC–LAC split is constrained by the TC concentrations, and any errors in the split will result in a 38% error in light extinction in the misapportioned mass. LAC is usually the smaller fraction of TC, typically 10–15%. Therefore, even a large error in the misapportionment of LAC would result in a relatively small error in carbonaceous light extinction. For example, if the reported LAC is 10% of the TC, but the actual LAC is 20% of the TC, this would result in an underestimation of carbonaceous light extinction of only 3.6%. Consequently, the reconstructed total light extinction and RHR metrics are relatively insensitive to errors in the OC–LAC split and thus the method for estimating OC and LAC. This is illustrated in Appendix B, which reports the RHR tracking metrics for the 20% most-impaired days and 20% clearest days for each IMPROVE monitoring site where the OC and LAC were estimated by TOR, FTIR, and a combination of TC and fabs data (Copeland, personal communication, 2020).

Intercomparison of Carbonaceous Aerosol Measurement Methods for Long-term Speciated Aerosol Monitoring Programs and Recommendations

The benefits and drawbacks of each method for measuring carbonaceous aerosols have been summarized in previous discussions, including the degree to which each method meets the five requirements for implementation into a long-term monitoring program. Here the methods are intercompared with final recommendations.

Table 2 summarizes the three carbonaceous aerosol measurement methods and how they meet network requirements. All three methods meet the IMPROVE network goals, and since they are filter-based, they are easily implementable in remote settings and the IMPROVE monitoring

program. In addition, they all can produce OC and LAC values that are relatable to TOR. However, relating fabs to LAC is complicated by changing aerosol composition and optical properties in space and time and fabs trends could deviate from LAC trends. On the other hand, fabs is a direct measurement of fine particulate absorption and should be a better surrogate for tracking trends in ambient absorption as aerosol compositions change over time, which is important for RHR and climate science.

Table 2. Summary of how the three carbonaceous aerosol measurement methods meet the requirements for implementation into the IMPROVE long-term monitoring programs. Y and N are "yes" and "no", respectively, and H, M, L are "high", "medium", and "low", respectively.

	TOR			FTIR		TOA-HIPS	
	TC	OC	LAC	OC	LAC	TC	(fabs)
Calibrated to standards	Y	N	N	N	N	Y	Y-N
Stable and reproducible measurements	Y	N	N	N	N	Y	Y
Instrument/method universality	N			Y		Y	Y
Measures at relevant low and high concentrations	Y	Y	N (biased)	Y	N (biased)	Y	N (unbiased)
High precision	Y	Y	N	Y	N	Y	Y
Cost	H			M		M	L
Implementable in remote settings	Y	Y	Y	Y	Y	Y	Y
Relatable to TOR	Y	Y	Y	Y	Y	Y	Y (today)
Organic aerosol compositional information	M			H		L	L

One of the primary limitations with TOR is that the measurement is operationally defined and can depend on the instruments and methods used in the analyses. This is not the case for FTIR, TC measured by TOA, and HIPS. The issue for TOR is that the OC–LAC split cannot be calibrated due to a lack of atmospherically relevant reference standards, and the split is dependent on the organic and inorganic composition. The operationally defined OC and LAC concentrations combined with the inability to accomplish fundamental calibrations introduces the possibility of discontinuities and drifts in the long-term time series. The FTIR OC and LAC are calibrated to the TOR OC and LAC concentrations and suffer from the same issues.

Measurements of TC can be calibrated to standards and have been shown to be independent of instruments and methods, and long-term trends in TC are expected to reflect changes in the atmospheric concentrations and not changes in analytical protocols. Fabs measured by HIPS has been shown to be instrument independent but is not fundamentally calibrated for loaded filters. fabs is calibrated to blank filters and has been shown to be linear with increasing absorbance gels (White et al., 2016) and increasing concentrations of soot uniformly deposited on filters. However, samples collected in the IMPROVE monitors are not uniformly deposited on the filters and fabs measurements have been shown to have filter loading artifacts, causing low fabs values at high loadings that affect 6–12% of the IMPROVE data. Retrospective analyses of 15 years of IMPROVE samples have demonstrated that HIPS fabs measurements are stable and reproducible, and long-term trends should reflect changes in ambient absorption.

TOR TC and OC are quantifiable at low concentrations measured in the IMPROVE program. However, high fractions of LAC, and thus FTIR LAC, are near or below the LQL and have high uncertainty. These low values also appear to be overestimated, which could bias aggregated values. HIPS fabs also have a significant fraction of values near or below the LQL, but since HIPS is calibrated to clean filters, the low values are not likely biased.

From a cost standpoint, TOR analysis is the most expensive. FTIR is a relatively inexpensive analysis that is conducted on IMPROVE Teflon filters. However, FTIR OC and LAC are moderately expensive due to the need to maintain the analysis of filters by TOR at a subset of network sites and the collection of samples on the quartz fiber filters. HIPS fabs is an inexpensive analysis that is currently conducted in the IMPROVE and CSN monitoring networks, and the measurement of TC is a moderately expensive analysis due to the need to maintain the collection of samples on separate quartz fiber filters.

One benefit of the FTIR method is that the FTIR data contain additional information on the organic and inorganic composition that can be used to assess the organic mass to carbon ratios needed to reconstruct PM mass and light extinction as well as information concerning the origin and history of the carbonaceous aerosols. This is also the case for the TOR data, where in addition to TC, OC, and LAC concentrations, TOR produces carbon concentrations for the different thermal subfractions and estimates of multiwavelength transmittance attenuation. The TOR subfractions and multiwavelength data are not discussed in this document, but the thermal fractions have been shown to be somewhat related to the composition of the carbonaceous aerosols, and the multiwavelength attenuation data is useful for distinguishing brown from black carbon concentrations. The thermal fractions are highly method dependent and not suitable for trends.

In long-term monitoring programs such as IMPROVE, the most important requirement is the ability to track long-term trends and ensure the changes in values are due to the changes in ambient aerosol concentrations and properties as opposed to analytical artifacts. This is ideally accomplished by fundamentally calibrating the system. In the measurement methods discussed, only TC fully meets this requirement, and fabs meets it partially, though it has been shown to be stable and reproducible over decades. Based on this, maintaining the current TOR OC and LAC analyses along with the HIPS fabs measurements provides the most flexibility in that TC and fabs would be measured and could be used for trends, but TOR OC and LAC concentrations would continue to be measured and reported and used in various analyses

The second-highest priority requirement is cost. IMPROVE and other monitoring programs are cost constrained, requiring annual cost savings that have led to the discontinuation of monitoring sites, filter analyses, and procedures that could influence the quality of the data. The current TOR analysis is a relatively expensive measurement, and a combined TC-only and fabs measurement would decrease costs, protecting other aspects of the monitoring programs. Consequently, if network operational costs need to be significantly reduced, then it is recommended that a TC-fabs system be used to measure carbonaceous aerosols in IMPROVE.

References

Alfaro, S. C., Lafon, S., Rajot, J. L., Formenti, P., Gaudichet, A., and Maille, M. (2004), Iron oxides and light absorption by pure desert dust: An experimental study, *Journal of Geophysical Research-Atmospheres*, *109*(D8), 10.1029/2003jd004374.

Atkinson, R. W., Analitis, A., Samoli, E., Fuller, G. W., Green, D. C., Mudway, I. S., Anderson, H. R., and Kelly, F. J. (2016), Short-term exposure to traffic-related air pollution and daily mortality in London, UK, *Journal of Exposure Science and Environmental Epidemiology*, *26*(2), 125-132, 10.1038/jes.2015.65.

Baumgardner, D., Popovicheva, O., Allan, J., Bernardoni, V., Cao, J., Cavalli, F., Cozic, J., Diapouli, E., Eleftheriadis, K., Genberg, P. J., Gonzalez, C., Gysel, M., John, A., Kirchstetter, T. W., Kuhlbusch, T. A. J., Laborde, M., Lack, D., Muller, T., Niessner, R., Petzold, A., Piazzalunga, A., Putaud, J. P., Schwarz, J., Sheridan, P., Subramanian, R., Swietlicki, E., Valli, G., Vecchi, R., and Viana, M. (2012), Soot reference materials for instrument calibration and intercomparisons: a workshop summary with recommendations, *Atmospheric Measurement Techniques*, *5*(8), 1869-1887, 10.5194/amt-5-1869-2012.

Bladt, H., Schmid, J., Kireeva, E. D., Popovicheva, O. B., Perseantseva, N. M., Timofeev, M. A., Heister, K., Uihlein, J., Ivleva, N. P., and Niessner, R. (2012), Impact of Fe content in laboratory-produced soot aerosol on its composition, structure, and thermo-chemical properties, Aerosol Science and Technology, 46(12), 1337-1348, 10.1080/02786826.2012.711917.

Blando, J. D., Porcja, R. J., and Turpin, B. J. (2001), Issues in the quantitation of functional groups by FTIR spectroscopic analysis of impactor-collected aerosol samples, Aerosol Science and Technology, 35(5), 899-908, 10.1080/02786820126852.

Bond, T. C., Anderson, T. L., and Campbell, D. (1999), Calibration and intercomparison of filter-based measurements of visible light absorption by aerosols, Aerosol Science and Technology, 30(6), 582-600, 10.1080/027868299304435.

Bond, T. C., and Bergstrom, R. W. (2006), Light absorption by carbonaceous particles: An investigative review, Aerosol Science and Technology, 40(1), 27-67, 10.1080/02786820500421521.

Bond, T. C., Doherty, S. J., Fahey, D. W., Forster, P. M., Berntsen, T., DeAngelo, B. J., Flanner, M. G., Ghan, S., Karcher, B., Koch, D., Kinne, S., Kondo, Y., Quinn, P. K., Sarofim, M. C., Schultz, M. G., Schulz, M., Venkataraman, C., Zhang, H., Zhang, S., Bellouin, N., Guttikunda, S. K., Hopke, P. K., Jacobson, M. Z., Kaiser, J. W., Klimont, Z., Lohmann, U., Schwarz, J. P., Shindell, D., Storelvmo, T., Warren, S. G., and Zender, C. S. (2013), Bounding the role of black carbon in the climate system: A scientific assessment, Journal of Geophysical Research-Atmospheres, 118(11), 5380-5552, 10.1002/jgrd.50171.

Boparai, P., Lee, J. M., and Bond, T. C. (2008), Revisiting thermal-optical analyses of carbonaceous aerosol using a physical model, Aerosol Science and Technology, 42(11), 930-U915, 10.1080/02786820802360690.

Cachier, H., Bremond, M. P., and Buat-Menard, P. (1989a), Determination of atmospheric soot carbon with a simple thermal method, Tellus Series B-Chemical and Physical Meteorology, 41(3), 379-390, 10.1111/j.1600-0889.1989.tb00316.x.

Cachier, H., Bremond, M. P., and Buatmenard, P. (1989b), Thermal separation of soot carbon, Aerosol Science and Technology, 10(2), 358-364, 10.1080/02786828908959273.

Cadle, S. H., Groblicki, P. J., and Mulawa, P. A. (1983), Problems in the sampling and analysis of carbon particulate, Atmospheric Environment, 17(3), 593-600, 10.1016/0004-6981(83)90132-4.

Cadle, S. H., Groblicki, P. J., and Stroup, D. P. (1980), Automated carbon analyzer for particulate samples, Analytical Chemistry, 52(13), 2201-2206, 10.1021/ac50063a047.

Cao, J. J., Lee, S. C., Ho, K. F., Zhang, X. Y., Zou, S. C., Fung, K., Chow, J. C., and Watson, J. G. (2003), Characteristics of carbonaceous aerosol in Pearl River Delta Region, China during 2001 winter period, Atmospheric Environment, 37(11), 1451-1460, 10.1016/s1352-2310(02)01002-6.

Cavalli, F., Viana, M., Yttri, K. E., Genberg, J., and Putaud, J. P. (2010), Toward a standardised thermal-optical protocol for measuring atmospheric organic and elemental carbon: the EUSAAR protocol, Atmospheric Measurement Techniques, 3(1), 79-89, 10.5194/amt-3-79-2010.

Chen, L. W. A., Chow, J. C., Watson, J. G., and Schichtel, B. A. (2012), Consistency of long-term elemental carbon trends from thermal and optical measurements in the IMPROVE network, Atmospheric Measurement Techniques, 5(10), 2329-2338, 10.5194/amt-5-2329-2012.

Chen, L. W. A., Watson, J. G., Chow, J. C., DuBois, D. W., and Herschberger, L. (2010), Chemical mass balance source apportionment for combined PM2.5 measurements from U S non-urban and urban long-term networks, Atmospheric Environment, 44(38), 4908-4918, 10.1016/j.atmosenv.2010.08.030.

Chiappini, L., Verlhac, S., Aujay, R., Maenhaut, W., Putaud, J. P., Sciare, J., Jaffrezo, J. L., Liousse, C., Galy-Lacaux, C., Alleman, L. Y., Panteliadis, P., Leoz, E., and Favez, O. (2014), Clues for a standardised thermal-optical protocol for the assessment of organic and elemental carbon within ambient air particulate matter, Atmospheric Measurement Techniques, 7(6), 1649-1661, 10.5194/amt-7-1649-2014.

Chow, J.C.; Watson, J.G.; Crow, D.; Lowenthal, D.H.; Merrifield, T.M. (2001). Comparison of IMPROVE and NIOSH carbon measurements. Aerosol Sci. Technol., 34(1):23-34.

Chow, J.C. and Watson, J.G. (2002). PM2.5 carbonate concentrations at regionally representative Interagency Monitoring of Protected Visual Environment sites. J. Geophys. Res., 107(D21):ICC 6-1-ICC 6-9.

Chow, J., Watson, J., Chen, L. W. A., Chang, O., and G, P.-M. (2005), Comparison of the DRI/OGC and Model 2001 Thermal/Optical Carbon Analyzers, final report prepared for the IMPROVE Steering Committee, Desert Research Institute, Reno, Nevada, January 18.

Chow, J. C., Watson, J. G., Chen, L. W. A., Arnott, W. P., Moosmuller, H., and Fung, K. (2004), Equivalence of elemental carbon by thermal/optical reflectance and transmittance with different temperature protocols, Environmental Science & Technology, 38(16), 4414-4422, 10.1021/es034936u.

Chow, J. C., Watson, J. G., Chen, L. W. A., Chang, M. C. O., Robinson, N. F., Trimble, D., and Kohl, S. (2007), The IMPROVE-A temperature protocol for thermal/optical carbon analysis: maintaining consistency with a long-term database, Journal of the Air & Waste Management Association, 57(9), 1014-1023, 10.3155/1047-3289.57.9.1014.

Chow, J. C., Watson, J. G., Chen, L. W. A., Rice, J., and Frank, N. H. (2010), Quantification of PM2.5 organic carbon sampling artifacts in US networks, Atmospheric Chemistry and Physics, 10(12), 5223-5239, 10.5194/acp-10-5223-2010.

Chow, J. C., Watson, J. G., Crow, D., Lowenthal, D. H., and Merrifield, T. (2001), Comparison of IMPROVE and NIOSH carbon measurements, Aerosol Science and Technology, 34(1), 23-34, 10.1080/027868201300081923.

Chow, J. C., Watson, J. G., Lowenthal, D. H., Chen, L. W. A., and Magliano, K. L. (2006), Particulate carbon measurements in California's San Joaquin Valley, Chemosphere, 62(3), 337-348, 10.1016/j.chemosphere.2005.04.094.

Chow, J. C., Watson, J. G., Pritchett, L. C., Pierson, W. R., Frazier, C. A., and Purcell, R. G. (1993), The DRI thermal optical reflectance carbon analysis system - Description, evaluation and applications in United States air quality studies, Atmospheric Environment Part a-General Topics, 27(8), 1185-1201, 10.1016/0960-1686(93)90245-t.

Conny, J. M., Klinedinst, D. B., Wight, S. A., and Paulsen, J. L. (2003), Optimizing thermal-optical methods for measuring atmospheric elemental (black) carbon: A response surface study, Aerosol Science and Technology, 37(9), 703-723, 10.1080/02786820300920.

Conny, J. M., Norris, G. A., and Gould, T. R. (2009), Factorial-based response-surface modeling with confidence intervals for optimizing thermal-optical transmission analysis of atmospheric black carbon, Analytica Chimica Acta, 635(2), 144-156, 10.1016/j.aca.2008.12.046.

Cormier, S. A., Lomnicki, S., Backes, W., and Dellinger, B. (2006), Origin and health impacts of emissions of toxic by-products and fine particles from combustion and thermal treatment of hazardous wastes and materials, Environmental Health Perspectives, 114(6), 810-817, 10.1289/ehp.8629.

Coury, C., and Dillner, A. M. (2008), A method to quantify organic functional groups and inorganic compounds in ambient aerosols using attenuated total reflectance FTIR spectroscopy and multivariate chemometric techniques, Atmospheric Environment, 42(23), 5923-5932, 10.1016/j.atmosenv.2008.03.026.

Currie, L. A., Benner, B. A., Kessler, J. D., Klinedinst, D. B., Klouda, G. A., Marolf, J. V., Slater, J. F., Wise, S. A., Cachier, H., Cary, R., Chow, J. C., Watson, J., Druffel, E. R. M., Masiello, C. A., Eglinton, T. I., Pearson, A., Reddy, C. M., Gustafsson, O., Quinn, J. G., Hartmann, P. C., Hedges, J. I., Prentice, K. M., Kirchstetter, T. W., Novakov, T., Puxbaum, H., and Schmid, H. (2002), A critical evaluation of interlaboratory data on total, elemental, and isotopic carbon in the carbonaceous particle reference material, NIST SRM 1649a, Journal of Research of the National Institute of Standards and Technology, 107(3), 279-298, 10.6028/jres.107.022.

Debus, B., Takahama, S., Weakley, A. T., Seibert, K., and Dillner, A. M. (2019), Long-term strategy for assessing carbonaceous particulate matter concentrations from multiple Fourier transform infrared (FT-IR) instruments: Influence of spectral dissimilarities on multivariate calibration performance, Applied Spectroscopy, 73(3), 271-283, 10.1177/0003702818804574.

Debus, B., Weakley, A. T., Takahama, S., Schichtel, B. A., Copeland, S., Wexler, A. S., and Dillner, A. M. (2020), Direct quantification of major particulate matter species from a single Teflon filter using infrared spectroscopy - Application to large-scale monitoring networks, submitted for publication.

Dillner, A. M., and Takahama, S. (2015a), Predicting ambient aerosol thermal-optical reflectance (TOR) measurements from infrared spectra: organic carbon, Atmospheric Measurement Techniques, 8(3), 1097-1109, 10.5194/amt-8-1097-2015.

Dillner, A. M., and Takahama, S. (2015b), Predicting ambient aerosol thermal-optical reflectance measurements from infrared spectra: elemental carbon, Atmospheric Measurement Techniques, 8(10), 4013-4023, 10.5194/amt-8-4013-2015.

DRI (2012), DRI Model 2001 Thermal/Optical Carbon Analysis (TOR/TOT) of Aerosol Filter Samples - Method IMPROVE_A, Standard Operating Procedure, Desert Research Institute, Reno, Nevada.

El-Zanan, H. S., Lowenthal, D. H., Zielinska, B., Chow, J. C., and Kumar, N. (2005), Determination of the organic aerosol mass to organic carbon ratio in IMPROVE samples, Chemosphere, 60(4), 485-496, 10.1016/j.chemosphere.2005.01.005.

Ellis, R. A., Jacob, D. J., Sulprizio, M. P., Zhang, L., Holmes, C. D., Schichtel, B. A., Blett, T., Porter, E., Pardo, L. H., and Lynch, J. A. (2013), Present and future nitrogen deposition to national parks in the United States: critical load exceedances, Atmospheric Chemistry and Physics, 13(17), 9083-9095, 10.5194/acp-13-9083-2013.

Fung, K. (1990), Particulate carbon speciation by MnO2 oxidation, Aerosol Science and Technology, 12(1), 122-127, 10.1080/02786829008959332.

Grahame, T. J., and Schlesinger, R. B. (2007), Health effects of airborne particulate matter: Do we know enough to consider regulating specific particle types or sources?, Inhalation Toxicology, 19(6-7), 457-481, 10.1080/08958370701382220.

Hakami, A., Henze, D. K., Seinfeld, J. H., Chai, T., Tang, Y., Carmichael, G. R., and Sandu, A. (2005), Adjoint inverse modeling of black carbon during the Asian Pacific Regional Aerosol Characterization Experiment, Journal of Geophysical Research-Atmospheres, 110(D14), 10.1029/2004jd005671.

Hand, J. L., Prenni, A. J., Copeland, S., Schichtel, B. A., and Malm, W. C. (2020), Thirty years of the Clean Air Act Amendments: Impacts on haze in remote regions of the United States (1990-2018), Atmospheric Environment, 243, 117865, 10.1016/j.atmosenv.2020.117865.

Hand, J. L., Prenni, A. J., Schichtel, B. A., Malm, W. C., and Chow, J. C. (2019), Trends in remote PM2.5 residual mass across the United States: Implications for aerosol mass reconstruction in the IMPROVE network, Atmospheric Environment, 203, 141-152, 10.1016/j.atmosenv.2019.01.049.

Hand, J. L., Schichtel, B. A., Malm, W. C., and Frank, N. H. (2013a), Spatial and temporal trends in PM2.5 organic and elemental carbon across the United States, Advances in Meteorology, dx.doi.org/10.1155/2013/367674.

Hand, J. L., Schichtel, B. A., Malm, W. C., and Pitchford, M. L. (2013b), Widespread reductions in sulfate across the United States since the early 1900s, presented at 19th International Conference on Nucleation and Atmospheric Aerosols, Fort Collins, CO, June 24-28.

Hand, J. L., Schichtel, B. A., Pitchford, M. L., Malm, W. C., and Frank, N. H. (2012), Seasonal composition of remote and urban fine particulate matter in the United States, J. Geophys. Res., 117, D05209, doi:10.1029/2011JD017122.

Heald, C. L., Jacob, D. J., Turquety, S., Hudman, R. C., Weber, R. J., Sullivan, A. P., Peltier, R. E., Atlas, E. L., de Gouw, J. A., Warneke, C., Holloway, J. S., Neuman, J. A., Flocke, F. M., and Seinfeld, J. H. (2006), Concentrations and sources of organic carbon aerosols in the free troposphere over North America, Journal of Geophysical Research-Atmospheres, 111(D23), 10.1029/2006jd007705.

Hopke, P. K., Ito, K., Mar, T., Christensen, W. F., Eatough, D. J., Henry, R. C., Kim, E., Laden, F., Lall, R., Larson, T. V., Liu, H., Neas, L., Pinto, J., Stolzel, M., Suh, H., Paatero, P., and Thurston, G. D. (2006), PM source apportionment and health effects: 1. Intercomparison of source apportionment results, Journal of Exposure Science and Environmental Epidemiology, 16(3), 275-286, 10.1038/sj.jea.7500458.

Huntzicker, J. J., Johnson, R. L., Shah, J. J., and Cary, R. A. (1982), Analysis of organic and elemental carbon in ambient aerosols by a thermal-optical method, in Particulate Carbon: Atmospheric Life Cycle, edited by G. T. Wolff and R. L. Klimisch, pp. 79-88, Springer, Boston, 978-1-4684-4156-7, doi:10.1007/978-1-4684-4154-3_6.

Hyslop, N. P., Trzepla, K., and White, W. H. (2012), Reanalysis of archived IMPROVE PM2.5 samples previously analyzed over a 15-year period, Environmental Science & Technology, 46(18), 10106-10113, 10.1021/es301823q.

Hyslop, N. P., Trzepla, K., and White, W. H. (2015), Assessing the suitability of historical PM2.5 element measurements for trend analysis, Environmental Science & Technology, 49(15), 9247-9255, 10.1021/acs.est.5b01572.

Hyslop, N. P., Trzepla, K., Yatkin, S., White, W. H., Ancelet, T., Davy, P., Butler, O., Gerboles, M., Kohl, S., McWilliams, A., Saucedo, L., Van Der Haar, M., and Jonkers, A. (2019), An inter-laboratory evaluation of new nulti-element reference materials for atmospheric particulate matter measurements, Aerosol Science and Technology, 53(7), 771-782, 10.1080/02786826.2019.1606413.

Hyslop, N. P., and White, W. H. (2008), An evaluation of Interagency Monitoring of Protected Visual Environments (IMPROVE) collocated precision and uncertainty estimates, Atmospheric Environment, 42(11), 2691-2705, 10.1016/j.atmosenv.2007.06.053.

Hyslop, N. P., and White, W. H. (2009), Estimating precision using duplicate measurements, Journal of the Air & Waste Management Association, 59(9), 1032-1039.

Jacobson, M. Z. (2010), Short-term effects of controlling fossil-fuel soot, biofuel soot and gases, and methane on climate, Arctic ice, and air pollution health, Journal of Geophysical Research-Atmospheres, 115, 10.1029/2009jd013795.

Janssen, N. A. H., Hoek, G., Simic-Lawson, M., Fischer, P., van Bree, L., ten Brink, H., Keuken, M., Atkinson, R. W., Anderson, H. R., Brunekreef, B., and Cassee, F. R. (2011), Black carbon as an additional indicator of the adverse health effects of airborne particles compared with PM10 and PM2.5, Environmental Health Perspectives, 119(12), 1691-1699, 10.1289/ehp.1003369.

Karanasiou, A., Minguillon, M. C., Viana, M., Alastuey, A., Putaud, J. P., Maenhaut, W., Panteliadis, P., Mocnik, G., Favez, O., and Kuhlbusch, T. A. J. (2015), Thermal-optical analysis for the measurement of elemental carbon (EC) and organic carbon (OC) in ambient air a literature review, Atmospheric Measurement Techniques Discussions, 8, 9649-9712, 10.5194/amtd-8-9649-2015.

Kim, E., and Hopke, P. K. (2006), Characterization of fine particle sources in the Great Smoky Mountains area, Science of the Total Environment, 368(2-3), 781-794, 10.1016/j.scitotenv.2006.02.048.

Kirchstetter, T. W., Agular, J., Tonse, S., Fairley, D., and Novakov, T. (2008), Black carbon concentrations and diesel vehicle emission factors derived from coefficient of haze measurements in California: 1967-2003, Atmospheric Environment, 42(3), 480-491, 10.1016/j.atmosenv.2007.09.063.

Klouda, G. A., Filliben, J. J., Parish, H. J., Chow, J. J., Watson, J. G., and Cary, R. A. (2005), Reference material 8785: Air particulate matter on filter media, Aerosol Science and Technology, 39(2), 173-183, 10.1080/027868290916453.

Li, Y., Schichtel, B. A., Walker, J. T., Schwede, D. B., Chen, X., Lehmann, C. M. B., Puchalski, M. A., Gay, D. A., and Collett, J. L. (2016), Increasing importance of deposition of reduced nitrogen in the United States, Proceedings of the National Academy of Sciences of the United States of America, 113(21), 5874-5879, 10.1073/pnas.1525736113.

Lim, H. J., and Turpin, B. J. (2002), Origins of primary and secondary organic aerosol in Atlanta: Results' of time-resolved measurements during the Atlanta supersite experiment, Environmental Science & Technology, 36(21), 4489-4496, 10.1021/es0206487.

Mader, B. T., Flagan, R. C., and Seinfeld, J. H. (2001), Sampling atmospheric carbonaceous aerosols using a particle trap impactor/denuder sampler, Environmental Science & Technology, 35(24), 4857-4867, 10.1021/es011059o.

Malm, W. C., and Hand, J. L. (2007), An examination of aerosol physical and optical properties of aerosols collected in the IMPROVE program, Atmospheric Environment, 41, 3407-3427, 10.1016/j.atmosenv.2006.12.012.

Malm, W. C., Schichtel, B. A., Hand, J. L., and Collett, J. L. (2017), Concurrent temporal and spatial trends in sulfate and organic mass concentrations measured in the IMPROVE monitoring program, Journal of Geophysical Research-Atmospheres, 122(19), 10341-10355, 10.1002/2017jd026865.

Malm, W. C., Schichtel, B. A., Hand, J. L., and Prenni, A. J. (2020), Implications of organic mass to carbon ratios increasing over time in the rural United States, Journal of Geophysical Research-Atmospheres, 125(5), 10.1029/2019jd031480.

Malm, W. C., Schichtel, B. A., and Pitchford, M. L. (2011), Uncertainties in PM2.5 gravimetric and speciation measurements and what we can learn from them, J. Air Waste Manage. Assoc., 61, 1131-1149, doi:10.1080/10473289.2001.603998.

Malm, W. C., Schichtel, B. A., Pitchford, M. L., Ashbaugh, L. L., and Eldred, R. A. (2004), Spatial and monthly trends in speciated fine particle concentration in the United States, J. Geophys. Res., 109, doi:10.1029/2003JD003739.

Malm, W. C., Sisler, J. F., Huffman, D., Eldred, R. A., and Cahill, T. A. (1994), Spatial and seasonal trends in particle concentration and optical extinction in the United States, Journal of Geophyiscal Research, 99(D1), 1347-1370, 10.1029/93JD02916.

Maria, S. F., Russell, L. M., Turpin, B. J., Porcja, R. J., Campos, T. L., Weber, R. J., and Huebert, B. J. (2003), Source signatures of carbon monoxide and organic functional groups in Asian Pacific Regional Aerosol Characterization Experiment (ACE-Asia) submicron aerosol types, Journal of Geophysical Research-Atmospheres, 108(D23), 10.1029/2003jd003703.

Martin, M. V., Heald, C. L., Lamarque, D. B., Tilmes, S., Emmons, L. K., and Schichtel, B. A. (2015), How emissions, climate, and land use change will impact mid-century air quality over the United States: A focus on effects, Atmospheric Chemistry and Physics, 15(5), 2805-2823, doi:10.5194/acp-15-2805-2015.

Mizohata, A., and Ito, K. (1985), Analysis of organic and elemental carbon in atmospheric aerosols by thermal method, in Annual Report of the Radiation Center of Osaka Prefecture, vol. 26, pp. 51-55, Sakai, Osaka, Japan.

Moosmuller, H., Engelbrecht, J. P., Skiba, M., Frey, G., Chakrabarty, R. K., and Arnott, W. P. (2012), Single scattering albedo of fine mineral dust aerosols controlled by iron concentration, Journal of Geophysical Research-Atmospheres, 117, 10.1029/2011jd016909.

Murphy, D. M., Chow, J. C., Leibensperger, E. M., Malm, W. C., Pitchford, M., Schichtel, B. A., Watson, J. G., and White, W. H. (2011), Decreases in elemental carbon and fine particle mass in the United States, Atmospheric Chemistry and Physics, 11(10), 4679-4686.

Nash, D. G., Swanson, N. B., Preston, W. T., Yelverton, T. L. B., Roberts, W. L., Wendt, J. O. L., and Linak, W. P. (2013), Environmental implications of iron fuel borne catalysts and their effects on diesel particulate formation and composition, Journal of Aerosol Science, 58, 50-61, 10.1016/j.jaerosci.2013.01.001.

Nicolosi, E. M. G., Quincey, P., Font, A., and Fuller, G. W. (2018), Light attenuation versus evolved carbon (AVEC) - A new way to look at elemental and organic carbon analysis, Atmospheric Environment, 175, 145-153, 10.1016/j.atmosenv.2017.12.011.

NIOSH (1999), NIOSH Method 5040 Issue 3 (Interim): Elemental Carbon (diesel exhaust), 4th edition, National Insitute for Occupational Safety and Health, Cincinnati, http://www.cdc.gov/niosh/docs/2003-154/pdfs/5040.pdf.

Novakov, T. (1982). Soot in the atmosphere. In Particulate Carbon: Atmospheric Life Cycle, Wolff, G. T., Klimisch, R. L., Eds.; Plenum Press: New York, NY, 19-41

Novakov, T. (1982), Characterization of aerosol sulfur, carbon, and nitrogen by ESCA and thermal-analysis, Transactions of the American Nuclear Society, 41, 193-193, ISSN 003-18x.

Novakov, T., and Corrigan, C. E. (1995), Thermal characterization of biomass smoke particles, Mikrochimica Acta, 119(1-2), 157-166, 10.1007/bf01244864.

Park, R. J., Jacob, D. J., Chin, M., and Martin, R. V. (2003), Sources of carbonaceous aerosols over the United States and implications for natural visibility, Journal of Geophysical Research-Atmospheres, 108(D12), 10.1029/2002jd003190.

Piazzalunga, A., Bernardoni, V., Fermo, P., Valli, G., and Vecchi, R. (2011), Technical Note: On the effect of water-soluble compounds removal on EC quantification by TOT analysis in urban aerosol samples, Atmospheric Chemistry and Physics, 11(19), 10193-10203, 10.5194/acp-11-10193-2011.

Polidori, A., Turpin, B. J., Lim, H. J., Cabada, J. C., Subramanian, R., Pandis, S. N., and Robinson, A. L. (2006), Local and regional secondary organic aerosol: Insights from a year of semi-continuous carbon measurements at Pittsburgh, Aerosol Science and Technology, 40(10), 861-872, 10.1080/02786820600754649.

Pollard, M., Jaklevic, J., and Howes, J. (1990), Fourier-transform infrared and ion-chromatographic sulfate analysis of ambient air samples, Aerosol Science and Technology, 12(1), 105-113, 10.1080/02786829008959330.

Ram, K., and Sarin, M. M. (2009), Absorption coefficient and site-specific mass absorption efficiency of elemental carbon in aerosols over urban, rural, and high-altitude sites in India, Environmental Science & Technology, 43(21), 8233-8239, 10.1021/es9011542.

Ramanathan, V., and Carmichael, G. (2008), Global and regional climate changes due to black carbon, Nature Geoscience, 1(4), 221-227, 10.1038/ngeo156.

Reff, A., Turpin, B. J., Offenberg, J. H., Weisel, C. P., Zhang, J., Morandi, M., Stock, T., Colome, S., and Winer, A. (2007), A functional group characterization of organic PM2.5 exposure: Results from the RIOPA study, Atmospheric Environment, 41(22), 4585-4598, 10.1016/j.atmosenv.2007.03.054.

Ridley, D. A., Heald, C. L., Ridley, K. J., and Kroll, J. H. (2018), Causes and consequences of decreasing atmospheric organic aerosol in the United States, Proceedings of the National Academy of Sciences of the United States of America, 115(2), 290-295, 10.1073/pnas.1700387115.

Rigler, M., Drinovec, L., Lavric, G., Vlachou, A., Prevot, A. S. H., Jaffrezo, J. L., Stavroulas, I., Sciare, J., Burger, J., Kranjc, I., Tursic, J., Hansen, A. D. A., and Mocnik, G. (2020), The new instrument using a TC-BC (total carbon-black carbon) method for the online measurement of carbonaceous aerosols, Atmospheric Measurement Techniques, 13(8), 4333-4351, 10.5194/amt-13-4333-2020.

Rupprecht, G., Patashnick, H., Beeson, D. E., Green, R. N., and Meyer, M. B. (1995), A new automated monitor for the measurement of particulate carbon in the atmosphere, in Proceedings of the U.S. EPA and Air & Waste Management Association Conference on Particulate Matter: Health and Regulatory Issues, Bhardwaja, P. J. (ed.), Air & Waste Management Association, Pittsburgh.

Russell, L. M. (2003), Aerosol organic-mass-to-organic-carbon ratio measurements, Environmental Science & Technology, 37(13), 2982-2987, 10.1021/es026123w.

Russell, L. M., Bahadur, R., and Ziemann, P. J. (2011), Identifying organic aerosol sources by comparing functional group composition in chamber and atmospheric particles, Proceedings of the National Academy of Sciences of the United States of America, 108(9), 3516-3521, 10.1073/pnas.1006461108.

Ruthenburg, T. C., Perlin, P. C., Liu, V., McDade, C. E., and Dillner, A. M. (2014), Determination of organic matter and organic matter to organic carbon ratios by infrared spectroscopy with application to selected sites in the IMPROVE network, Atmospheric Environment, 86, 47-57, 10.1016/j.atmosenv.2013.12.034.

Samoli, E., Atkinson, R. W., Analitis, A., Fuller, G. W., Green, D. C., Mudway, I., Anderson, H. R., and Kelly, F. J. (2016), Associations of short-term exposure to traffic-related air pollution with cardiovascular and respiratory hospital admissions in London, UK, Occupational and Environmental Medicine, 73(5), 300-307, 10.1136/oemed-2015-103136.

Schauer, J. J., Mader, B. T., Deminter, J. T., Heidemann, G., Bae, M. S., Seinfeld, J. H., Flagan, R. C., Cary, R. A., Smith, D., Huebert, B. J., Bertram, T., Howell, S., Kline, J. T., Quinn, P., Bates, T., Turpin, B., Lim, H. J., Yu, J. Z., Yang, H., and Keywood, M. D. (2003), ACE-Asia intercomparison of a thermal-optical method for the determination of particle-phase organic and elemental carbon, Environmental Science & Technology, 37(5), 993-1001, 10.1021/es020622f.

Schichtel, B. A., Hand, J. L., Barna, M. G., Gebhart, K. A., Copeland, S., Vimont, J., and Malm, W. C. (2017), Origin of fine particulate carbon in the rural United States, Environmental Science & Technology, 51(17), 9846–9855, 10.1021/acs.est.7b00645.

Schichtel, B. A., Malm, W. C., Bench, G., Fallon, S., McDade, C. E., Chow, J. C., and Watson, J. G. (2008), Fossil and contemporary fine particulate carbon fractions at 12 rural and urban sites in the United States, J. Geophys. Res., 113(D02311), doi:10.1029/2007JD008605.

Schmid, H., Laskus, L., Abraham, H. J., Baltensperger, U., Lavanchy, V., Bizjak, M., Burba, P., Cachier, H., Crow, D., Chow, J., Gnauk, T., Even, A., ten Brink, H. M., Giesen, K. P., Hitzenberger, R., Hueglin, C., Maenhaut, W., Pio, C., Carvalho, A., Putaud, J. P., Toom-Sauntry, D., and Puxbaum, H. (2001), Results of the "carbon conference" international aerosol carbon round robin test stage I, Atmospheric Environment, 35(12), 2111-2121, 10.1016/s1352-2310(00)00493-3.

Sharma, S., Brook, J. R., Cachier, H., Chow, J., Gaudenzi, A., and Lu, G. (2002), Light absorption and thermal measurements of black carbon in different regions of Canada, Journal of Geophysical Research-Atmospheres, 107(D24), 10.1029/2002jd002496.

Strader, R., Lurmann, F., and Pandis, S. N. (1999), Evaluation of secondary organic aerosol formation in winter, Atmospheric Environment, 33(29), 4849-4863, 10.1016/s1352-2310(99)00310-6.

Subramanian, R., Khlystov, A. Y., and Robinson, A. L. (2006), Effect of peak inert-mode temperature on elemental carbon measured using thermal-optical analysis, Aerosol Science and Technology, 40(10), 763-780, 10.1080/02786820600714403.

Takahama, S., Dillner, A. M., Weakley, A. T., Reggente, M., Burki, C., Lbadaoui-Darvas, M., Debus, B., Kuzmiakova, A., and Wexler, A. S. (2019), Atmospheric particulate matter characterization by Fourier transform infrared spectroscopy: a review of statistical calibration strategies for carbonaceous aerosol quantification in US measurement networks, Atmospheric Measurement Techniques, 12(1), 525-567, 10.5194/amt-12-525-2019.

Takahama, S., Johnson, A., and Russell, L. M. (2013), Quantification of carboxylic and carbonyl functional groups in organic aerosol infrared absorbance spectra, Aerosol Science and Technology, 47(3), 310-325, 10.1080/02786826.2012.752065.

Tanner, R. L. (1982), An ambient experimental-study of phase-equilibrium in the atmospheric system - Aerosol H+, NH4+,SO4(2-), NO3--NH3(G), HNO3(G), Atmospheric Environment, 16(12), 2935-2942, 10.1016/0004-6981(82)90044-0.

US EPA (2000), Quality Assurance Project Plan: $PM_{2.5}$ Speciation Trends Network Field Sampling, U. S. E. P. Agency, Office of Air Quality Planning and Standards, Research Triangle Park, NC 27711, EPA-454/R-01-001.

Venkataraman, C., Reddy, C. K., Josson, S., and Reddy, M. S. (2002), Aerosol size and chemical characteristics at Mumbai, India, during the INDOEX-IFP (1999), *Atmospheric Environment*, *36*(12), 1979-1991, 10.1016/s1352-2310(02)00167-x.

Watson, J. G., Chow, J. C., and Chen, L. W. A. (2005), Summary of organic and elemental carbon/black carbon analysis methods and intercomparisons, *Aerosol and Air Quality Research*, *5*(1), 65-102, 10.4209/aaqr.2005.06.0006.

Watson, J. G., Chow, J. C., Lowenthal, D. H., Pritchett, L. C., Frazier, C. A., Neuroth, G. R., and Robbins, R. (1994), Differences in the carbon composition of source profiles for diesel-powered and gasoline-powered vehicles, *Atmospheric Environment*, *28*(15), 2493-2505, 10.1016/1352-2310(94)90400-6.

Weakley, A. T., Takahama, S., Wexler, A. S., and Dillner, A. M. (2018), Ambient aerosol composition by infrared spectroscopy and partial least squares in the chemical speciation network: Multilevel modeling for elemental carbon, *Aerosol Science and Technology*, *52*(6), 642-654, 10.1080/02786826.2018.1439571.

White, W. H., Trzepla, K., Hyslop, N. P., and Schichtel, B. A. (2016), A critical review of filter transmittance measurements for aerosol light absorption, and de novo calibration for a decade of monitoring on PTFE membranes, *Aerosol Science and Technology*, *50*(9), 984-1002, 10.1080/02786826.2016.1211615.

White, W. H. (2017), The Dance of Carbon, Iron, and Light Absorption. Presented at the IMPROVE Steering Committee Meeting in Ely Minnesota, http://vista.cira.colostate.edu/improve/wp-content/uploads/2017/11/13_White-Ely_Oct-2017.pdf

White, W.H., J.A. Giacomo, N.P. Hyslop, L.M. Kline, K. Trzepla, Verifying Multi-Decadal Consistency of Light-Absorption Measurements in a Filter-Based Haze Monitoring Network, AGU Winter Meeting, San Francisco, 11 December 2019.

Yang, H., and Yu, J. Z. (2002), Uncertainties in charring correction in the analysis of elemental and organic carbon in atmospheric particles by thermal/optical methods, *Environmental Science & Technology*, *36*(23), 5199-5204, 10.1021/es025672z.

Yu, J. Z., Xu, J. H., and Yang, H. (2002), Charring characteristics of atmospheric organic particulate matter in thermal analysis, *Environmental Science & Technology*, *36*(4), 754-761, 10.1021/es015540q.

Appendix A

Relating HIPS Filter Absorption to TOR Light Absorbing Carbon

William Malm

If measurements of filter absorption (fabs) and TC are to replace the current TOR OC–LAC system, it is essential that the relationships between fabs and LAC and fabs and ambient absorption and the wavelength dependence of fabs are understood and quantified. In this appendix, only the relationship between fabs and LAC is explored and quantified. To accomplish this, the contributions of iron oxides to fabs as well as filter loading artifacts in the fabs and TOR LAC values need to be assessed.

Filter Loading Effect on fabs

Filter absorption measurements made using transmission-based instruments can suffer from filter loading artifacts. Heavy deposits of absorbing particles on filters can "shadow" other absorbing particles, while scattering particles can increase the reflectance of incident light. Both effects would cause an underestimation in the fabs measurement. On the other hand, increased light scattering by particles could increase the absorption by LAC. These are well-known artifacts (e.g., Bond et al., 1999), and various methods are used to reduce them. The measurement of both reflectance and transmittance by HIPS reduces but may not eliminate these effects (Bond et al., 1999).

White (personal communication, 2021) assessed the potential loading artifacts on the HIPS measurement in several analyses and experiments. In one assessment, fabs measurements from collocated IMPROVE and CSN samplers were compared. CSN samplers use a larger filter and lower flow rate than IMPROVE, and the resulting sample deposits on the CSN filters were more than a factor of 10 lower. The ratio of the CSN to IMPROVE fabs data as a function of IMPROVE filter absorption optical depth, (τ_{abs}) is presented in Figure A1. As shown, at τ_{abs} somewhere below 0.5 to 0.4, the ratios have high variability due to large errors but are scattered around the one-to-one line, indicating little to no bias in either measurement. However, at τ_{abs} above 0.4 to 0.5, there is a decreasing trend in the ratio. This trend indicates that the more heavily loaded IMPROVE filters have a negative loading artifact, and fabs data at τ_{abs} ~1.0 are underestimated by more than 30%. A τ_{abs} of 0.5 is equivalent to fabs of about 1.5 Mm^{-1}.

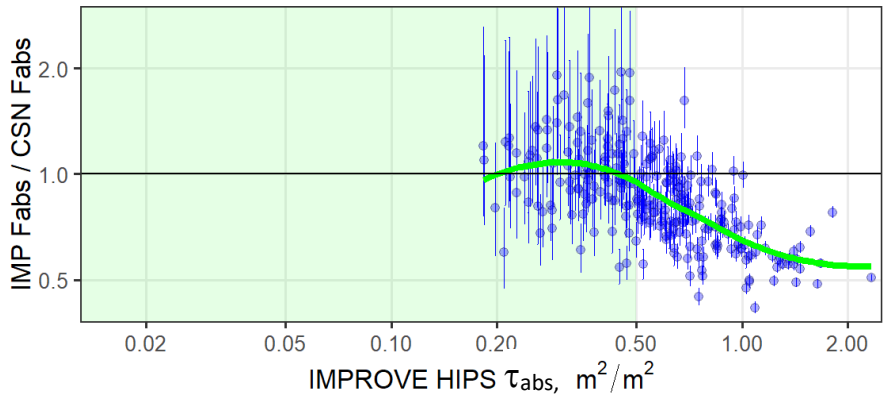

Figure A1. Ratio of fabs measured by collocated IMPROVE and CSN samplers as a function of the filter absorption optical depth, τ_{abs}, measured on the IMPROVE filters. The trend in the data is visualized by the green smooth curve, which is an unweighted fit by the LOESS function from the R STATS package. Error bars represent measurement error in the ratios. (White 2020, personal communication)

Comparison of TOR LAC to fabs

The HIPS instrument is calibrated to 0 absorption while the TOR LAC is not. Figure A2 is a plot of the ratios of the TOR LAC to fabs values for three time periods against the filter absorption optical depth, τ_{abs} (White, personal communication, 2020). As shown, the ratio is relatively constant across the range of τ_{abs}, but below τ_{abs} = 0.1, the ratio increases by a factor of 2. It is unlikely that such a change is due to atmospheric changes in the aerosol absorption properties and may be indicative of low TOR LAC concentrations being biased high. Also shown in Figure A2 is an increase in the TOR LAC/fabs ratio at high τ_{abs}. This is further evidence of fabs being biased low due to a filter loading effect.

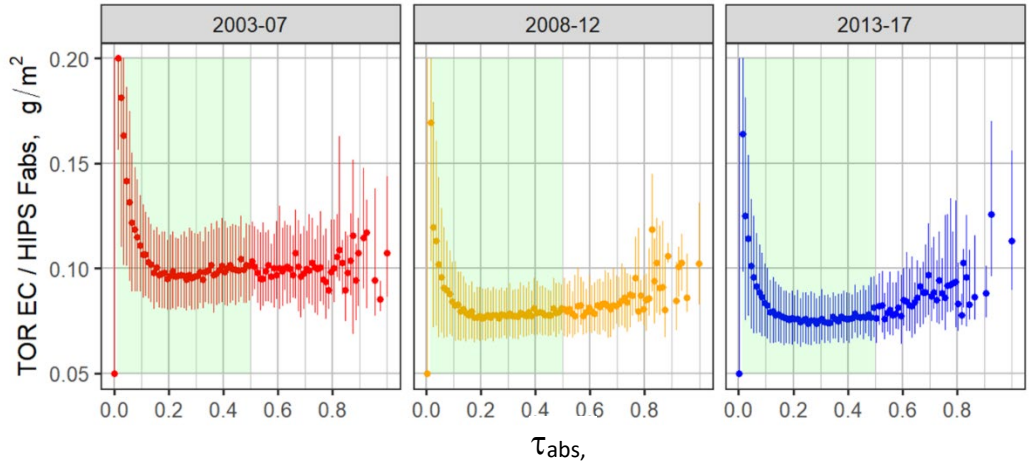

Figure A2. Ratio of TOR LAC to HIPS fabs vs. the filter absorption optical depth, τ_{abs}, for three time periods, 2003–2007, 2008–2012, and 2013–2017. Data from all IMPROVE sites with at least 50 samples in all three time periods were used (White, personal communication, 2020).

Contribution of Fe to fabs

In the following discussion, TOR LAC is referred to as just LAC. From an RHR perspective, it is the contribution of LAC to ambient babs that is of interest. So, a first step in using fabs to represent babs or LAC is to correct fabs for Fe absorption.

White et al. as well as others have shown that Fe contributes to light absorption in the atmosphere and thus to fabs. Therefore, it is assumed that the fabs is a linear combination of contributions from LAC and Fe, such that

$$fabs_i = a_1 LAC_i + a_2 Fe_i \qquad \text{(A1)}$$

where i refers to the i^{th} sample, and a_1 and a_2 are the MAE efficiencies of LAC and Fe, respectively. The coefficients a_1 and a_2 in equation A1 can be estimated using linear regression models such as OLS. Applying equation A1 to a dataset where fabs and LAC are not exactly linearly related to each other will result in a weighted average relationship between cfabs and LAC and Fe. Furthermore, OLS regressions are unduly influenced by larger values. LAC concentrations on the average are more than an order of magnitude greater than Fe concentrations, and the magnitude of a_2 may be artificially suppressed, which results in an underestimation or undetermined Fe MAEs.

The unequal weighting in the regression analysis can be reduced by normalizing the fabs and Fe values by the LAC concentrations, transforming equation A1 to

$$\frac{fabs_i}{LAC_i} = a_1 + a_2 \frac{Fe_i}{LAC_i}. \qquad \text{(A2)}$$

Solving equation A2 using an OLS-type regression gives greater weight to filter samples with high relative contributions from Fe to fabs and thus more-stable a_1 coefficients, i.e., FeMAE. In equation A2, a_1 is now an intercept term that corresponds to an average MAE when Fe concentrations are near zero. This is equivalent to the MAE for fabs being corrected for Fe contributions and will be referred to as cfabsMAE.

Although there are currently 157 monitoring sites in IMPROVE, only 136 sites with the most complete records, shown in Figure A3, will be used in the following analysis. The data from these sites are available on the IMPROVE web site at http://vista.cira.colostate.edu/improve/.

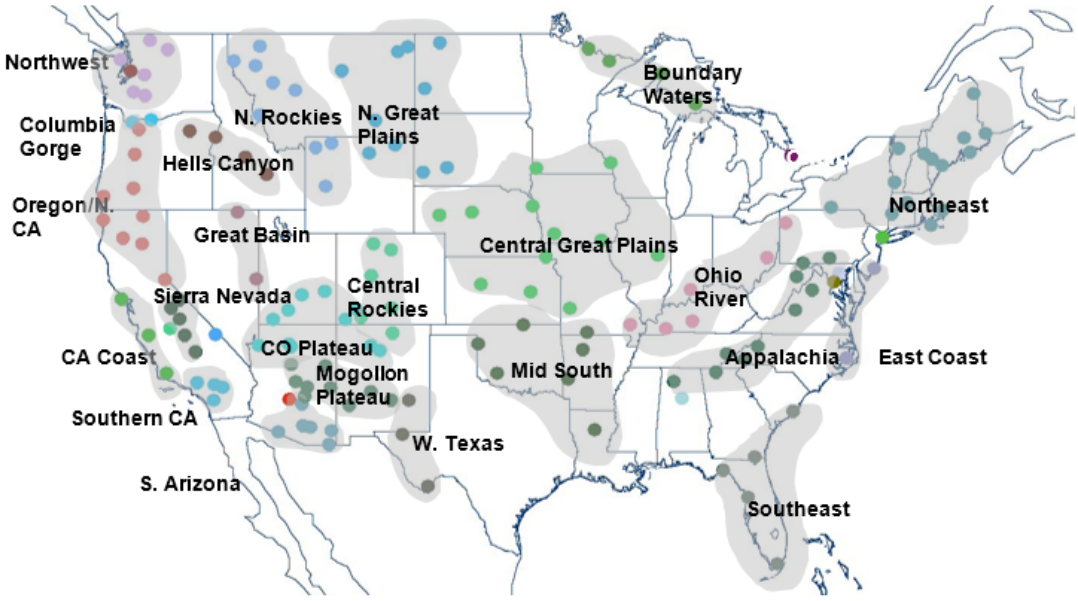

Figure A3. Map showing locations of IMPROVE monitoring sites as well as the grouping of the sites into regions.

The 136 monitoring sites used in this analysis and operating in the IMPROVE network during 2008–2018 were grouped into 23 regions (Malm et al., 2002; Hand et al., 2012). The regions were selected based upon topography and the expected spatial extent of fine aerosols. The groupings were further refined by examining the individual monthly aerosol composition patterns for each site within a region.

Figure A4 shows a plot of fabs/LAC versus Fe/LAC for 9 years of data for the Mid-South region. The slope of the line, as stated above, is the FeMAE, while the intercept is cfabsMAE. For this case, FeMAE is 4.7±0.05 m^2/gm, while cfabsMAE is 12.2±0.08 m^2/gm.

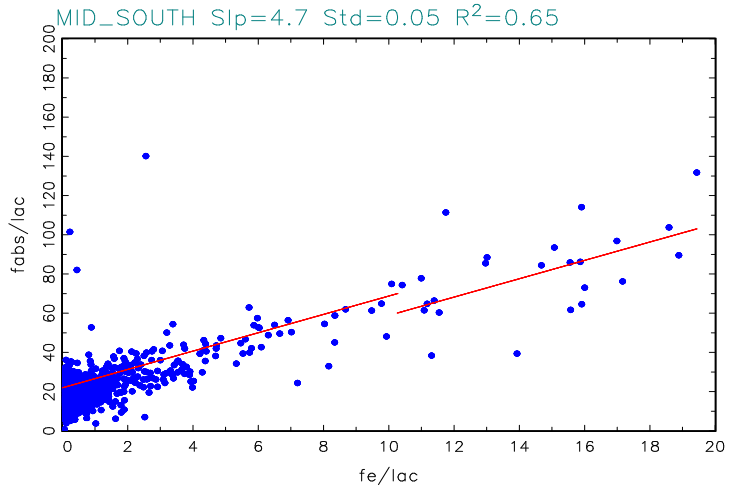

Figure A4. Scatter plot of fabs/LAC vs. Fe/LAC.

Figure A5 is a plot of a_1 and a_2 derived from an OLS regression analysis using equation A2 for each of the 23 regions. The right-hand axis shows a_1 values, i.e., cfabs/LAC or cfabsMAE, represented by blue bars, while the left-hand axis shows a_2 values, i.e., cfabs/Fe or FeMAE, represented by enclosed circles. Cfabs/Fe (FeMAE) values for the Northeast, East Coastal,

Boundary Waters, Northern Rockies, and Northeast regions are not shown because of very few elevated Fe/LAC ratios resulting in very low R^2 values and meaningless regression coefficients.

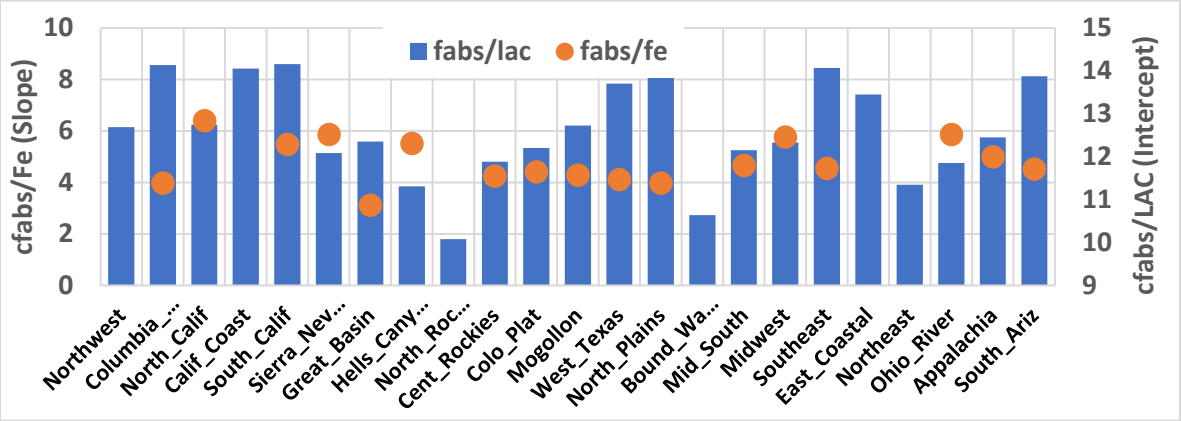

Figure A5. Plot of cfabs/LAC as blue bars and fabs/Fe as orange filled circles. Right axis is cfabs/LAC while the left axis represents fabs/Fe.

The FeMAE varies between 3.5 and 6.4 m^2/gm with an average of 4.8±0.88 m^2/gm. The term cfabs/LAC varies from a low of 10.1 m^2/gm in the Northern Rockies region to the highest values near 14 m^2/gm in the Southern California, California Coast, Northern Plains, Southeast, West Texas, and Columbia River Gorge regions. The average cfabsMAE is 12.6±1.17 m^2/gm. The regressions discussed above assume a linear relationship between cfabs and LAC.

Is the Relationship between cfabs and LAC Linear and Constant across CONUS?

In the following analysis, fabs has been corrected (cfabs) for Fe absorption by assuming an FeMAE of 5 m^2/gm and using

$$Cfabs = fabs - 5.0 \times Fe. \quad (A3)$$

Figure A6 shows a scatter plot of cfabs versus LAC for the Ohio River region for all daily data collected from 2008 through 2015. A regression model between cfabs and LAC can be formed using the relationship

$$cfabs_i = a_o + a_1 \times LAC_i \quad (A4)$$

where i refers to the i^{th} observation and cfabs is defined in equation A3.

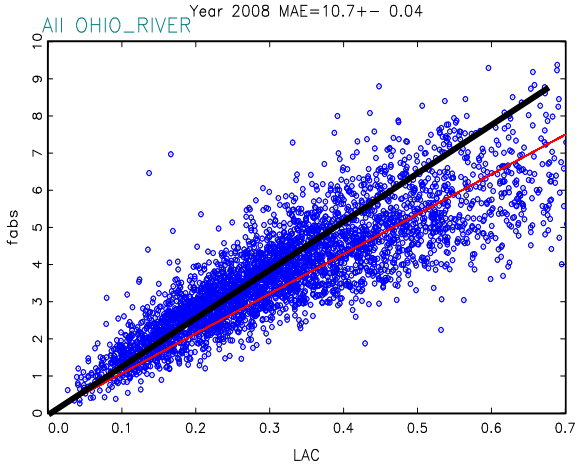

Figure A6. Scatter plot of cfabs vs. LAC for the Ohio River valley region. Units for LAC are $\mu g/m^3$, and cfabs units are Mm^{-1}. Black line represents an OLS regression line between the two variables for LAC concentrations <0.3 $\mu g/m^3$, while the red line is an OLS regression line for all data.

The red line in Figure A6 corresponds to an OLS regression between cfabs and LAC with the intercept set equal to zero, and the black line is an OLS regression between the same variables but only for LAC values <0.3 $\mu g/m^3$. If the fabs is linearly related to LAC and Fe as defined in equations A1 and A2, then a_o in equation A4 should be zero. This implies that the MAE is approximately constant with little spatial and temporal variability.

The slope of the OLS line represented by the regression coefficient between cfabs and LAC shows an estimation of the corrected filter MAE (cfabsMAE = Δcfabs/ΔLAC). The slope for all the data in Figure A6 is 10.4 m^2/gm. The slope of the data points corresponding to LAC < 0.3 $\mu g/m^3$ is 13.1 m^2/gm. Figure A6 clearly shows that there is a nonlinear relationship between cfabs and LAC, with the cfabs/LAC ratio deceasing as LAC increases. With the intercept set equal to zero, lower LAC concentration data points are biased above the OLS line, while higher values are biased below the regression line. For the most part, under lower concentrations (LAC < 0.3 $\mu g/m^3$), the relationship between cfabs and LAC is approximately linear with an intercept approaching zero.

Another way to show the nonlinearity between cfabs and LAC is to implement an OLS regression allowing for an intercept. Figure A7 shows the OLS regression line with a slope of 8.2±0.08 m^2/gm and an intercept of 1.16±0.03 Mm^{-1}. With an intercept term, the OLS regression line is weighted toward the higher cfabs and LAC values, which results in a lower cfabsMAE. The slope of LAC levels below 0.3 $\mu g/m^3$, as shown above, is 13.1 m^2/gm.

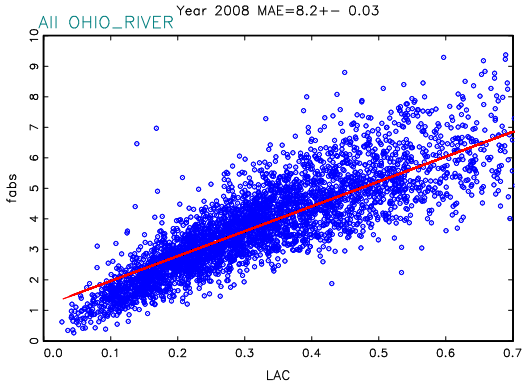

Figure A7. Same data as in Figure A6, but the OLS regression line in red was not fit through zero.

OLS regressions between cfabs and LAC were conducted for all data in each of the 23 regions in Figure A3 for 2008–2015. Figure A8 is a plot of the OLS intercept term as a function of the average LAC concentrations in each region. As the average LAC concentrations decrease, the intercept tends toward zero, implying a more linear relationship between the two variables at low concentrations of LAC, which is consistent with Figure A6. Figure A9, a scatter plot of cfabs versus LAC for the Great Basin region, is an example of where the intercept term is near zero and there is a near-linear relationship between the two variables.

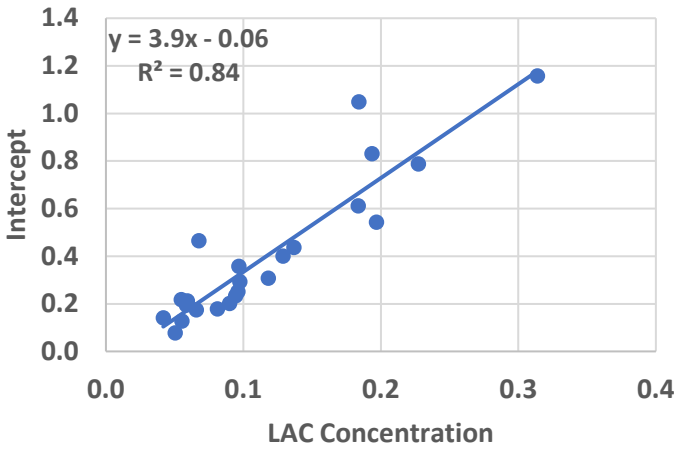

Figure A8. Intercept term vs. average LAC concentrations from the OLS regression between cfabs and LAC data for all IMPROVE sites in one of the 23 regions defined in Figure A3, using data from 2008 through 2018.

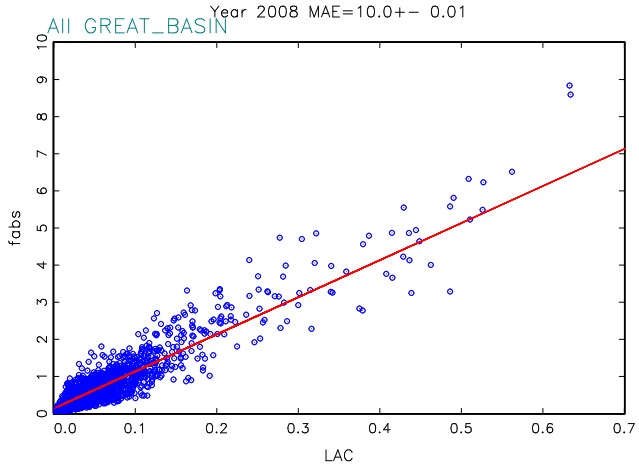

Figure A9. Scatter plot of cfabs vs. LAC for the Great Basin region using all data from 2008 through 2018.

Figure A10 is a plot of the OLS regression slope (cfabsMAE) as a function of the intercept term for each of the 23 regions. As the intercept approaches zero, the slope, on the average, approaches 11 as indicated by the regression equation of cfabsMAE = 11.0 - 2.28 × Intercept.

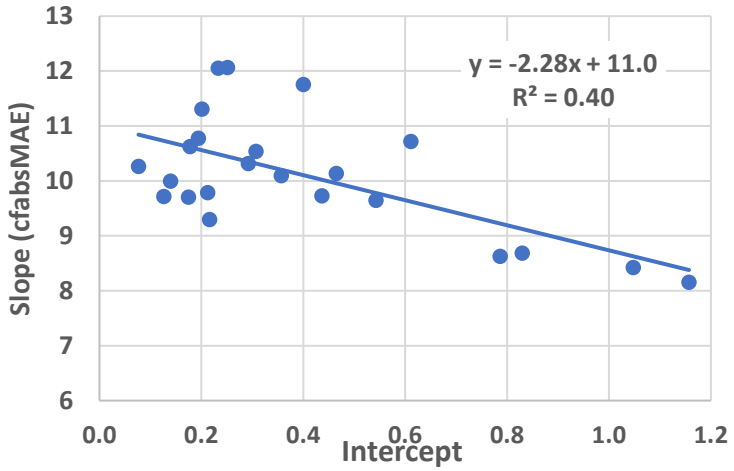

Figure A10. Scatter plot of the OLS regression slope (cfabsMAE) and the intercept term for each of the 23 regions using 2008–2018 data.

The correlation between the slope and intercept term and LAC concentration is generally continuous across all regions of CONUS and suggests possible underlying analytic artifacts in the measurement systems or possibly a similarity in chemical and optical characteristics of the absorbing aerosols across most of CONUS. At lower concentrations of LAC, cfabsMAE is elevated compared to higher concentrations. However, even at lower values of the intercept term, the implied cfabsMAE varies from a low of about 9 m^2/gm to a maximum near 12 m^2/gm.

A nonlinear equation that better describes the relationship between cfabs and LAC is given by

$$cfabs = a_o(1 - e^{-LAC}). \quad \text{(A5)}$$

Equation A5 can be approximated using a Maclurin series expansion as

$$cfabs = a_o\left(LAC - \frac{LAC^2}{2!} + \frac{LAC^3}{3!} \ldots\ldots\ldots\ldots\ldots\ldots\ldots\right). \quad \text{(A6)}$$

Under low LAC concentrations, equation A6 reduces to cfabs = cfabsMAE × LAC, and for higher concentrations, the higher-order terms in equation A6 attenuate the cfabs/LAC relationship and effectively adjust for the nonlinearity between cfabs and LAC. Figure A11 shows the same data as presented in Figures A5 and A6 but using equation A5 to optimize the relationship between cfabs and LAC. In Figure A11, a_o = 13.86±0.05, which is close to the linear regression line of 13.1 m^2/gm when LAC numbers were constrained to be <0.3 µg/m^3.

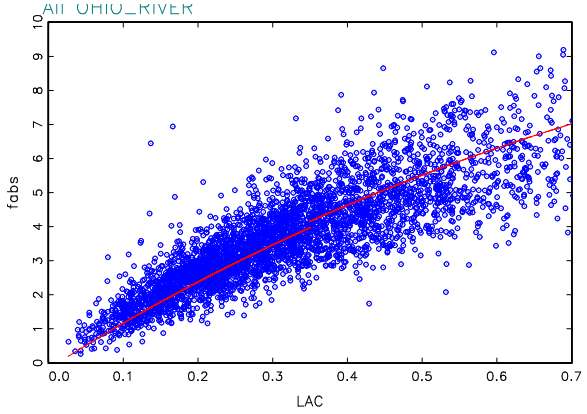

Figure A11. Scatter plot of cfabs vs. LAC for the Ohio River valley region. Units for LAC are µg/m^3 and cfabs units are Mm^{-1}. Red line is the OLS regression of equation A5 to the data.

The relationship between cfabs and LAC shown in Figure A11 is similar for most regions of CONUS. Figure A12 shows a_o values, which can be interpreted as cfabsMAE for low LAC concentrations for each of the 23 regions of CONUS, as filled circles; a filled circle corresponding to 12 m^2/gm is shown for reference. The lower a_o values of around 12 occur at the Colorado Plateau, Great Basin, Northern California-Oregon, and Idaho regions, where LAC levels are lowest, while the four highest a_o values are found in the Columbia River Gorge, Southern California, West Texas, and Southeast regions.

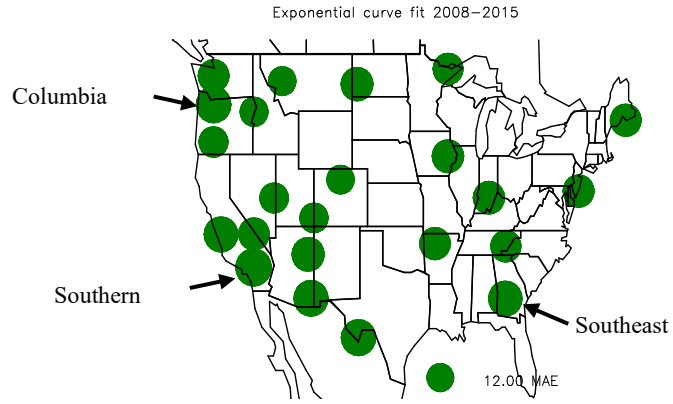

Figure A12. a_o for the fit of equation A5 to the cfabs and LAC data in each of the 23 regions defined in Figure A3 for 2008–2018.

The spatial variability of fabsMAE over CONUS is further highlighted in Figure A13 where the derived fabsMAE using two of the methods described above are compared. The methods are the OLS regressions defined in equation A4 with the intercept set equal to zero and a_o from the fit to the exponential function in equation A5. The average fabsMAE values derived using equation A4 are the weighted averages of the fabsMAE over the entire range of fabs and LAC values and are lower than a_o from the exponential fit, which is weighted toward lower fabs and LAC values.

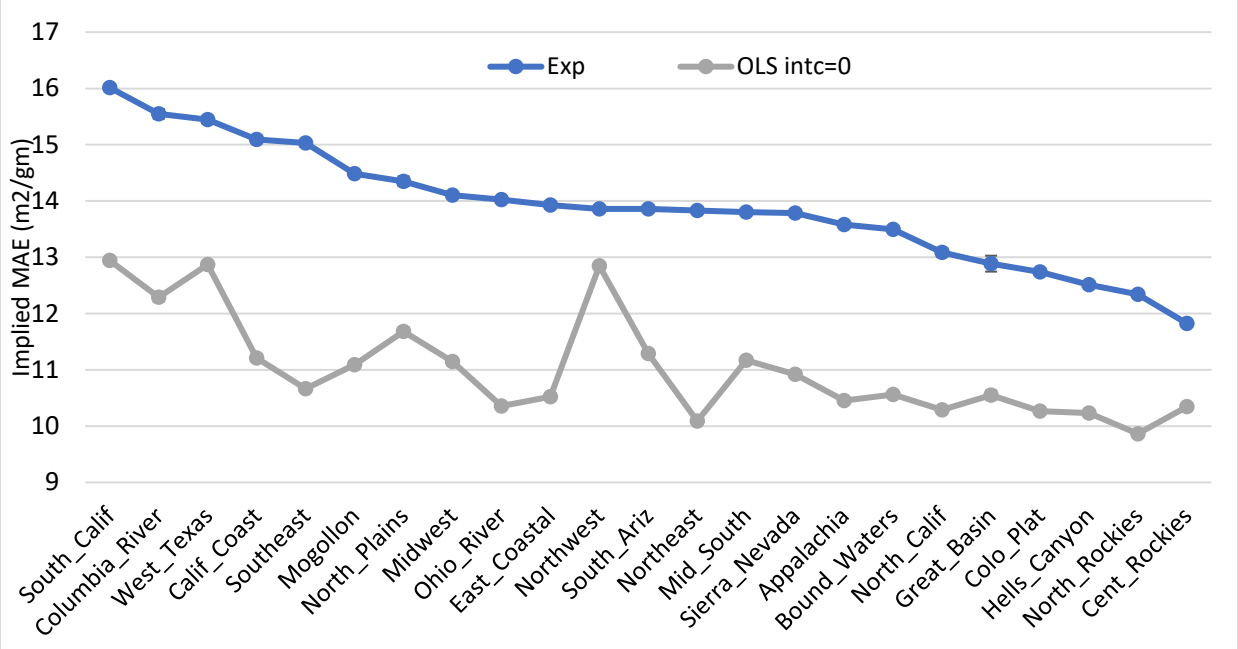

Figure A13. Derived cfabsMAE for the 23 regions across the United States. Exp is the a_o term from the fit of the exponential curve in equation A5; cfabs/LAC is the a_1 term in the linear OLS regression defined in equation A2; and OLS intc = 0.

The average of fabsMAE over the 23 regions for the two techniques is 13.9±1.06 and 11.03±0.92 m^2/gm, respectively. The MAEs calculated using the exponential fit reflect low LAC concentrations and are remarkably stable with 19 of 23 regions within about 14±10%. The included uncertainty bars for each datapoint are the standard errors associated with the respective regression coefficients that represent the estimated fabsMAE values and in most cases are so small they do not show up in the data plot.

Interestingly, the variability in estimated cfabsMAE associated with the two techniques across the 23 sites is about the same with commiserate standard deviations of about one. The correlation between the two techniques is high at >0.70. The difference between the highest and lowest fabsMAE values is about 4 m^2/gm for the two estimation techniques, which is well above the estimated uncertainties.

If fabsMAE values were approximately constant across the range of LAC concentrations and spatially invariant over CONUS, then the decrease in the ratio, cfabs/LAC, as a function of LAC concentrations suggests that either fabs is underestimated as filter loading increases or that LAC is overestimated. As discussed, fabs has a known filter loading artifact and is underestimated at higher fabs and LAC loadings, which would explain at least some of the cfabs/LAC to LAC relationship.

A potential additional contribution to the change in the ratio is the variability in the composition of the carbonaceous aerosols. The sources of the carbonaceous aerosols vary widely across CONUS. In the western mountainous regions, much of the LAC is associated with fire activity, in more-urban areas transportation is a source of carbonaceous aerosols, and in the eastern United States biogenic emissions play a large role in the formation of organic aerosols (Schichtel et al., 2017). Because of the highly varied molecular form of carbonaceous aerosols as both a function of source types and aging, the MAE of LAC may indeed decrease as LAC concentrations increase and may vary across CONUS.

Further Exploration of fabsMAE as a Function of LAC Concentration

To further explore how the cfabs/LAC ratio varies as a function of LAC concentration, the 2008–2018 cfabs-LAC data in each of the 23 regions were first sorted by cfabs then divided into deciles, i.e., ten groups each containing 10% of the data, then averaged together. In Figure A14, the 11-year average LAC and cfabs values for each region were plotted against each other for each decile. In each graph in Figure A14, the title is labeled with the cfabs decile used to group and average the data together.

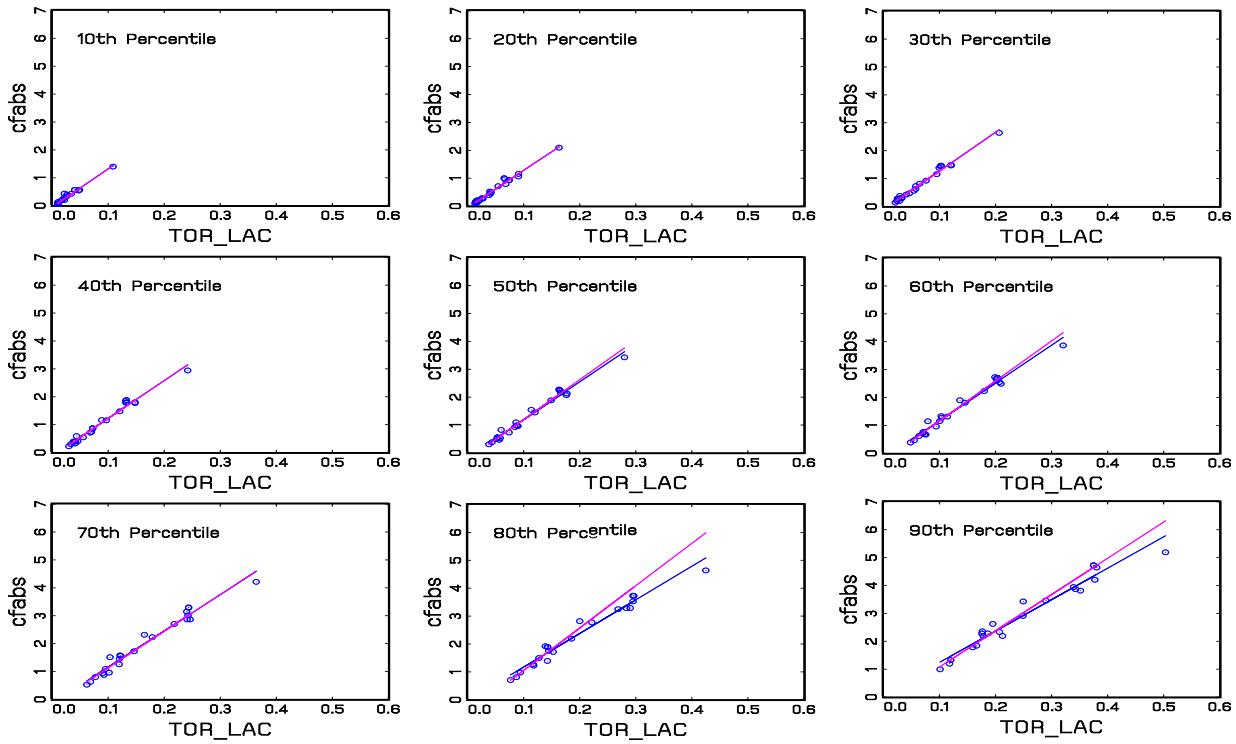

Figure A14. Average cfabs and LAC values for the 23 regions in each decile of cfabs data. Data from 2008 through 2018 were used in the analysis. The magenta OLS regression line used data where the average cfabs was less than 3 Mm^{-1}. The blue OLS regression used all data in each decile.

Two OLS regressions were carried out for the data in each decile. The first regression used data where cfabs < 3 Mm^{-1}, which is plotted as the magenta line, and the second regression used all data, which is plotted as the blue line. The slopes of the regression lines are the average cfabsMAE over all of CONUS for the given decile. For the lower deciles, the cfabs < 0.3 Mm^{-1} regression lines are the same because no cfabs values exceed the 3 Mm^{-1} threshold.

In Figure A15, the derived cfabsMAEs for each decile are plotted for the two regression analyses. The error bars are the standard errors of the regression coefficients representing cfabsMAE values. As shown, the cfabsMAEs derived from data with cfabs < 3 Mm^{-1} are similar across the deciles. This implies that for these lower cfabs values, the cfabsMAEs are about the same for all of CONUS.

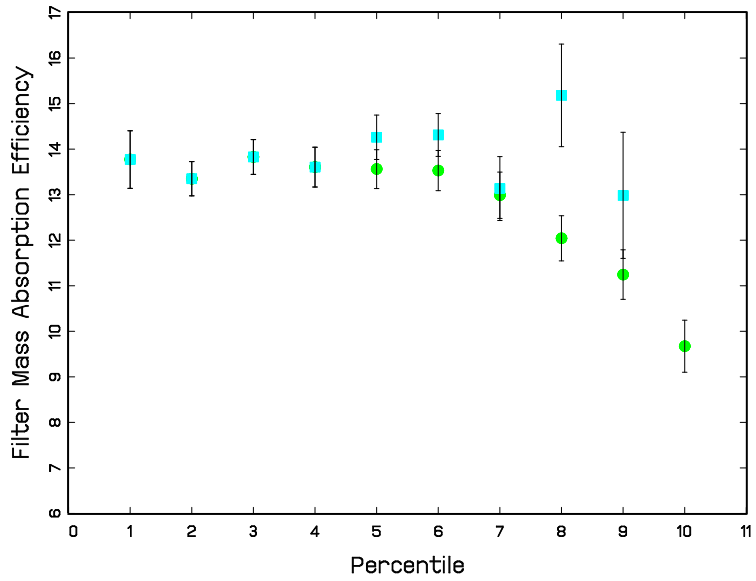

Figure A15. cfabsMAE derived from the regression analysis of the data in each cfabs decile of data in Figure A14. Green circles and cyan squares are the results of the OLS regression using all data and data with cfabs < 3 Mm^{-1} in each decile, respectively.

For the higher deciles where the average cfabs values in a number of regions exceed 3 Mm^{-1}, the ratio of cfabs to LAC decreases in a nonlinear fashion with increasing LAC concentrations. The average cfabsMAE is nearly constant up to the 60th percentile at 13.8±0.68 m^2/gm and decreases to 9.7±0.57 m^2/gm at the 90th decile. These results are consistent with the interpretation of the a_o term in equation A5 as the cfabsMAE of the lower cfabs values where the average CONUS-wide a_o term was 13.9±1.06 m^2/gm.

Notice also that at the higher deciles in Figure A14, the average cfabsMAE as represented by the regression line is systematically lower at very low cfabs values and higher at higher cfabs values. The observed nonlinearity between cfabs and LAC at higher and lower cfabs and LAC concentration values is consistent with Figures A1 and A2 where LAC is biased high relative to fabs at low concentrations, and at higher LAC concentrations, fabs is biased low because of filter loading effects.

Because of the highly varied molecular form of carbonaceous aerosols both as a function of source types and aging, the change in the cfabs/LAC ratio (cfabsMAE) as a function of LAC concentration could in part be real. The absorption efficiency of LAC may indeed decrease as LAC concentrations increase. A more aged, higher concentration LAC level may have a lower MAE.

Variability of cfabsMAE as a Function of Assumed FeMAE

Figure A16 shows a plot of the a_o coefficient in equation A5 as a function of LAC concentration for the 23 regions of CONUS. The blue dots represent an FeMAE of 3 m^2/gm and orange dots correspond to an FeMAE of 6 m^2/gm.

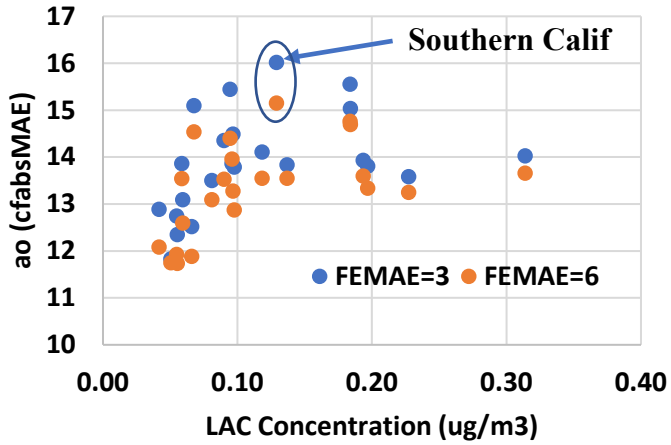

Figure A16. Regression coefficient a_o is the cfabsMAE for low LAC concentration derived from the exponential fit of LAC to cfabs using equation A5. Blue and orange dots are a_o derived assuming that the FeMAE = 3 and 6 m^2/g, respectively, for the 23 regions of CONUS.

First notice the difference in a_o as a function of assuming different FeMAE values. Increasing FeMAE reduces a_o but not by the same fraction in all regions. Increasing FeMAE adjusts cfabs down to a greater extent in regions where soil dust is higher.

Figure A17 shows the differences in a_o resulting by assuming values of FeMAE of 3 m^2/gm and 6 m^2/gm for the different regions of CONUS. The filled circles represent the magnitude of change of cfabsMAE resulting from the change in FeMAE of 3 to 6 m^2/gm; the legend shows the circle size for 1 m^2/gm. The effect of increasing FeMAE is greater in the Southwest and West in general than the eastern United States. It should be noted, however, that the increase in a_o is greatest in southern Arizona and New Mexico and the Mogollon Rim, Arizona. Southern California, Sierra Nevada, and West Texas have increased a_o values but less than those regions in Arizona. The regions with increased a_o values correspond to regions of CONUS with more-elevated levels of soil dust with corresponding levels of increased Fe concentrations.

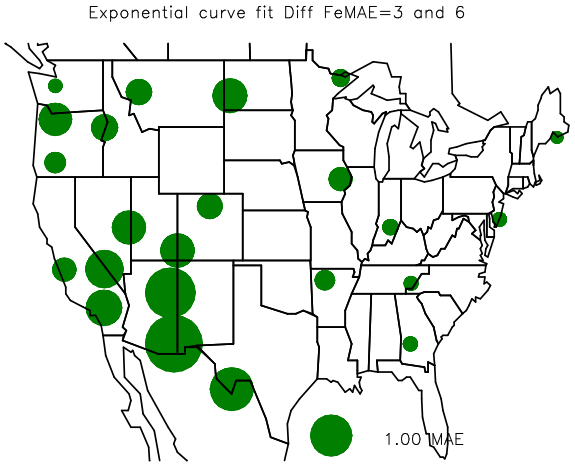

Figure A17. Differences in the a_o term from the fit of the exponential function between cfabs and LAC (equation A5) assuming FeMAE is equal to 3 and 6 m^2/gm. a_o can be loosely interpreted as cfabsMAE for cfabs < 3 Mm^{-1}.

Deviation from Estimate

The overarching goal of the above analysis is to use measurements of fabs to derive an estimate of LAC concentrations measured using IMPROVE TOR analysis. LAC derived from an fabs measurement is estimated using

fabsLAC = cfabs/cfabsMAE. (A7)

Average cfabsMAE values for each of the regions can be derived from OLS regression of cfabs against LAC data using various models as discussed above. Figure A18 is a scatter plot of measured LAC and LAC estimated from fabs using equation A7 where cfabsMAE was set to a constant 12 m^2/gm. The red line is the one-to-one line. The data are from all IMPROVE monitoring sites for 2008–2018. These data were sorted by the measured cfabs, and every 50 data points were averaged together, resulting in 4010 data points. A linear OLS regression of predicted LAC and measured LAC as the dependent and independent variables, respectively, has an $R^2 = 0.94$ with a slope of 0.76±0.003 and intercept of 0.27±0.0009, suggesting that the predicted LAC underestimates the measured concentrations. However, as shown in Figure A18, the agreement between the two variables is near the one-to-one line below about 0.5 $\mu g/m^3$. Above 0.5 $\mu g/m^3$, the ratio of the predicted to measured LAC decreases with increasing LAC concentration until about 1.5 $\mu g/m^3$, where the ratio remains relatively constant at about 0.6. The mean absolute deviation (MAD), normalized root mean square error (NRMSE), and average bias (AB), defined in Table A1, between the predicted and measured LAC are 0.041, 0.351, and -0.068, respectively.

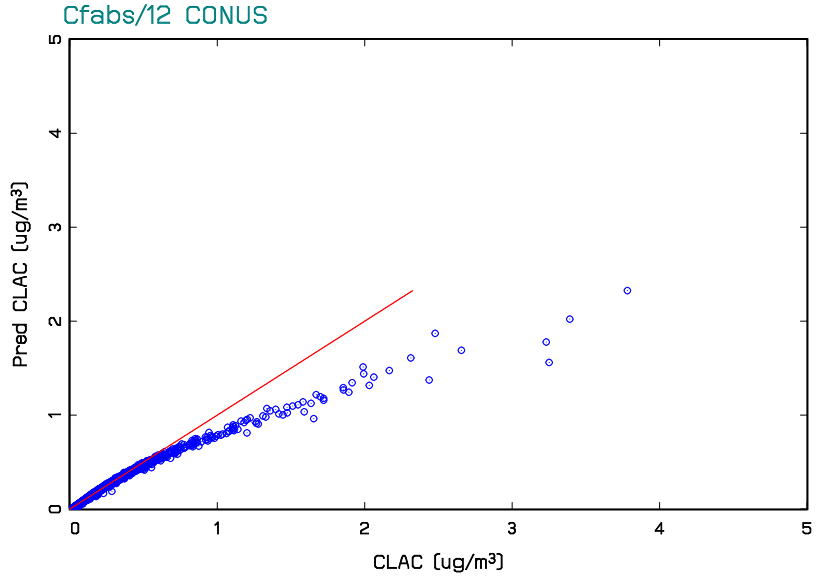

Figure A18. Scatter plot of measured LAC and predicted LAC where predicted LAC = cfabs/12. Red line is the one-to-one line. Data from all IMPROVE sites from 2008 to 2018 with a 50-point average were used.

Table A1. Performance statistics

Median of the absolute difference (MAD)	$median(\lvert P_i - M_i \rvert)/\bar{M}^*$
Normalized root mean square error (NRMSE)	$\sqrt{\frac{1}{N}\sum_{1}^{N}(P_i - M_i)^2}/\bar{M}$

Average bias (AB)	$= \frac{1}{N}\sum_{1}^{N}(P_i - M_i)/\bar{M}$

$* \bar{M} = \frac{1}{N}\sum_{1}^{N} M_i$

More-refined estimates of cfabsMAE as a function of LAC concentrations can be approximated using relationships between cfabs and LAC consistent with Figures A13 and A14. cfabsMAE is approximately constant for cfabs values less than about 3 Mm^{-1} and then decreases to <8 m^2/gm for cfabs > 8 Mm^{-1}. In the following analysis, the cfabsMAE is estimated using

cfabsMAE = fl × lightly + fh × heavy (A8)

where

$f_l = 1 - (cfabs - 3)/9$ (A9)

and

fh = 1 - fl. (A10)

fl and fh loosely refer to the fraction of filter aerosol material that corresponds to lightly loaded MAEs and more heavily loaded MAE values, respectively. Lightly and heavy refer to the cfabsMAE values for the lightly and more heavily loaded filters, respectively. When fl is greater than one, fl is set equal to one, and when fl becomes negative, fl is set to zero. cfabsMAE is then calculated as

cfabsMAE = fl × 12 + fh × 8. A11

The use of equations A9–11 will be referred to as the loading model. Figure A19 shows a scatter plot of TOR LAC and predicted LAC concentrations using the above equations. The data points correspond to the cfabs deciles for each of the 23 regions, resulting in 230 data points. All of CONUS and the entire range of LAC and fabs values found in each region are represented. The solid line is the one-to-one line, and an OLS regression between the two variables yields an R^2 of 0.98 and intercept of -0.003±0.0018 with a slope of 1.04±0.009. The MAD, NRMSE, and AB are 0.057, 0.11, and $2.7x10^{-6}$, respectively. The error bars in Figure A19 are plus and minus of the average NRMSE error associated with each data point of 0.11.

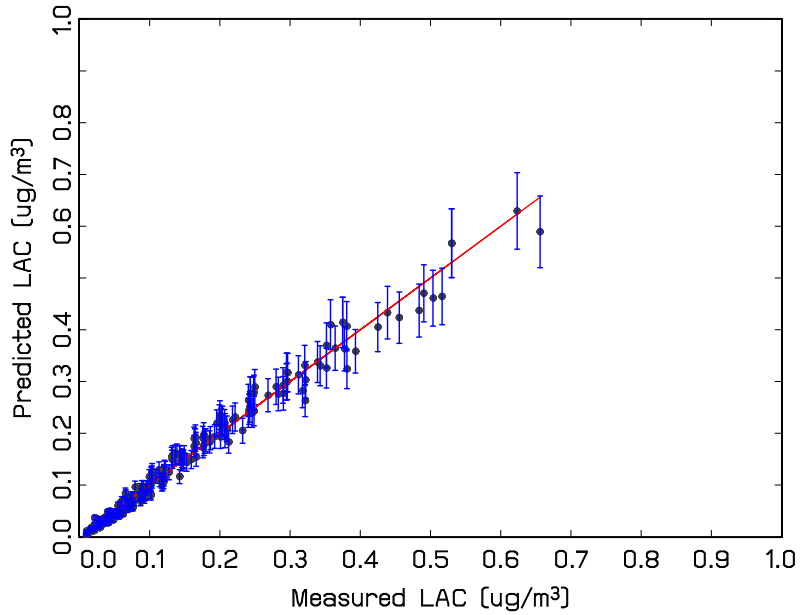

Figure A19. Scatter plot of measured and predicted LAC using the filter loading model. Each data point corresponds to one decile for each of the 23 regions. Red line is the one-to-one line.

Even though the agreement between measured and derived LAC from fabs data is very good, there are some biases evident in Figure A19. Predicted LAC values are biased a bit low below measured LAC concentrations of about 0.1 µg/m^3, and from about 0.1 µg/m^3 to 0.3 µg/m^3, the predicted concentrations are above the one-to-one line.

Figure A20a–b shows the same data presented in Figure A18 but with the more heavily loaded filters corrected for an apparent decrease in cfabsMAE. Equation A9, the fraction corresponding to lightly loaded filters, was replaced with $f_l = 1 - (fabs - 3)/12$, resulting in the scaling from fl to fh extending into higher fabs values. Figure A19a shows LAC concentrations plotted against cfabs levels, while A19b shows the same data but with LAC concentrations plotted against predicted LAC concentrations. In Figure A19a, the red line is the predicted cfabs as a function of LAC, while in Figure A20b it is the one-to-one line. The R^2 for Figure A20b is 0.98; the slope and intercept are 0.99±0.002 and 0.002±0.00006, respectively. The MAD, NRMSE, and AB values are 0.041, 0.139, and -0.017, respectively.

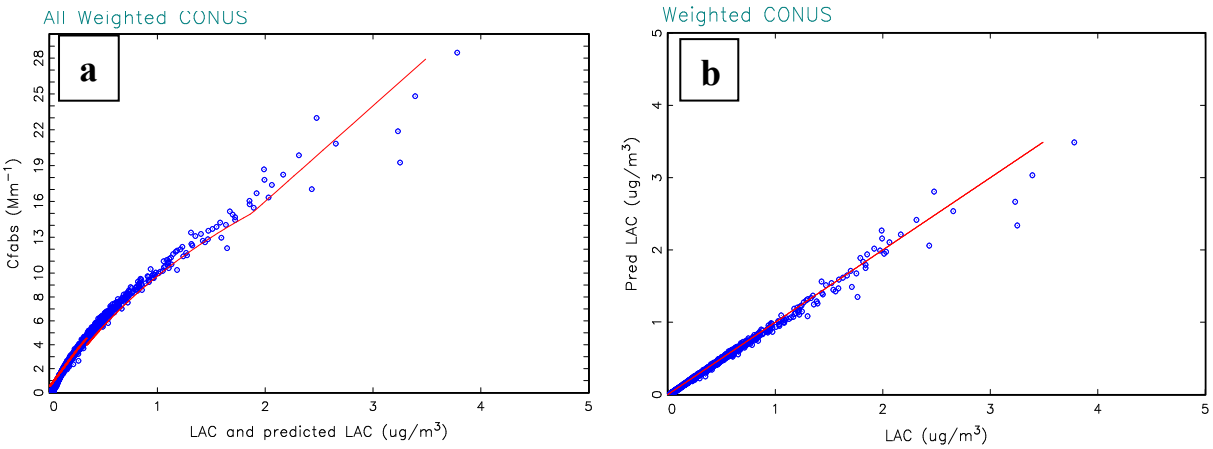

Figure A20. (a) Scatter plot of measured LAC vs. cfabs. Data are from all IMPROVE sites from 2008 to 2018 using a 50-point average. Red line represents predicted cfabs values using the filter loading model. (b) Scatter plot of measured LAC vs. predicted LAC using the filter loading model.

Figure A21 is a scatter plot of the same data shown in Figure A19 but without the 50-point averaging. Every 24-sample data point is shown. As before, the red line is the one-to-one line. An OLS regression with an intercept of zero between measured and predicted values yields an R^2 = 0.78 and a slope of 0.78±0.0009. The MAD, NRMSE, and AB values are 0.133, 0.856, and -0.018, respectively.

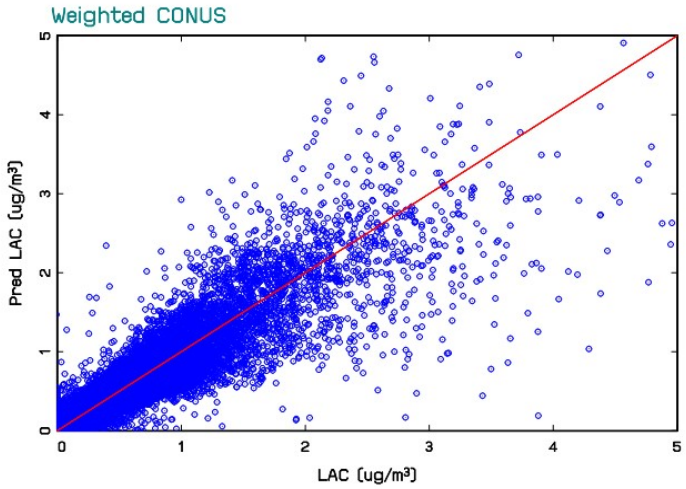

Figure A21. Scatter plot of measured vs. predicted LAC using the filter loading model. Data are from all IMPROVE sites from 2008 to 2018. Each data point is one 24-hour sample. The scatter plot contains 221487 data points.

Whereas the above analysis grouped data from all monitoring sites into one analysis, the following analysis will explore the average deviation of LAC values derived from fabs measurements using the aforementioned cfabsMAE model from measured LAC levels for each of the 23 regions independently. Any region-specific model will yield the smallest deviation between modeled and predicted LAC. However, it is desirable to use one model that best fits individual measurements for each of the monitoring sites. Figure A22 is a plot of the average deviation between observed LAC and fabs-derived LAC for three different models for 2008–2018. The blue bar is the weighted filter loading model, the gray bar refers to the exponential model with a_o = 13 for all regions as opposed to optimizing a_o to each region, and the orange bar refers to an assumed average cfabsMAE of 12 m^2/gm.

The exponential model with a constant a_o = 13 has an average deviation of 0.066±0.0098 with maximum deviations of about 0.25 and -0.08. The average deviation of the weighted filter loading model is -0.025±0.099, while for the constant cfabsMAE model it is -0.058±0.099. The weighted model varies from a maximum deviation of about 0.15 to a minimum of -0.20, while the constant cfabsMAE model varies from a maximum of about 0.12 to a minimum of -0.20. Southern California has the highest deviations for the weighted and exponential models, while the Central Rockies, Northern Rockies, and Hells Canyon regions have the most negative deviations.

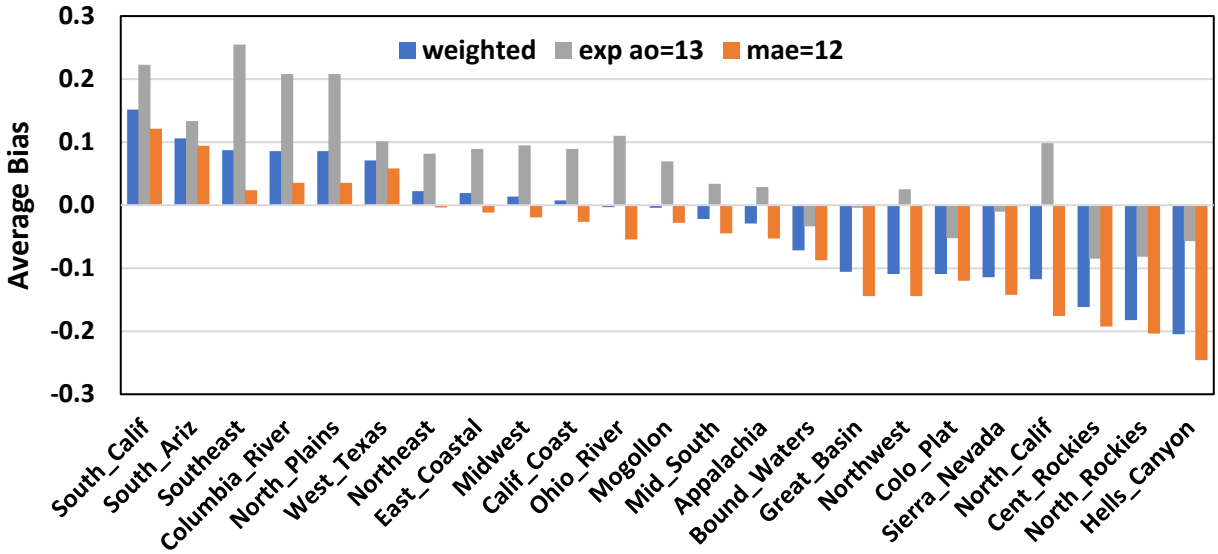

Figure A22. Average bias between measured LAC and LAC predicted using the weighted filter loading model, the exponential model with a_o = 13, and LAC = cfabs/12 for each of the 23 regions.

Figure A23 shows the NRMSE for the three models. The average NRMSE errors for the weighted filter loading and constant cfabsMAEs models are 0.79±0.68 and 0.82±0.73, respectively, while the exponential model with a_o = 13 has an NRMSE error of 1.19±0.62. The northwestern coastal regions have the largest NRMSE errors, at well over 2.0, while there is not a clear regional trend for regions with lower NRMSE values. The weighted model performs marginally better on a region by region and average basis.

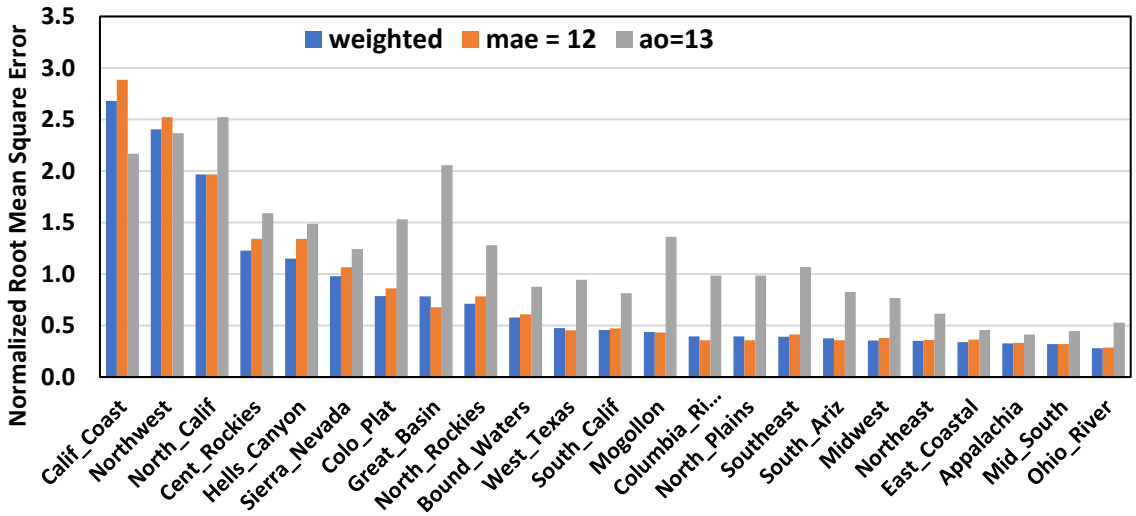

Figure A23. Normalized root mean square between measured LAC and LAC predicted using the weighted filter loading model, the exponential model with a_o = 13, and LAC = cfabs/12 for each of the 23 regions.

Appendix B

Scott Copeland

Introduction

This report details a number of statistical comparisons between OC and EC measurements determined by TOR, FTIR, and HIPS. In general, they considered intercomparability of the measurements, their relative biases and precisions. This appendix takes estimates of EC OC from each of the three techniques and examines how they affect the metrics used to track progress under the Regional Haze Rule with its revisions.

Methods

Annual means of the "most impaired days" and annual means on the "clearest" days are determined for each site and year that meets the RHR completeness criteria using the standard OC and EC by TOR. OC and EC were then also estimated from FTIR and by using TC and subtracting Cfabs/12, were Cfabs is corrected for iron concentrations as Cfabs=fabs-5*fe, where fe concentration is iron in ug/m3. Values below zero are set equal to zero.

FTIR OC and EC, and TC - Fabs derived OC and EC are determined after patching and substitution, but before calculating impairment. Therefore, sample days can move in and out of most impaired days. In general, the shift in days is driving the larger differences seen.

IMPROVE 2 Method:

Masses

OMC=1.8*(o1+o2+o3+o4+op)
LAC=e1+e2+e3-op

Extinctions

EOMC=2.8*Small_OMC
+6.1*Large_OMC
ELAC=10*LAC

Evaluation Method for TC-Fabs:

Masses

TC*=o1+o2+o3+o4+e1+e2+e3
TMC=1.8*(o1+o2+o3+o4+op)+(e1+e2+e3-op)
LAC=(Fabs-5*fe)/12
OMC=TMC-LAC

Extinctions

EOMC=2.8*Small_OMC
+6.1*Large_OMC
ELAC=10*LAC

*TC would be measured directly, not derived from fractions

Results

See the document: RHR_Metrics_for_Different_OC_LAC_Measures_12_9_21_10_90.pdf at http://vista.cira.colostate.edu/improve/wp-content/uploads/2021/10/RHR_Metrics_for_Different_OC_LAC_Measures_12_9_21_10_90.pdf